Protein-protein interaction within multi-protein complexes from *Paracoccus versutus* and *Paracoccus denitrificans*: characterization of the recognition surfaces by high resolution NMR and X-ray crystallography

Ph.D Course in Biochemistry and Molecular Biology
XX cycle, 2004-2007

Chiara Cavalieri

Department of Biochemistry and Molecular Biology
University of Parma

Ph.D program coordinator:

Prof. Gian Luigi Rossi, Department of Biochemistry and Molecular Biology, University of Parma

Tutors:

Prof. Gian Luigi Rossi, Department of Biochemistry and Molecular Biology, University of Parma
Dott. Marcellus Ubbink, Leiden Institute of Chemistry, Leiden University

CONTENTS

CHAPTER 1

Introduction

Paracoccus versutus and *Paracoccus denitrificans* are phylogenetically closely related species that belong to the α-cluster of purple bacteria. Usually these organisms are found in soil, sewage or sludge, environments where the availability of suitable carbon and energy sources as well as of terminal electron acceptors is subject to ever-fluctuating conditions. The possibility for the cells to survive in these variable environments is the consequence of the ability of the bacterium to redirect electron fluxes to alternative branches within its respiratory network (short-term adaptation) as well as to change the makeup of the respiratory network (long-term adaptation) in response to environmental changes.
In the situation in which these bacteria experience a shortage of heterotrophic substrates (as sugars or alcohols) they can switch to autotrophic growth, during which hydrogen or thiosulfate are oxidized by hydrogenase or thiosulfate-oxidizing enzymes, respectively, and the carbon supply is accomplished by the fixation of atmospheric carbon dioxide. These bacteria are also able to grow on C_1 substrates, such as methanol or methylamine, a process considered as autotrophic growth too, because these carbon sources are oxidized merely with the purpose of gaining energy *(1)*

The methylamine dehydrogenase electron transfer chain

In these organisms, the oxidation of methylamine to formaldehyde and ammonia is catalysed by methylamine dehydrogenase (MADH), an inducible periplasmic enzyme. This reaction

$$CH_3NH_3^+ + H_2O \Rightarrow CH_2O + NH_4^+ + 2H^+ + 2e^-$$

is the first step in the metabolism of methylamine which can serve as a sole source of carbon and energy for these bacteria.

In both *P. denitrificans* and *P. versutus* the natural electron acceptor for MADH is a periplasmic type I blue copper protein, amicyanin, which mediates electron transfer from MADH to a membrane bound terminal oxidase, cytochrome aa_3, probably via one or more soluble electron carrier proteins. Cytochrome aa_3 finally reduces cytoplasmic O_2 to H_2O, effectively creating a proton gradient across the periplasmic membrane, which can drive the cell's energy production Both amicyanin and MADH are induced in these bacteria only when the cell uses methylamine as sole source of energy and in *P. denitrificans* the amicyanin is demonstrated to be the obligatory mediator of electron transfer from MADH. In fact the inactivation by gene replacement of the amicyanin gene, that is located immediately downstream of that for MADH, resulted in loss of the ability to grow on methylamine *(2)*.

MADH

MADH of *P. denitrificans* is a dimer of heterodimers, each one composed of a heavy chain (H) of 43 kDa and a light chain (L) of 14 kDa, the latter containing tryptophan tryptophylquinone (TTQ) as the redox cofactor. The crystal structure of this enzyme has been determined to 1.75 Å resolution *(3)*. The H subunit consists of seven antiparallel four-stranded β-sheets arranged in a propeller-like pattern about a pseudo-7-fold rotational axis of symmetry (figure 1A), while the L subunit consists of a tight structure composed of five β-strands which form two antiparallel β-sheets and contains the TTQ prosthetic group (figure1B). This subunit is crosslinked by six disulfide bridges and contains an additional covalent bond between two tryptophans, one of which has been modified to include an orthoquinone function at C6 and C7, to form the redox cofactor (figure 2).

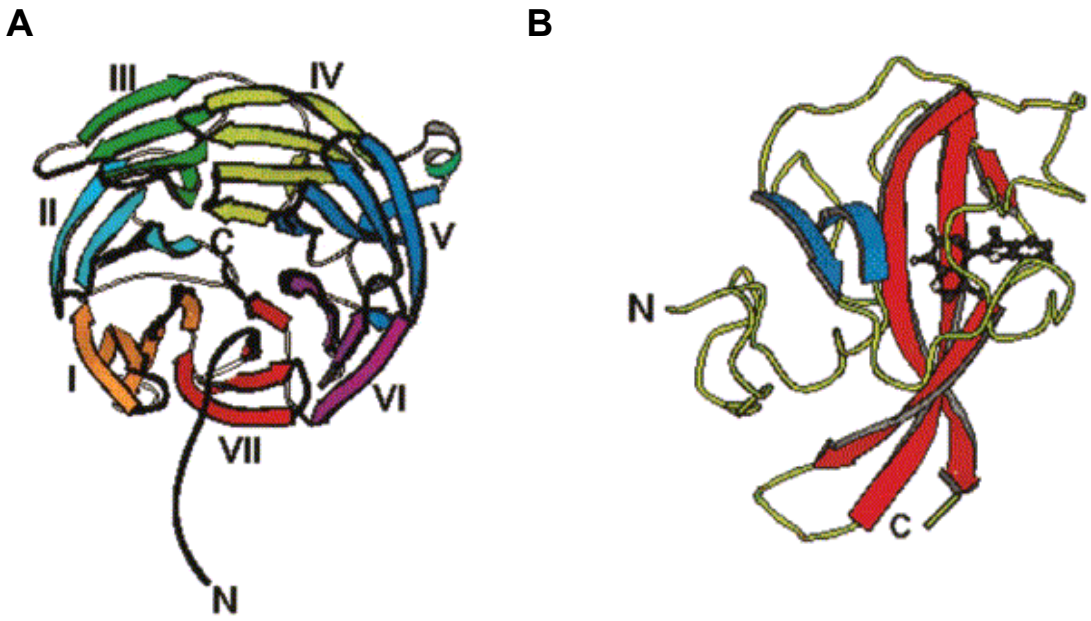

Figure 1. Schematic ribbon drawings of the H **(A)** and the L **(B)** subunits of *P.denitrificans* MADH

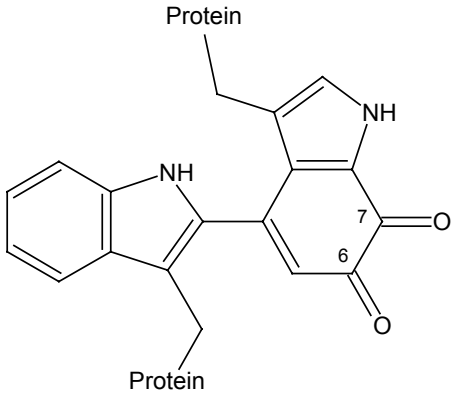

Figure 2. Tryptophan tryptophylquinone (TTQ), the cofactor of MADH

The oxidation of methylamine catalysed by MADH produces the two-electron reduced (aminoquinol) form of TTQ (figure 3A); then the coenzyme is reoxidized by the one-electron carrier amicyanin in two subsequent steps, the first one leading to formation of the aminosemiquinone form of TTQ (figure 3B).

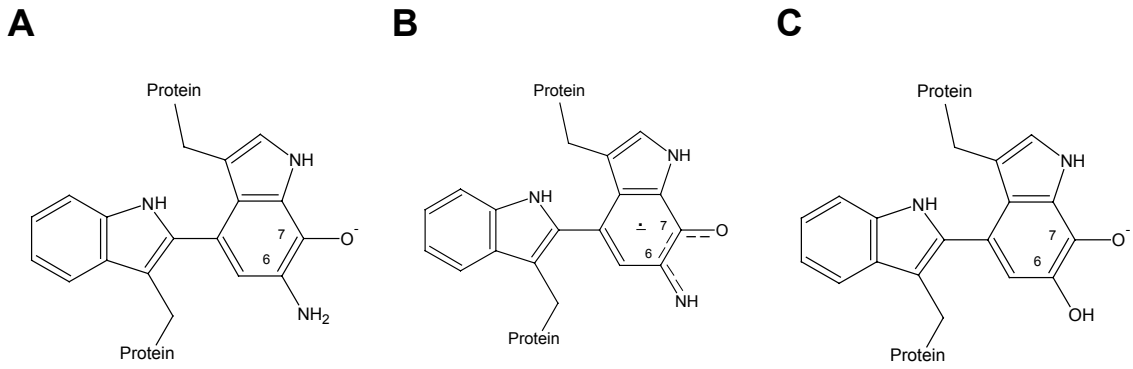

Figure 3. Reduced forms of the TTQ cofactor: **A)** N-quinol, **B)** N-semiquinone and **C)** O-quinol

Transfer of the first electron from the TTQ aminoquinol (N-quinol) to the amicyanin copper is a process activated by monovalent cations and gated by deprotonation of the methylamine-derived amino group *(4)*. In the case of the corresponding O-quinol (figure 3C), resulting from TTQ reduction by dithionite, electron transfer is slow and nearly independent of the presence of ions *(5)*.

It has been established that the dissociation constant of the binary complex between MADH and amicyanin in solution is in the micromolar range *(6)*.

Amicyanin and the binary complex

Amicyanin is a member of the type I blue copper proteins family (cupredoxin) in which two histidines, one cysteine and one methionine provide the four ligands for the redox-active copper centre. The *P. denitrificans* and *P. versutus* proteins have 105 and 106 amino acid residues, respectively, and are structurally strongly related with a 63% identity of their primary structures. The three-dimensional structure of the oxidized form of amicyanin from *Paracoccus versutus* has been solved by X-ray crystallography *(7)* and the NMR solution structure of the diamagnetic reduced protein is also available *(8)*. These structural studies show that the protein has a β-sandwich topology with nine β-strands forming two mixed β-sheets (figure 4A). This overall structural motif is very similar to that of other structurally characterized cupredoxins, with the greatest omology to plastocyanin *(9)*. The only notable difference between amicyanin and most other cupredoxin structures is the presence

of twenty additional residues at the N-terminus with no counterparts in other blue copper proteins; a portion of these residues forms the first β-strand of the structure.

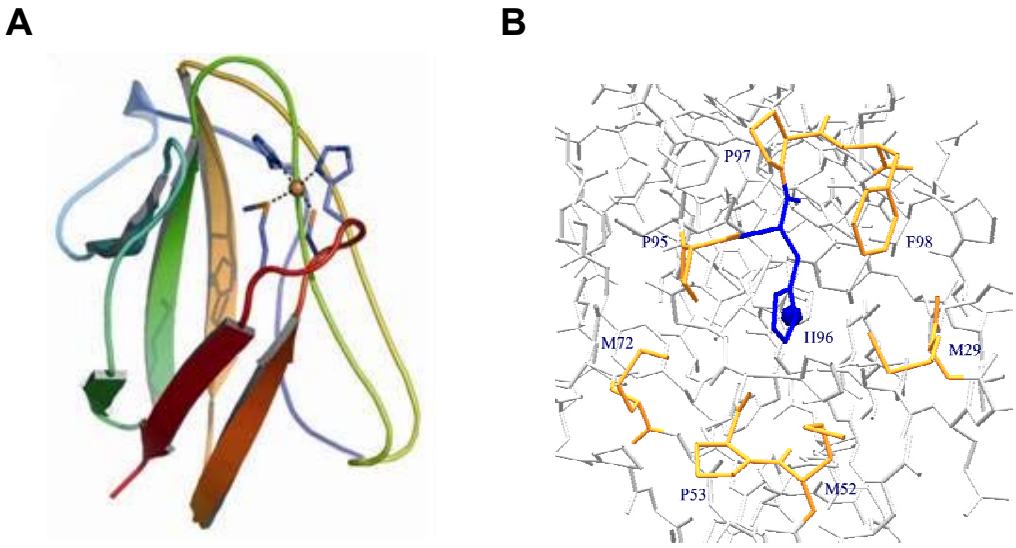

Figure 4. **A)** Representation of the three-dimensional structure of *P.versutus* amicyanin; **B)** The residues in orange form the hydrophobic patch that in *P.versutus* amicyanin surrounds the exposed copper ligand His 96

The single copper atom representing the redox center of amicyanin is found at one end of the β-sandwich. It is strongly coordinated by a cysteine sulphur, the N^{δ} atoms of two histidines and by the sulphur atom of a distant methionine. Another feature of amicyanin, that is common to all structurally investigated cupredoxins, is the presence of a hydrophobic patch on the protein surface, which surrounds the exposed imidazole ring of the C-terminal histidine ligand (His 96 in the *P. versutus* protein). This patch, that in amicyanin is composed of seven residues, is particularly important because it has been proposed as the main portal of entry end exit of electrons into and out of the protein active site (figure 4B).

In fact this hydrophobic part of the amicyanin surface is the region that mainly interacts with MADH in the crystal structure of the binary complex from *P.denitrificans*. In the structure of this complex, determined at 2.5 Å resolution *(10)*, one amicyanin molecule, of molecular mass 12 kDa, interacts with each protomer (the heterodimer) of MADH; the major intermolecular interactions occur between amicyanin and the light subunit of the enzyme, where the interface is also largely hydrophobic (figure 5). The distance between the TTQ reactive oxygen (O6) and

copper is 16.8 Å , while the distance between the closest TTQ atom and copper is 9.3 Å and one of the copper ligands, His 95, lies between the two redox centers thus facilitating electron transfer between them.

Figure 5.Crystal structure of the binary complex of amicyanin and MADH from *P.denitrificans*

Cytochrome c-551i and the ternary complex

In the last few years particular attention has been drawn to structural and electron-transfer properties of individual components of the periplasmic respiratory chain of methylotrophs. Besides amicyanin, that has been shown to be essential for *P.denitrificans* growth on methylamine, other redox proteins of this bacterium have been studied extensively using physico-chemical methods. However, some controversy has remained concerning the identity of the physiological electron acceptor for amicyanin.

When grown on methanol or methylamine, *P. denitrificans* synthesizes three periplasmic soluble *c*-type cytochromes: cytochrome *c*-550, also present during heterotrophic growth, and two inducible cytochromes, *c*-551i and *c*-553i, that are present just during methylotrophic growth conditions *(11)*. Cytochrome *c*-551i, of molecular mass 17.5 kDa, is shown to be *in vitro* the most efficient electron acceptor

from amicyanin and it co-crystallizes with the MADH-amicyanin binary complex to form a ternary complex in which one cytochrome molecule binds each amicyanin molecules; the crystal structure of this ternary complex has been solved at 2.4 Å resolution (figure 6) *(12)*. In this structure amicyanin is in contact with both MADH and the cytochrome and the association between the first two proteins is very similar to that observed in the binary complex, involving both H and L subunits of MADH. The distance between copper and the nearest atom of the heme is about 21 Å and that between copper and iron is 24.8 Å. From these structural studies it is evident that the amicyanin-cytochrome interface is considerably different from the MADH-amicyanin interface: it is smaller and more polar; moreover, the connections between amicyanin and cytochrome *c*-551i are more numerous than those between amicyanin and MADH.

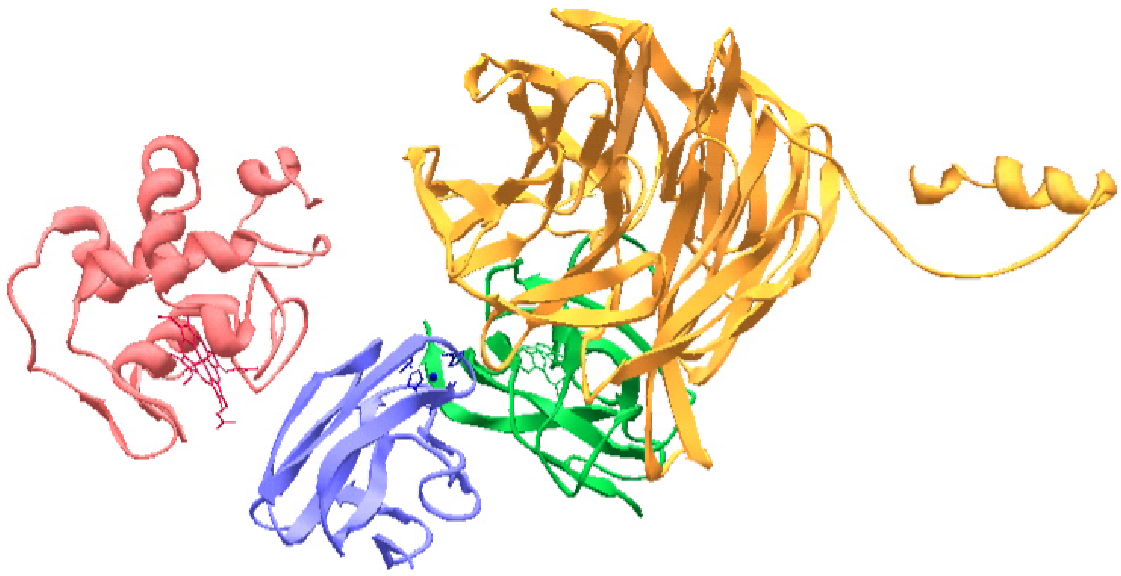

Figure 6. Crystal structure of the ternary complex between amicyanin, MADH and *c* -551i from *P.denitrificans*

Nevertheless it, has been reported that gene knock-out of cytochrome *c*-551i, and even of the other two soluble *c*-type cytochromes, does not affect the growth of *P.denitrificans* on methylamine, a finding which has been considered inconsistent with the role of cytochrome *c*-551i as the physiological redox partner of amicyanin. On the other side this cytochrome is important for this bacterium to grow on methanol and it is supposed to be the natural electron acceptor of methanol dehydrogenase (MDH) *(13)*. In spite of the question concerning the physiological role of cytochrome *c*-551i, the crystal structure of this ternary complex, has been used as a base to propose pathways for inter-molecular electron transfer *(12,14)* and to interpret the rates measured in solution *(5,15,16)*. Both the binary and ternary complexes in the crystalline state are catalitycally and electron transfer competent, as demonstrated by single crystal polarized absorption microspectrophotometry *(14,17)* and continuous-wave electron paramagnetic resonance, using polycrystalline powders *(17,18)*. However, the rate of electron transfer between the amicyanin copper and the cytochrome has been found to be considerably slower than cytochrome reduction in solution *(17,19)*.

Aim of the work

In the present work, both systems from *P. versutus* and *P. denitrificans* have been investigated, studying protein-protein interactions in different multi-protein complexes, both in the solid state, using X-ray crystallography, and in solution, using multi-dimensional high-resolution nuclear magnetic resonance (NMR) spectroscopy (see chapter 2) and stopped-flow kinetics. In particular, NMR techniques, never used before to study these systems, have been used with the aim to identify the amicyanin binding interfaces. Subsequently, where possible, these have been compared with the recognition surfaces found in the crystal structures of the corresponding complexes. Stopped-flow experiments have been performed to study the kinetics of electron transfer between MADH and amicyanin in the *P. versutus* system in different conditions to determine the parameters present in the equations derived from the Marcus theory *(20)*. The results have been compared with those previously published for the same system from *P. denitrificans*.

Stopped-flow kinetics

Since many biologically important processes function by producing changes in the millisecond time range, it is useful to study a variety of physiological and pathological systems in this time range.

One of the most frequently used rapid kinetics techniques requires rapid mixing and stopped-flow. Small volumes of solutions are driven from high performance syringes through a high efficiency mixer just before passing into a measurement flow cell. As the solutions flow through, a steady state equilibrium is established and the resultant solution is only a few milliseconds old as it passes through the cell. The mixed solution then passes into a stopping syringe which allows the flow to be instantaneously stopped. Using appropriate spectroscopic techniques, the kinetics of the reaction can be measured in the cell. The most common method of following the kinetics is to use either absorbance or fluorescence spectroscopy.

A simplified schematic of the basic components of a stopped-flow instrument is shown in figure 7.

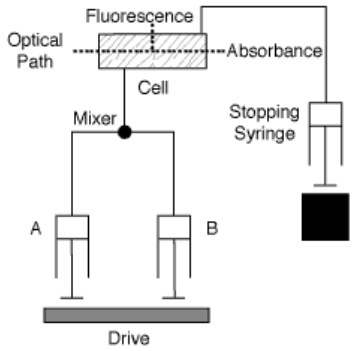

Figure 7. Schematic representation of a single mixing stopped-flow instrument

A wide variety of options include multi-mixing where more that two solutions are mixed together, variable ratio mixing using syringes of different sizes and microvolume mixing for applications where only very small quantities of reactants are available. Regardless of which configurations the stopped-flow uses, the time resolution of this method is limited by the time required for the reactants to flow from the final point of mixing to the observation cell. This time is referred to as the dead time of the instrument.

CHAPTER 2

NMR techniques

The basic theory of NMR

Nuclear spin and quantization of energy

The phenomenon of magnetic resonance results from the interaction of the magnetic moment of an atomic nucleus with an external magnetic field. The cause of this magnetic moment is the quantum mechanical angular momentum (spin angular momentum). In order to understand this, imagine the nucleus as a small positive charged particle which is spinning around its own axis thus representing an electric current. Due to this current the atomic nucleus behaves as a small electromagnet. The nucleus therefore possesses a magnetic moment, μ, which is proportional to its spin,*I* :

$$\mu = \frac{\gamma I h}{2\pi}$$

where γ is called the *gyromagnetic ratio* and is a fundamental nuclear constant which has a different value for every nucleus and *h* is the Planck's constant.
The sensitivity of a nucleus in NMR depends on gamma (high gamma means high sensitivity).

Of course, this picture is a classical model which has nothing to do with reality. The quantum mechanical property 'spin' does not mean that the nucleus is spinning around its own axis.
In many atoms (such as ^{12}C) these spins are paired against each other, such that the nucleus of the atom has no overall spin. However, in some atoms (such as ^{1}H and ^{13}C) the nucleus does possess an overall spin (see table 1).

Table 1. Features of some magnetic active nuclei that are of special interest in NMR spectroscopy of biomolecules

Isotope	Spin,*I*	Natural abundance (%)	Gyromagnetic ratio, γ [10^7*rad/(T*s)]	Relative sensitivity[1]	Absolute sensitivity[2]
^{1}H	1/2	99.98	26.7519	1.00	1.00
^{2}H	1	0.016	4.1066	$9.65 \cdot 10^{-6}$	$1.45 \cdot 10^{-6}$
^{13}C	1/2	1.108	6.7283	$1.59 \cdot 10^{-2}$	$1.76 \cdot 10^{-4}$
^{14}N	1	99.63	1.9338	$1.01 \cdot 10^{-3}$	$1.01 \cdot 10^{-3}$
^{15}N	1/2	0.37	-2.712	$1.04 \cdot 10^{-3}$	$3.85 \cdot 10^{-6}$
^{17}O	5/2	0.037	-3.6279	$2.91 \cdot 10^{-2}$	$1.08 \cdot 10^{-5}$
^{31}P	1/2	100	10.841	$6.63 \cdot 10^{-2}$	$6.63 \cdot 10^{-2}$

[1]The relative intensity is given at constant magnetic field and equal number of nuclei.

[2] The absolute intensity is the product of the relative intensity multiplied by the natural abundance.

The overall spin,*I*, is important. Quantum mechanics tells us that a nucleus of spin I will have 2*I* + 1 possible orientations. So, as an example, a nucleus with spin 1/2 (as ^{1}H) will have two possible orientations. In the absence of an external magnetic field, these orientations are of equal energy. If a magnetic field is applied, then the energy levels split. Each level is given a magnetic quantum number, m (see figure 1).

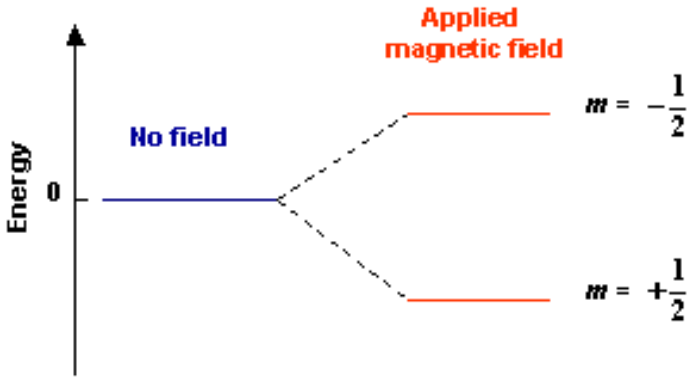

Figure 1. Energy levels for a nucleus with spin quantum number 1/2

When the nucleus is in a magnetic field, the initial populations of the energy levels are determined by thermodynamics, as described by the Boltzmann distribution:

$$\frac{N_\beta}{N_\alpha} = e^{-\Delta E/(k_B T)}$$

where:

N_β and N_α are the populations of the state β and α respectively;

ΔE is the energy difference between the two state;

k_B is the Boltzmann constant;

T is the temperature in Kelvin.

This is very important, and it means that the lower energy level will contain slightly more nuclei than the higher level. It is possible to excite these nuclei into the higher level with electromagnetic radiation. The frequency of radiation needed is determined by the difference in energy between the energy levels. The energy of a particular energy level is given by:

$$E = -\frac{\gamma h}{2\pi} m B$$

where B is the strength of the homogenous magnetic field.

The difference in energy between levels (the transition energy) can be found from

$$\Delta E = \frac{\gamma h B}{2\pi}$$

This means that if the magnetic field, B, is increased, so is ΔE. It also means that if a nucleus has a relatively large gyromagnetic ratio, then ΔE is correspondingly large.

The absorption of radiation by a nucleus in a magnetic field

Imagine a nucleus (of spin 1/2) in a magnetic field. This nucleus is in the lower energy level (i.e. its magnetic moment does not oppose the applied field). The nucleus is spinning around its axis and in the presence of a magnetic field this axis of rotation will precess around the magnetic field:

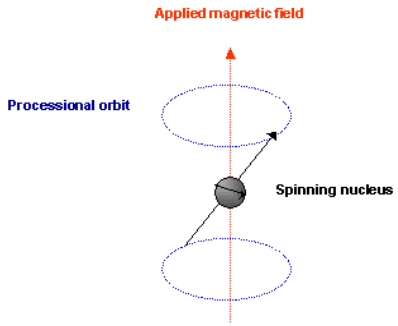

The frequency of precession is termed the *Larmor frequency*, which is identical to the transition frequency.
The potential energy of the precessing nucleus is given by:

$$E = -\mu\ B\cos\theta$$

where θ is the angle between the direction of the applied field and the axis of nuclear rotation.

If energy is absorbed by the nucleus, then the angle of precession, θ, will change. For a nucleus of spin 1/2, absorption of radiation "flips" the magnetic moment so that it opposes the applied field (the higher energy state), as shown in figure 2.

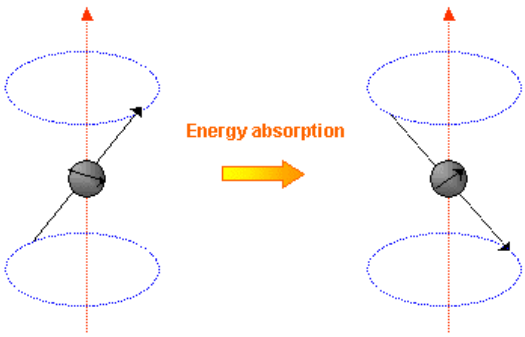

Figure 2. Transition between two spin energy state after absorption of energy

It is important to realise that only a small proportion of "target" nuclei in the lower energy state are in excess relative to the higher energy state, causing absorption of radiation, so there is the possibility that by exciting these nuclei the populations of the higher and lower energy levels will become equal. If this occurs, then there will be no further absorption of radiation: the spin system is saturated. The possibility of saturation means that we must be aware of the relaxation processes which re-establish the Boltzmann equilibrium.

Relaxation processes

How do nuclei in the higher energy state return to the lower state? Emission of radiation is insignificant because the probability of re-emission of photons varies with the cube of the frequency and at radio frequencies re-emission is negligible. We must focus on non-radiative relaxation processes.
Ideally the relaxation rates sholud be fast , but not too fast. If the relaxation rate is fast, then saturation is reduced. If the relaxation rate is too fast, line-broadening in the resultant NMR spectrum is observed.
There are two major relaxation processes:

- Spin - lattice (longitudinal) relaxation
- Spin - spin (transverse) relaxation

Spin - lattice relaxation

Nuclei in an NMR experiment are in a sample that is called the lattice. Nuclei in the lattice are in vibrational and rotational motion, which creates a complex magnetic field. The magnetic field caused by motion of nuclei within the lattice is called the lattice field. This lattice field has many components. Some of these components will be equal in frequency and phase to the Larmor frequency of the nuclei of interest. These components of the lattice field can interact with nuclei in the higher energy state, and cause them to lose energy (returning to the lower state). The energy that a nucleus loses increases the amount of vibration and rotation within the lattice (resulting in a tiny rise in the temperature of the sample).
The *spin-lattice relaxation time,* t_1 (the average lifetime of nuclei in the higher energy state), is dependent on the gyromagnetic ratio of the nucleus and the mobility of the

lattice. As mobility increases, the vibrational and rotational frequencies increase, making it more likely for a component of the lattice field to be able to interact with excited nuclei. However, at extremely high mobilities, the probability of a component of the lattice field being able to interact with excited nuclei decreases.

Spin - spin relaxation

Spin-spin relaxation describes the interaction between neighbouring nuclei with identical precessional frequencies but differing magnetic quantum states. In this situation the nuclei can exchange quantum states; a nucleus in the lower energy level will be excited, while the excited nucleus relaxes to the lower energy state. There is no net change in the populations of the energy states, but the average lifetime of a nucleus in the excited state will decrease. This can result in line-broadening. The *spin-spin relaxation time* is conventionally called t_2.

Chemical shift

The magnetic field at the nucleus is not equal to the applied magnetic field because the electrons around the nucleus shield it from the applied field.

Consider the s-electrons in a molecule. They have spherical symmetry and circulate in the applied field producing a magnetic field which opposes the applied field (figure 3). This means that the applied field strength must be increased for the nucleus to absorb at its transition frequency. This upfield shift is also termed diamagnetic shift. Electrons in p-orbitals have no spherical symmetry. They produce comparatively large magnetic fields at the nucleus, which give a low field shift. This "deshielding" is also called paramagnetic shift.

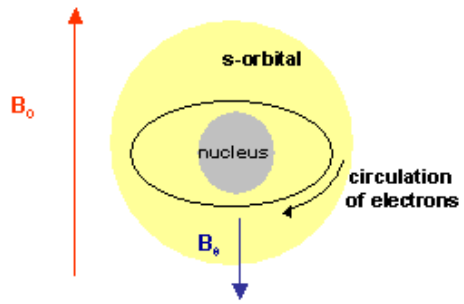

Figure 3. Creation of the B_e field, by the circulation of electrons, in opposition to the external B_o field.

So, the actual strength of the magnetic field is different for nuclei that have different electronic environments (i.e. nucleus magnetically different). As consequence of that the transition between two spin states should be induced by absorption of a photon of frequency ν_1, directly proportional to the actually magnetic field, B_1, that is experienced at a considered nucleus:

$$\Delta E = h\nu_1 = h B_1 \gamma = h(B_0 - B_e)\gamma$$

where:

ΔE is the difference between two spin states;

h is the Planck's constant;

ν_1 is the frequency of the B_1 field;

B_0 is the strength of the external homogeneous magnetic field;

B_e is the small magnetic field generated by the circulation of electrons;

γ is the gyromagnetic ratio.

The chemical shift is the difference between resonance frequency of the nucleus and a standard, relative to the standard itself. Conventionally in the scale of NMR spectra the chemical shift is not expressed in frequency, but in ppm (part per million) and it is indicated with δ:

$$\delta = \frac{\nu_1 - \nu_{ref}}{\nu_{ref}} 10^6$$

where:

ν_1 is the resonance frequency of the observed nucleus;

ν_{ref} is the resonance frequency of the nuclei of a reference compound (for ^{1}HNMR the reference is usually tetramethylsilane, TMS)

Continuous wave spectroscopy

Transitions between different energy levels occur if the frequency of radiation is equivalent to the energy difference between the two levels. In the old days of NMR, experiments were carried out by varying the frequency of radiation at constant magnetic field and measuring the absorption of radiation by the different nuclei. Equivalently, the magnetic field strength could be varied at constant radiation frequency. Until the nineteen-seventies all NMR spectrometers worked with this continuous wave technique.

Pulsed Fourier Transform NMR Spectroscopy

A far better resolution and sensitivity in NMR was achieved by the introduction of pulsed Fourier transform techniques (FT-NMR). In FT-NMR the resonances are not measured one after another but all nuclei are excited at the same time by a radio frequency pulse. Normally a radio emitter works at fixed frequency. However, if the radiation is emitted as a very short pulse (some μs in NMR) the pulse frequency becomes ill-defined. A short radio frequency pulse contains many frequencies in a broad band around the fixed work frequency and thus excites the resonances of all spins in a sample at the same time.
The excited spins emit the absorbed radiation after the pulse. The emitted signal is a superposition of all excited frequencies. Its evolution in time is recorded. The intensities of the several frequencies, which give the observed signal in their superposition, are calculated by a mathematical operation, the Fourier transformation, which translates the time data into the frequency domain. The resulting NMR spectrum looks like an ordinary cw spectrum but its sensitivity is several orders of magnitudes better.

The 90-FID pulse sequence

By the application of the Fourier transformation you can convert the time domain signal into a frequency domain signal, but how you can create the first one? Consider a case of a nucleus of spin equal of ½. When a group of these spins is placed in an external static magnetic field (B_0) each spin aligns in one of the two possible orientations, conventionally called α (+1/2, parallel to B_0) and β (-1/2, antiparallel to B_0) and the distribution between this two energy states is given by the Boltzmann

equation. In this situation at the thermal equilibrium the net magnetization is along the direction of B_0 (conventionally the z axis) because the x and y components sum up to zero (figure 4).

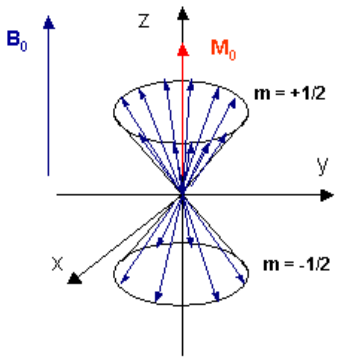

Figure 4. Distribution of the nuclei between the two spin energy levels in an external magnetic field B_0 and the resulting magnetization vector M_0 along z

In this condition you cannot detect any signals. But if you perturb this situation of equilibrium, by an electromagnetic pulse, you can detect an electric signal. This electric signal is the *Free Induction Decay* (FID) that is registered and further converted into the frequency domain by the application of the FT.

There are infinite numbers of possibilities to create a time domain signal and the simplest one is with a single 90° pulse. In this case the net magnetization, M_0, initially along the z axis (i.e. the B_0 direction), is rotated down into xy plane with a 90° pulse, B_1, (figure 5A) and the net magnetization vector begins to precess about the z axis (figure 5B) with the Larmor frequency and its magnitude also decays with time due to relaxation processes.

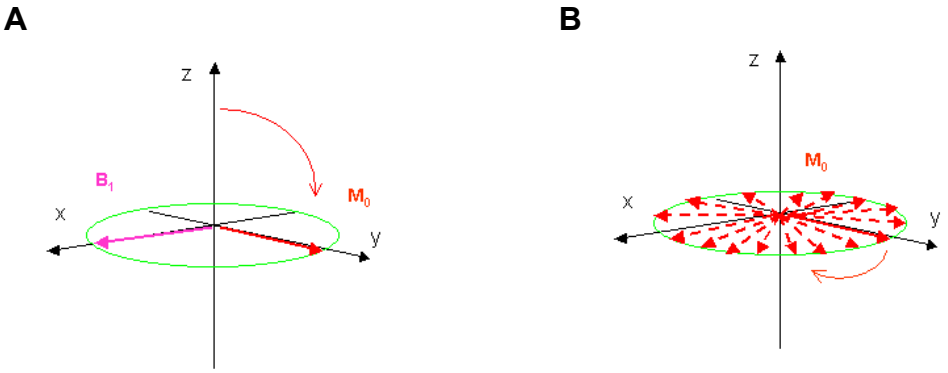

Figure 5. A) Effect of the application of a 90°-pulse along the x axis on the net magnetization vector M_0; **B)** Representation of the precession of the M_0 around the z axis after the 90°-pulse.

The 1D experiment

Each one-dimensional (1D) NMR experiment consists of two sections: preparation and detection. During preparation the spin-system is set to a defined state. During detection the resulting signal is recorded. In the simplest case the preparation consist in a 90°-pulse applied along the x axis (see precedent paragraph) which rotates the equilibrium magnetization from the z to the y axis. After this pulse each spin precesses with its own Larmor frequency around the z axis and induces an electric signal in the receiver coil. This signal decays due to the T_2 relaxation and is therefore called Free Induction Decay (FID) (figure 6).

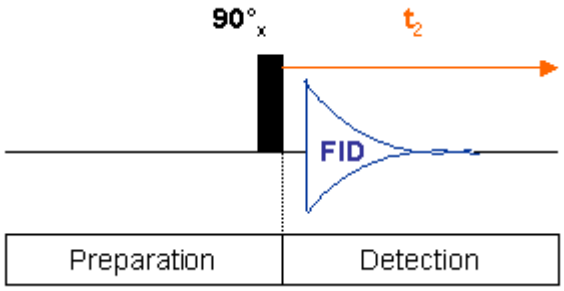

Figure 6. A 1D experiment

Usually the experiment is repeated several times and the data summed up to increase the signal-to-noise ratio. After summation the data are Fourier transformed to yield the final 1D spectrum (figure 7).

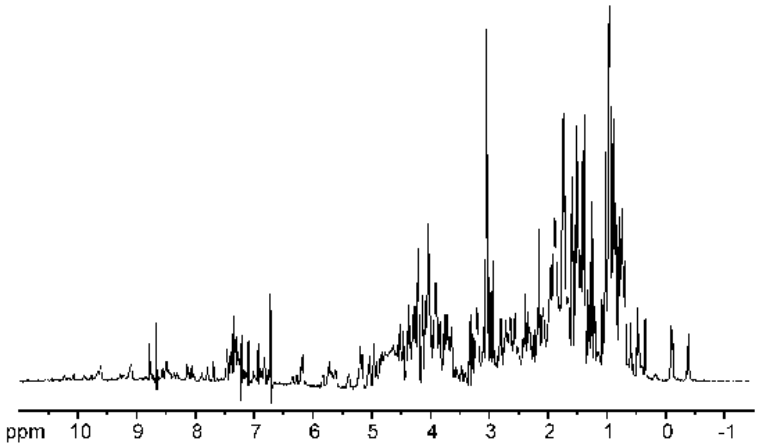

Figure 7. Example of a 1D NMR spectrum of a protein

The 2D experiments

As can be seen from the figure 7, 1D protein spectra are far too complex for interpretation as most of the signals overlap heavily. By the introduction of an additional spectral dimension these spectra are simplified and some extra information is obtained.

In addition to preparation and detection, which are already known from 1D experiment (see precedent paragraph), in 2D experiment there is an indirect evolution time t_1 and a mixing sequence (figure 8).

This scheme can be viewed as:

- Do something with the nuclei (preparation);
- Let them precess freely (evolution)
- Do something else (mixing);
- Detect the result (detection).

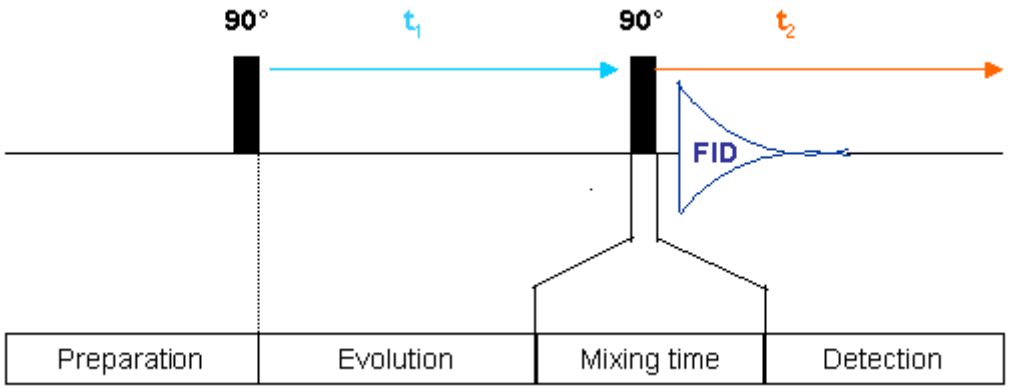

Figure 8. A 2D experiment

After preparation the spins can precess freely for a given time t_1 and during this time the magnetization is labelled with the chemical shift of the first nucleus. Then, during the mixing time the magnetization is transferred from the first nucleus to a second one.

Mixing sequences utilize two mechanisms for magnetization transfer:

- Scalar coupling (J-coupling)
- Dipolar interaction (NOE)

Finally, the data are acquired at the end of the experiment; during the detection phase (often called the direct evolution time) the magnetization is labelled with the chemical shift of the second nucleus. The experiment is repeated numerous times with increasing t_1.

The two-dimensional FT yields the 2D spectrum with two frequency axes. If the spectrum is *homonuclear* (signals of the same isotope, usually ^1H, are detected during the two evolution periods) it has a characteristic topology, as shown in the figure 9.

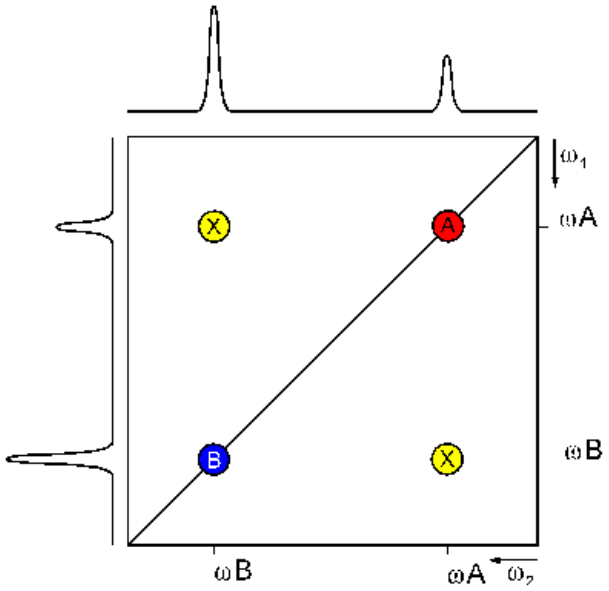

Figure 9. Characteristic topology of a 2D homonuclear NMR spectrum

A diagonal of signals (A and B) divides the spectrum in two equal halves and symmetrical to this diagonal there are more signals (X), called cross signals. The diagonal results from contributions of the magnetization that has not been changed by the mixing sequence (equal frequency in both dimensions, i.e. from the contributions which remained on the same nucleus during both evolution times).

The cross signals originate from nuclei that exchanged magnetization during the mixing time (frequencies of the first and second nucleus in each dimension, respectively). They indicate an interaction of these two nuclei. Therefore, the cross signals contain the really important information of 2D NMR spectra.

Homonuclear 2D experiments

There are three 2D spectra which are widely used for the structure determination of proteins with a mass of up to 10 kD**:**

- 2D-COSY
- 2D-TOCSY
- 2D-NOESY

2D-COSY

In the COSY (*Correlated Spectroscopy*) experiment the magnetization is transferred by scalar coupling. Protons that are more than three chemical bonds apart give no cross signal because the coupling constant between them (^{4}J) is close to zero. Therefore, only signals of protons which are two or three bonds apart are visible in a COSY spectrum (red signals in the figure 10). The cross signals between H^N and H^α protons are of special importance because the *phi* torsion angle of the protein backbone can be derived from the ^{3}J coupling between them.

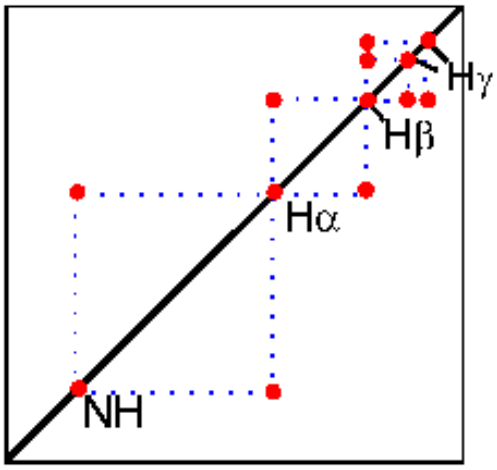

Figure 10. Topology of a 2D-COSY NMR spectrum

2D-TOCSY

In the TOCSY (*Total Correlation Spectroscopy*) experiment the magnetization is dispersed over a complete spin system of an amino acid by successive scalar coupling; this experiment correlates all protons of a spin system. Therefore, not only the signals that are visible in a COSY spectrum are present (red signals in the figure 11), but also additional signals (in green in the picture) which originate from the interaction of all protons of a spin system that are no directly connected via three chemical bonds.

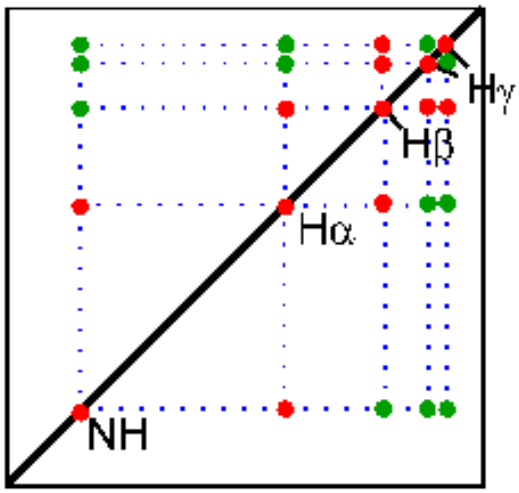

Figure 11. Topology of a 2D-TOCSY NMR spectrum

Thus, a characteristic pattern of signals results for each amino acid from which the amino acid can be identified. However, some amino acids have identical spin systems and therefore identical signal patterns; they are: cysteine, aspartic acid, phenylalanine, histidine, aspargine, tryptophane and tyrosine on the one hand and glutamic acid, glutamine and methionine on the other hand.

2D-NOESY

The NOESY (*Nuclear Overhauser Enhancement Spectroscopy*) experiment is crucial for the determination of protein structure. It uses dipolar interaction of spins (the NOE, *Nuclear Overhauser Enhancement*) for correlation of protons. The intensity of the NOE is in first approximation proportional to $1/r^6$, with r being the distance between the protons. The correlation between two protons depends on the distance between them, but normally a signal is only observed if their distance is smaller than 5 Å. The NOESY experiment correlates all protons which are close enough. It also correlates protons which are distant in the amino acid sequence but close in space due to tertiary structure of the protein and obviously this is most important information for the determination of the protein structures.

Heteronuclear 2D experiments

Apart from protons, proteins contain other magnetic active nuclei (see table 1) and for NMR of proteins ^{15}N and ^{13}C are of special importance. The use of these heteronuclei allows some new features in NMR which facilitate the structure determination, especially of larger proteins (>100 aa). The natural abundance of ^{15}N and ^{13}C is very low and their gyromagnetic ratios are markedly lower that of proton (see table 1). Therefore, two strategies are used for increasing the low sensitivity of these nuclei: isotopic enrichment of these nuclei in proteins and enhancement of the signal to noise ratio by the use of inverse NMR experiments in which the magnetization is transferred from protons to the hetero nucleus.

The HSQC experiment

The most important inverse NMR experiment is the HSQC (*Heteronuclear Single Quantum Correlation*) experiment; a typical pulse sequence of an HSQC experiment is shown in the figure 12. It correlates the heteroatom (^{13}C or ^{15}N) with the directly attached proton. So, each signal in a ^{15}N-HSQC spectrum represents a proton that is bound to a nitrogen atom (i.e. a NH, NH_2 or NH_3 group). An example of an HSQC spectrum is shown in the figure 13.

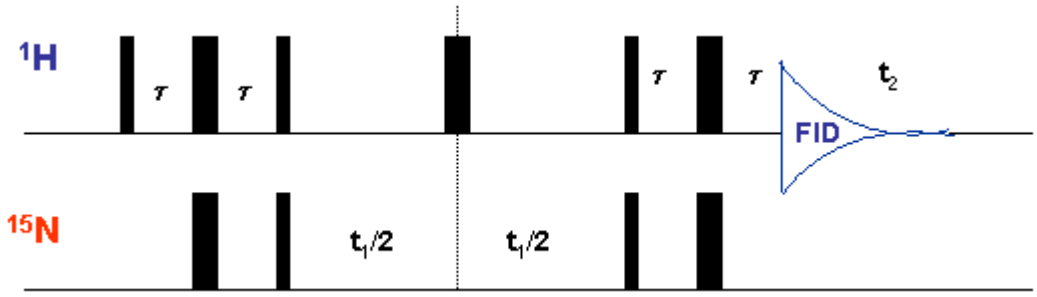

Figure 12. Typical pulse sequence of an HSQC experiment

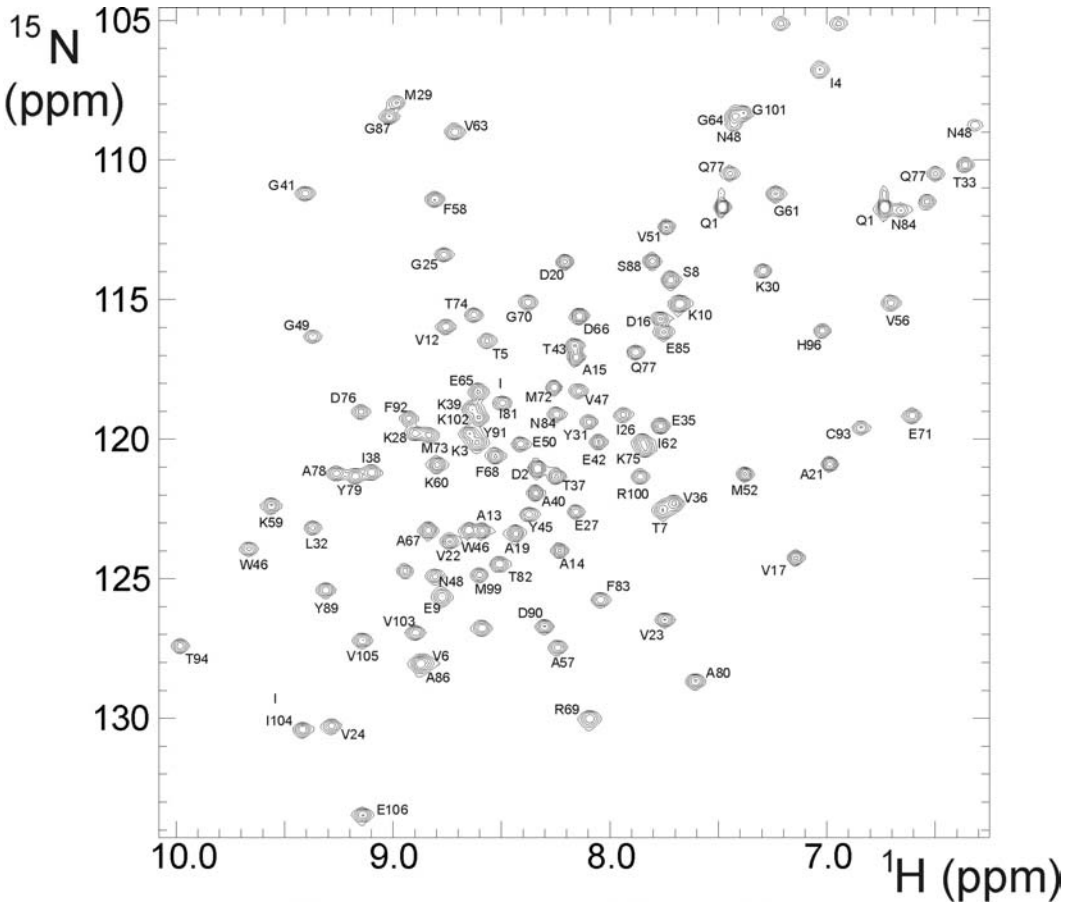

Figure 13. Annotated ^{15}N-HSQC spectrum of *P. versutus* Zn-substitute amicyanin

The TROSY experiment

Even with the most powerful and sensitive of modern nuclear magnetic resonance instruments, many interesting systems are impossible to solve because they are simply too big. This problem can be solved by the application of a particular type of 2D NMR experiment, called TROSY (*Transverse Relaxation Optimized Spectrocopy*) *(21)*. In fact in the TROSY technique the transverse nuclear spin relaxation, the most important event that causes the deterioration of NMR spectra for larger molecular structures, is suppressed, so it becomes possible to observe sharp signals also for very big proteins and protein complexes.

In the present work this approach was used, in combination with the use of perdeuterated form of amicyanin, to observe the resonances of this protein when it is in complex with the large enzyme methylamine dehydrogenase (MADH) (see figure 14) and also for the titration of the binary complex of these two proteins with its proposed acceptor of electrons in the MADH redox chain (i.e. cytochromes *c*-550 and *c*-551i for *P. versutus* and *P. denitrificans* respectively).

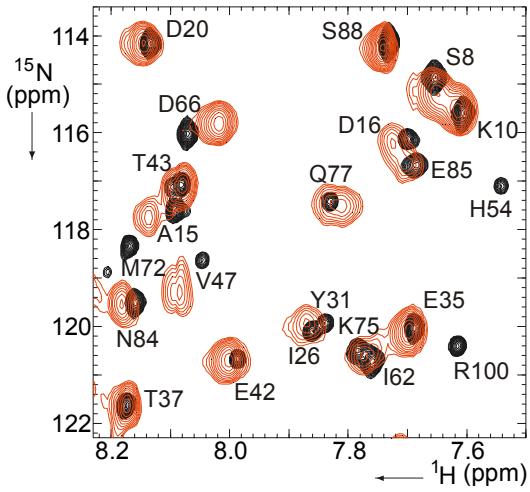

Figure 14. Regions of the TROSY spectra of Cu(I) amicyanin free (black contours) and bound to MADH (red contours).

The 3D experiments

- A three dimensional NMR experiment can be constructed from a two dimensional one by inserting an additional indirect evolution time and a second mixing period between the first mixing period and the direct data acquisition (see figure 15). Each of the different indirect time periods (t_1 and t_2) is incremented separately.

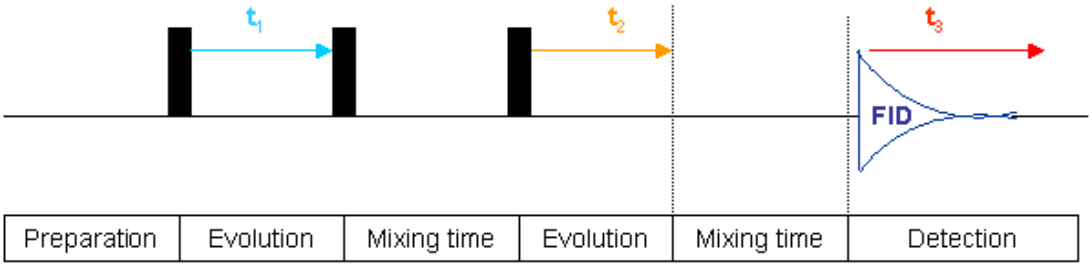

Figure 15. Schematic pulse sequence in a 3D NMR experiment

There are two principal classes of 3D experiments:

- Experiments consisting of “two 2D experiments after another”;
- The triple resonances experiments.

NOESY-HSQC, TOCSY-HSQC experiment

Two dimensional spectra, like NOESY and TOCSY, of larger proteins are often crowded with signals. Therefore, these spectra can be spreading out in a third dimension (usually ^{15}N or ^{13}C), so that the signals are distributed in a cube instead of a plane. This spreadout is achieved by combining HSQC and NOESY in a single 3D experiment. The NOESY experiment is extended by an HSQC step. Acquisition starts after this HSQC step instead of at the end of the NOESY mixing time. The resulting experiment is called 3D NOESY-HSQC. In a similar way a TOCSY-HSQC can be constructed by combining the TOCSY and the HSQC experiment.

In the present work these types of spectra were used to assign the HSQC spectra of both the *P. versutus* and *P. denitrificans* ^{15}N-Zn-substituted amicyanin.

HCCH-TOCSY

This experiment is alternative to the TOCSY-^{13}C-HSQC one, which shows a markedly reduced sensitivity for larger proteins. In both parts of the experiment the magnetization is transferred via direct ^{1}J couplings between the atoms, allowing a much faster magnetization transfer than in the TOCSY-HSQC. Magnetization is transferred (see blue arrows in the figure 16) from a sidechain proton (shown in red) to its attached carbon atom (shown in yellow), by ^{1}J coupling to the neighboring carbon atoms and finally to their attached protons. Therefore, a HCCH-TOCSY experiment looks in principle the same like a TOCSY-^{13}C-HSQC and the type of an amino acid can be recognized from the peak pattern in the usual way.

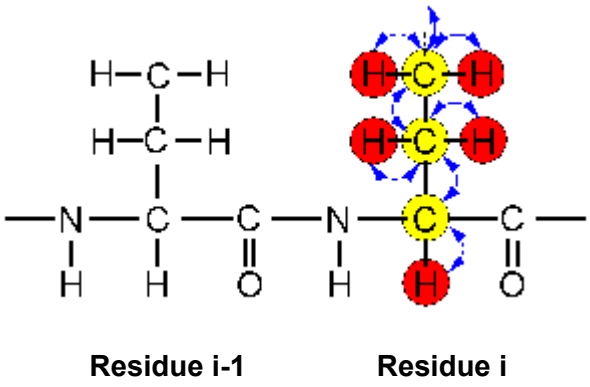

Figure 16. Scheme of the magnetization transfer in a HCCH-TOCSY experiment

Triple resonance experiments

Triple resonance experiments are the method of choice for the sequential assignment of larger proteins (>150 aa). These experiments are called “triple resonance” because three different nuclei (^{1}H, ^{13}C and ^{15}N) are correlated and are performed on ^{13}C,^{15}N doubly labelled proteins.

The most important advantage of the triple resonance spectra is their simplicity. They contain only a few signals on each frequency (often only one), so the problem of spectral overlap is therefore strongly reduced (this is the main reason why proteins of more than 20 kDa can be assigned with these type of experiments). However, the coordinates of clearly separated signals from different amino acids can accidentally

be identical (degeneration of signals); the correct choice of connectivities between amino acids is the main problem in the assignment of triple resonance spectra.

Another advantage of these spectra is their high sensitivity which is caused by an efficient transfer of magnetization. The magnetization is transferred via ^{1}J or ^{2}J couplings (i.e. via the covalent chemical bonds), therefore the transfer times are shorter and the losses due to relaxation are smaller than in homonuclear experiments.

There is a variety of triple resonance experiments and here just some of them are illustrated (those that were used in this work to assign the HSQC spectra of both the *P. versutus* and *P. denitrificans* ^{13}C-^{15}N-Cu(I)-amicaynin).

The names of triple resonance experiments sound very cryptic at first glance, but they are very descriptive. The names of all nuclei which are used for magnetization transfer during the experiment are listed in the order of their use, bracketing the names of nuclei which are used only for transfer and for detection.

HNCA

The HNCA experiment is the prototype of all triple resonance experiments. Starting at an amide proton (H) the magnetization is transferred to the directly attached nitrogen atom (N) which is measured as the first spectral dimension. Then the magnetization is transferred to the C_α nucleus (CA) which is measured as second dimension. Afterwards, the magnetization is transferred back the same way to the amide proton which is measured as the third (direct) dimension (see figure 17).

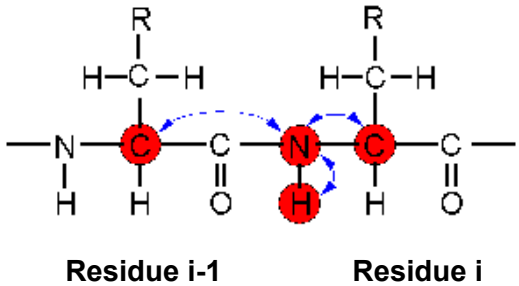

Figure 17. Scheme of the magnetization transfer in a HNCA experiment

In each step the magnetization is transferred via strong ^{1}J coupling between the nuclei; the coupling which connects the nitrogen atom with the C_α carbon of the preceding amino acid (^{2}J=7 Hz) is only marginally smaller than the coupling to the directly attached C_α atom (^{1}J =11 Hz). Thus, the nitrogen atom of a given amino acid is correlated with both C_α : its own and the one of the preceding residue. Therefore, it is possible to assign the protein backbone exclusively with and HNCA spectrum, though usually more triple resonance experiments are required.

HNCACB

In the HNCACB experiment *(22)* the magnetization starts at an amide proton (H) and it is transferred to the directly attached nitrogen atom (N) which is measured as the first spectral dimension. Then it is transferred to the C_α (CA) and C_β (CB) nuclei which are measured as second dimension. Afterwards, the magnetization is transferred back the same way to the amide proton which is measured as the third (direct) dimension (see figure 18, in which the detected nuclei are highlighted in red).

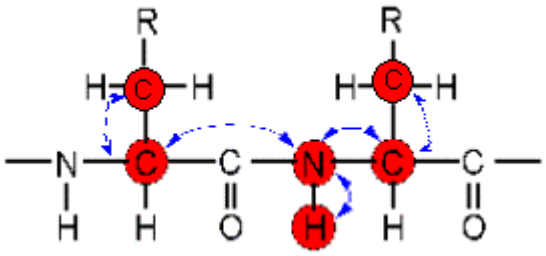

Figure 18. Scheme of the magnetization transfer in a HNCACB experiment

HNCO

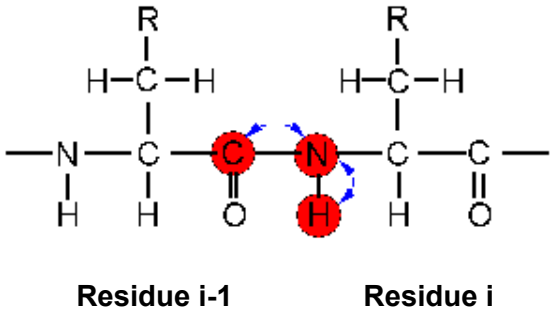

Figure 19. Scheme of the magnetization transfer in a HNCO experiment

In the HNCO experiment *(23)* the magnetization is transferred (blue arrows in the figure 19) from the H^N(i) proton via N(i) atom to the directly attached CO(i-1) carbon atom and return the same way to he H^N(i) nucleus which is directly detected. The frequencies of all three nuclei (in red in the picture) are detected.

HN(CA)CO

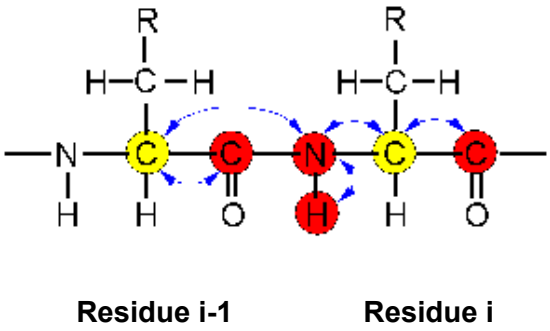

Figure 20. Scheme of the magnetization transfer in a HN(CA)CO experiment

In the HN(CA)CO experiment *(24)* the magnetization is transferred from the H^N(i) proton via the N(i) atom and the CA nucleus (the C_α(i)) to the CO(i) carbon atom and back the same way. The C_α atom (in yellow in the figure 20) acts only as relay nucleus and its frequency is not detected. In this experiment only the frequencies of H^N, N and CO (shown in red in the picture) are detected.

CC(CO)NH

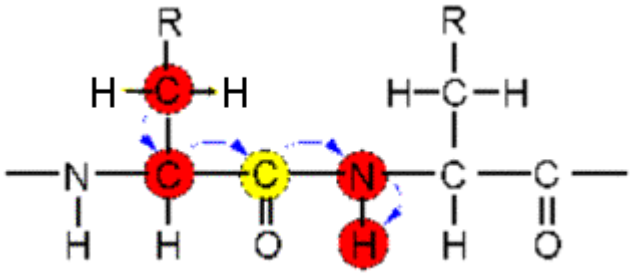

Figure 21. Scheme of the magnetization transfer in a CC(CO)NH experiment

In the CC(CO)NH experiment *(25)* the magnetization starts from the C_α and the C_β of the residue i-1 (shown in red in the figure 21) and it is transferred via the CO(i-1) (in yellow) to the N and H^N of the attached NH(i) group (in red) which are detected.

CHAPTER 3

Structural comparison of crystal and solution states of the 138 kDa complex of methylamine dehydrogenase and amicyanin from *Paracoccus versutus*

INTRODUCTION AND AIM OF THE WORK

The crystal structure of MADH *(26)* and both the solution *(27)* and crystal *(7)* structures of amicyanin from *P. versutus* have been determined but the binary complex has not been described either in solution or in the crystal. Cytochrome *c*-551i has not been found in this bacterium and cytochrome *c*-550 has been proposed as the further electron acceptor *(28)*. The final acceptor of the methylamine-derived electrons is likely to be the membrane-bound cytochrome oxidase aa_3.

In the present study, the binary complex of *P. versutus* MADH and amicyanin has been characterized functionally as well as structurally, both in the crystal and in solution. Functional analysis of the *P. versutus* system was performed by determining the temperature-dependent rate of electron transfer (et) from the N-quinol to amicyanin and calculating the values of two parameters of the semiclassical et theory *(20)*, the strength of electronic coupling between electron donor and electron acceptor at the transition state (H_{AB}) and the nuclear reorganization energy (λ). For pure electron transfer, an H_{AB} value lower than 80 cm^{-1} is expected, whereas higher values point to an adiabatic rate-limiting step *(4,29)*. The results confirm the findings described above for the *P. denitrificans* complex. The crystal structure of the binary complex has been obtained to 2.5 Å resolution and has been compared with the structure of the complex in solution using NMR spectroscopy. By perdeuteration and labelling with ^{15}N, amicyanin has been observed selectively in the complex. Chemical shift perturbation mapping shows good agreement with the interface observed in the crystal and is similar for both redox states of amicyanin. Interestingly, small secondary chemical shift effects, deep inside the protein can be correlated to small differences in the H-bond network between free and bound amicyanin. These results show that, despite the large size of the complex, details of the molecular interactions

can be obtained in solution. Furthermore, the interaction between both the uncomplexed amicyanin and the binary complex with the possible electron acceptor, cytochrome *c*-550, has been investigated by NMR experiments. In both cases the data do not show any perturbation in the amicyanin signals, suggesting that this cytochrome is not the physiological partner of amicyanin in the *P. versuts* respiratory chain.

EXPERIMENTAL PROCEDURES

Proteins production and purification

Amicyanin

Escherichia coli BL21 cells were transformed with the plasmid pET28a-ami *(30)* and cultured at 37°C in LB medium containing 50 mg/L kanamycin (Sigma-Aldrich, St. Louis, MO). Expression was induced by adding 1 mM isopropyl-β-galactoside when OD_{600}=0.7. After 16 hours, the cells were harvested by centrifugation at 6000 rpm for 20 minutes. Cells were lysed by sonication after adding DNase (Sigma-Aldrich, St. Louis, MO) and 0.5 mM phenylmethanesulphonylfluoride (Sigma-Aldrich, St. Louis, MO). In the presence of about 20 μM $CuSO_4$ to convert apo to holo-protein, $K_3Fe(CN)_6$ was slowly added in amounts sufficient to fully oxidize the bound metal. Holo-amicyanin was purified following the published procedure *(31)* with slight modifications. After sonication and centrifugation at 10000 rpm for 30 minutes, the supernatant was dialysed overnight in a 3500 MWCO dialysis tube against 2 L of 20 mM sodium phosphate buffer, pH 7, which was replaced twice. The supernatant was then loaded on a DEAE column equilibrated with 20 mM sodium phosphate, pH 7. The protein bound weakly to the column material and could be eluted in the absence of salt. The pH of the protein solution was lowered to 4.5 by slowly adding 50 mM acetate buffer, pH 4.5, and the solution was loaded on a CM column equilibrated with the same buffer. The protein was eluted using a linear gradient (0-50%) of 500 mM NaCl in the same buffer and collected as 1.5 ml fractions at the flow rate of 1-1.5 ml/min. Purity was checked by the A_{280}/A_{596} ratio (4.2 for pure protein) *(31)*. The yield was 80 mg/L (estimated from ε=3900 $M^{-1}cm^{-1}$ at 596 nm).

^{15}N-labelled protein was produced as above, using M9 minimal medium supplemented with 1 g/L $^{15}NH_4Cl$. The protein yield after purification was about $30mg/L$. ^{15}N-^{13}C-amicyanin was produced in a minimal medium as described above,

but using 2 g/L of $^{13}C_6$-glucose (as the sole carbon source) with a yield of 30 mg/L of pure protein. A minimal medium with D_2O substituting H_2O and 5 g/L CD_3COONa as the sole carbon source was used to produce ^{15}N-^{2}H-amicyanin (yield after purification: 30 mg/L). Due to possibly incomplete exchange of the amide protons it was only possible to establish that the deuteration level of non-exchangeable protons was between 83% and 99%, on the basis of mass spectrometry.

Zn-replacement

Substitution of copper with zinc was performed as described *(32)*. To remove the unfolded protein, zinc-amicyanin was passed through an anionic exchange column (Source 30Q) equilibrated with 20 mM sodium phosphate, pH 7. The protein was eluted with 100 mM NaCl in the same buffer.

MADH

MADH was expressed in *P. versutus* grown on a minimal medium containing 6.7 g Na_2HPO_4, 0.37 g KH_2PO_4 and 10 g $CH_3NH_2{\cdot}HCl$/L and 2 mM $MgSO_4$, a vitamin mix and a trace elements mix. MADH was purified as previously described *(33)*. The MADH purity was indicated by the A_{280}/A_{440} absorption ratio equal to 6.7 for pure protein *(34)*.

Cytochrome c-550

Cytochrome *c*-550 was prepared as described in *(35)*.

Crystallization

Crystals of the binary complex of *P. versutus* MADH-amicyanin were obtained by the hanging drop method. Two µl of protein solution (9.0 mg/ml MADH and 2.3 mg/ml amicyanin in 0.1 M phosphate buffer pH 6.5) were mixed with 2 µl of reservoir solution (28-29.5% PEG 8000, 0.2 M Li_2SO_4, 0.1 M phosphate, pH 6.5) and allowed to equilibrate at room temperature. The components of the crystallization medium of this binary complex are totally different from those used to crystallize the corresponding binary complex from *P. denitrificans (10)* in particular with respect to the use of PEG instead of a high phosphate concentration.

Structure determination

Crystals of the *P. versutus* MADH/amicyanin complex belonged to the orthorhombic space group $P2_12_12_1$ with unit cell dimensions of a = 55.6 Å, b = 131.0 Å and c = 171.7 Å with one complete complex per asymmetric unit at a solvent content of 36%. Diffraction data to 2.5 Å resolution were collected on beamline BW7B at EMBL/DESY, Hamburg, Germany, and integration and scaling were carried out using the HKL package *(36)*. Phase information was obtained by Molecular Replacement with MOLREP *(37)*, using the coordinates of MADH from *P. denitrificans* (PDB ID 2BBK *(3)*) and amicyanin from *P. versutus* (PDB ID 1ID2 *(7)*) as a search model. Additional model building was done in O *(38)* and Coot *(39)* and CNS *(40)* was used for refinement (table 1).

Table 1. Crystal structure statistics

Wavelength	0.8414 Å
Space group	$P2_12_12_1$
Unit cell dimensions	**a** = 55.6 Å; **b** = 131.0 Å; **c** = 171.7 Å
	α = **β** = **γ** = 90°
Resolution limits (last shell)	50.0 Å - 2.5 Å (2.6 Å - 2.5 Å)
Independent reflections	37332 (3897)
Completeness	84.1 % (80.9 %)
I / σ(I)	6.51 (2.25)
R_{merge}	0.143 (0.449)
$R_{p.i.m.}$*	0.069 (0.224)
R_{free}	0.283
R_{work}	0.235
r.m.s.d. in bond distances	0.012 Å
r.m.s.d. in bond angles	1.681°

Data collection and refinement statistics. Values in brackets are for the highest resolution shell.

* $R_{p.i.m.}$ according to Weiss and Hilgenfeld *(41)*.

Kinetic experiments

Measurements of intermolecular electron transfer

The two-electron reduction of MADH was achieved by exposing the enzyme either to a threefold molar excess of methylamine or to 2 mM dithionite. Excess reagent was removed by repeated ultrafiltration on Centricon-30 and complete reduction was confirmed by the characteristic absorption spectrum of the coenzyme *(42)*.

The kinetics of electron transfer between MADH and amicyanin was investigated by rapidly mixing a solution containing 1 µM reduced MADH (heterotetramer) with a solution containing increasing concentrations of oxidized amicyanin in the range 10-150 µM in a stopped-flow apparatus. The reduction of amicyanin by methylamine-reduced MADH was studied either in 10 mM potassium phosphate buffer, pH 7.5, containing 0.2 M KCl, or in 10 mM HEPES, adjusted to pH 7.5 with $Ca(OH)_2$. The reaction of amicyanin with dithionite-reduced MADH was performed in 10 mM potassium phosphate buffer, pH 7.5.

Spectral changes due to formation of the TTQ semiquinone were measured at 443 nm. At this isosbestic point in the spectra of the semiquinone and the oxidized states of TTQ the observed signal reflected only the conversion of the aminoquinol to the semiquinone state *(5)*. The molar extinction coefficient difference $\Delta\varepsilon$ = 26200 $M^{-1}cm^{-1}$ was used *(4)*. The time courses of the reaction in the temperature range 277-310 K were fitted to single exponential curves and k_{obs} were determined.

By assuming the same model *(43)* that was previously chosen to describe electron transfer between MADH and amicyanin from *P. denitrificans* *(5,44)*

$$MADH_{red} + amicyanin_{ox} \overset{K_d}{\rightleftarrows} MADH_{red} / amicyanin_{ox} \qquad (1)$$

$$MADH_{red} / amicyanin_{ox} \underset{k_4}{\overset{k_{ET}}{\rightleftarrows}} MADH_{sq} / amicyanin_{red} \qquad (2)$$

the equilibrium dissociation constant K_d for reaction (1) and k_{ET} for reaction (2) were determined by fitting the experimental data to equation (3); k_4 turned out to be very small (close to 0)

$$k_{obs} = \frac{k_{ET}[amicyanin]}{[amicyanin] + K_d} + k_4 \qquad (3)$$

The electron transfer parameters H_{AB} and λ were calculated by fitting the values of k_{ET} determined at different temperatures to the Marcus equation (4). The decay coefficient β, defined in equation 5, resulted from the fitting of the data.

$$k_{ET} = \frac{4\pi^2 H_{AB}^2}{h\sqrt{4\pi R\lambda T}} e^{-\frac{(\Delta G^0 - \lambda)^2}{4\lambda RT}} \qquad (4)$$

$$k_{ET} = 10^{13} e^{-\beta(r - r_o)} e^{-\frac{(\Delta G^0 - \lambda)^2}{4\lambda RT}} \qquad (5)$$

where $\Delta G°$, r and r_0 are, respectively, the driving force determined from the redox potential difference for the et reaction, the donor to acceptor distance and the close contact distance (3 Å). R is the universal gas constant and T the absolute temperature.

Electron transfer in the crystal

Single crystal polarized absorption spectra were recorded using a Zeiss MPM 800 microspectrophotometer. Crystals were oriented with the principal optical directions parallel to the electric vector of the incident light, as previously described *(17,45)*. A single crystal was placed in a flow cell with quartz windows, in the presence of either its mother liquor or a replacing medium containing 0.5 mM methylamine. Reduction of TTQ was complete before the beginning of the spectrophotometric measurements. The pH dependence of electron distribution between the two redox centers was investigated by replacing the crystal surrounding medium with a new one at different pH.

NMR spectroscopy

For the assignment of the backbone amide resonances of reduced Cu amicyanin, HNCACB *(22)*, HNCO *(23)*, HN(CA)CO *(24)*, CC(CO)NH *(25)* and [^{15}N-^{1}H] HSQC spectra were acquired at 300 K on a Bruker Avance DMX 600 MHz NMR spectrometer equipped with a TCI-Z-GRAD ATM cryo-probe using a 2.5 mM ^{13}C,^{15}N labelled sample of amicyanin, in 10 mM potassium phosphate, pH 6.8, 1 mM sodium ascorbate and containing 6% D_2O for lock. Zn-substituted amicyanin was assigned on the basis of NOESY-[^{15}N-^{1}H] HSQC and TOCSY-[^{15}N-^{1}H] HSQC spectra on a 1.0 mM ^{15}N labelled sample in the same buffer, but in the absence of ascorbate. These data were acquired using a TXI-Z-GRAD probe on the same spectrometer.
Chemical shift perturbation experiments were performed at 300 K on a Bruker DSX 750 MHz spectrometer. To study the interaction of amicyanin with MADH have been used 0.20−0.25 mM samples of ^{2}H-^{15}N labelled amicyanin in 20 mM potassium phosphate pH 8.1, 1 mM methylamine, 1 mM sodium ascorbate and 6% D_2O, to which aliquots of a concentrated stock of methylamine-reduced MADH were added. While, to study the interaction with cytochrome *c*-550 small aliquots of this protein were added to a 0.20−0.25 mM samples of ^{15}N labelled amicyanin or binary complex of MADH and ^{2}H-^{15}N labelled amicyanin. TROSY *(21)* spectra were acquired for 40 min−4 h, depending on the concentration of the protein added (MADH or cytochrome *c*-550). In the indirect dimension 80 complex points were acquired.

NMR data analysis

NMR data were processed using AZARA (http://www.bio.cam.ac.uk/azara/). Backbone assignment of Cu(I)-amicyanin was performed using the semi-automated procedure in Ansig-for-Windows *(46)*. All non-proline residues were assigned except for Asn55 for which no signals were observed. Amides in Zn-substituted amicyanin were assigned by comparison with Cu(I)-amicyanin and confirmed by analysis of the NOESY-[^{15}N-^{1}H] HSQC and TOCSY-[^{15}N-^{1}H] HSQC spectra. TROSY spectra were compared using Ansig-for-Windows. Amicyanin resonances of the bound form could be assigned by comparison with the free form, except for several residues in the Zn-substituted form, which had shifted much. For these a minimum perturbation was determined on the basis of the closest unassigned peak in the bound form. These were residues Val51, Val63, His96, Phe98, and Met 99. For the assigned residues,

the perturbation was quantified as $\Delta\delta_{avg} = (½(\Delta\delta N^2/25 + \Delta\delta H^2))^{0.5}$, where $\Delta\delta N$ and $\Delta\delta H$ are the chemical shift changes of ^{15}N and ^{1}H nuclei upon binding. Annotated HSQC spectra for Cu(I) and Zn amicyanin are shown in figure 1 and 2 respectively, while the assignments and perturbations tables are shown in Appendix A.

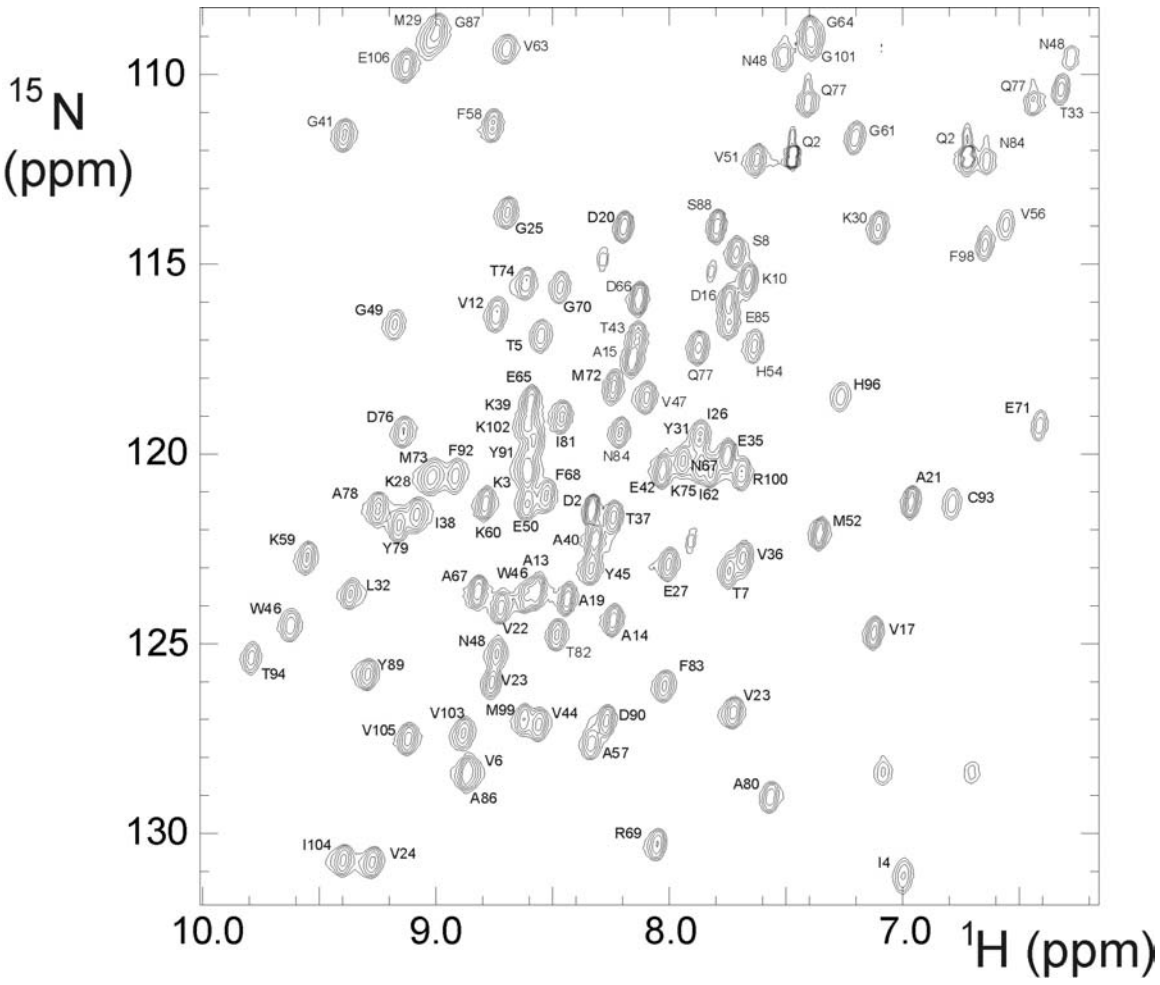

Figure 1. Annotated ^{15}N-HSQC spectrum of *P. versutus* Cu(I)-amicyanin

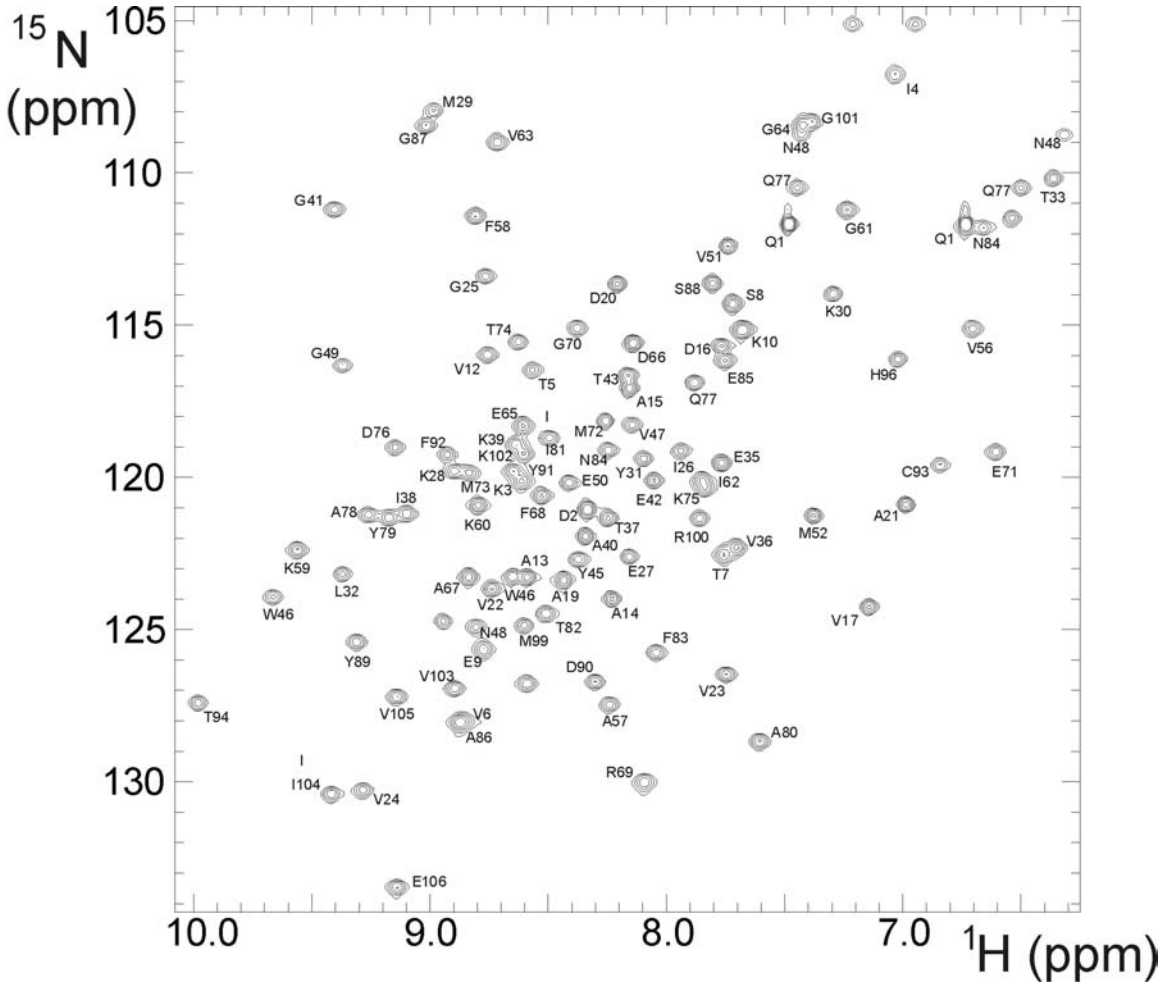

Figure 2. Annotated ^{15}N-HSQC spectrum of *P. versutus* Zn-substitute amicyanin

RESULTS

Description of the structure

The structure of *P. versutus* MADH has been reported previously *(26,47)* and it remains largely unchanged when forming an electron transfer complex with amicyanin (figure 3). The enzyme forms a compact $\alpha_2\beta_2$ heterotetramer consisting of a heavy (395 aa, 43.3 kDa) and a light peptide chain (131 aa, 14.2 kDa). The heavy (H) chain folds into a characteristic, seven-bladed β–propeller domain and contains an N-terminal extension (residues 1-80) that extends around the neighbouring light (L) chain, fixing it to the tetrameric enzyme. It does not contain cofactors and none of its residues is immediately involved in catalysis, but due to its rigid structure it forms a base for the smaller – but catalytically active – light chain. The L subunit consists mainly of loop regions with only four β-strands, stabilized by a total of six disulfide bridges. The active site of the enzyme is a tryptophan tryptophyl quinone moiety formed by Trp57, covalently linked to Trp108 (figure 4).

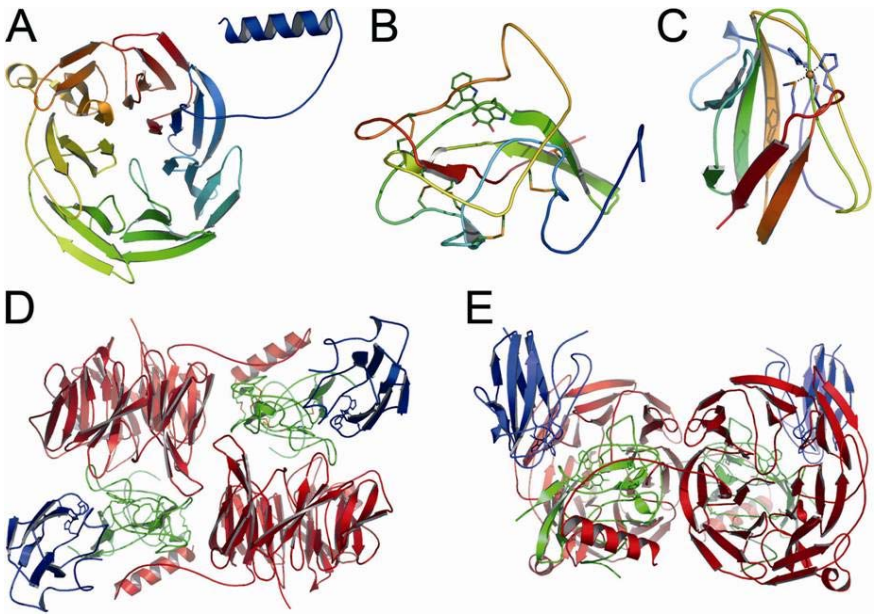

Figure 3 **A)** The large subunit of MADH; **B)** the small subunit of MADH; **C)** amicyanin, a type I copper protein with the typical cupredoxin fold; **D)** structure of the MADH/amicyanin complex, with in red and green the the H and L subunits of MADH respectively and in blue the amicyanin molecules; **E)** view of the complex rotated by 90 degrees towards the viewer in respect to D).

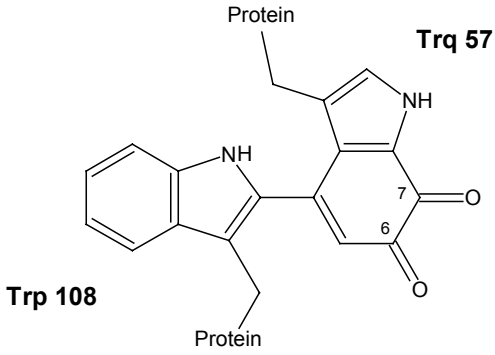

Figure 4. Tryptophan tryptophylquinone (TTQ), the cofactor of MADH

In the electron transfer complex, amicyanin (Ami, 106 aa, 11.7 kDa) interacts with MADH close to the interface of the L- and H-subunit. A water molecule (W90) is located close to the N_{ε} atom of His96 of amicyanin and hydrogen bonded to the carbonyl oxygen of Ser56, next to the tryptophylquinone moiety in the adjacent L-subunit. It is observed only close to one of the two amicyanin molecules bound to MADH, yet it suggests an obvious and direct path for electron transfer (Trp57 – Ser56 O - W90 - His96 - Cu). An analogous water molecule had not been modelled in the original structure of the *P. denitrificans* binary complex *(10)* but it was in subsequent higher resolution structures of the ternary complex. The same path across a water molecule (W56) was described in the structure of the ternary complex *(14)* and was reported to be three times more efficient than an alternative pathway involving a through-space jump from the indole ring of Trp107 ($C_{\eta 2}$) to the backbone oxygen atom of Pro94 *(48)*. The former pathway depends on the presence of the bridging water, but it seems geometrically more feasible than the latter pathway, where the indole proton of $C_{\eta 2}$ of Trp107 is not directed towards the amide oxygen of Pro94.

Access for substrate to the active site of the enzyme is possible on the opposite side of the L-subunit, where a substrate channel at the interface of L and H leads directly to the quinone site on Trp57.

Intermolecular electron transfer

The rate of electron transfer (k_{ET}) in the *P. versutus* binary complex was determined for substrate-reduced MADH, both in the presence and in the absence of monovalent cations, and for dithionite-reduced MADH, in the presence of monovalent cations. The dependence of the rate of electron transfer on temperature was analyzed to investigate the nature of the rate-limiting step and establish whether it is an adiabatic or a non-adiabatic process (Figure 5).

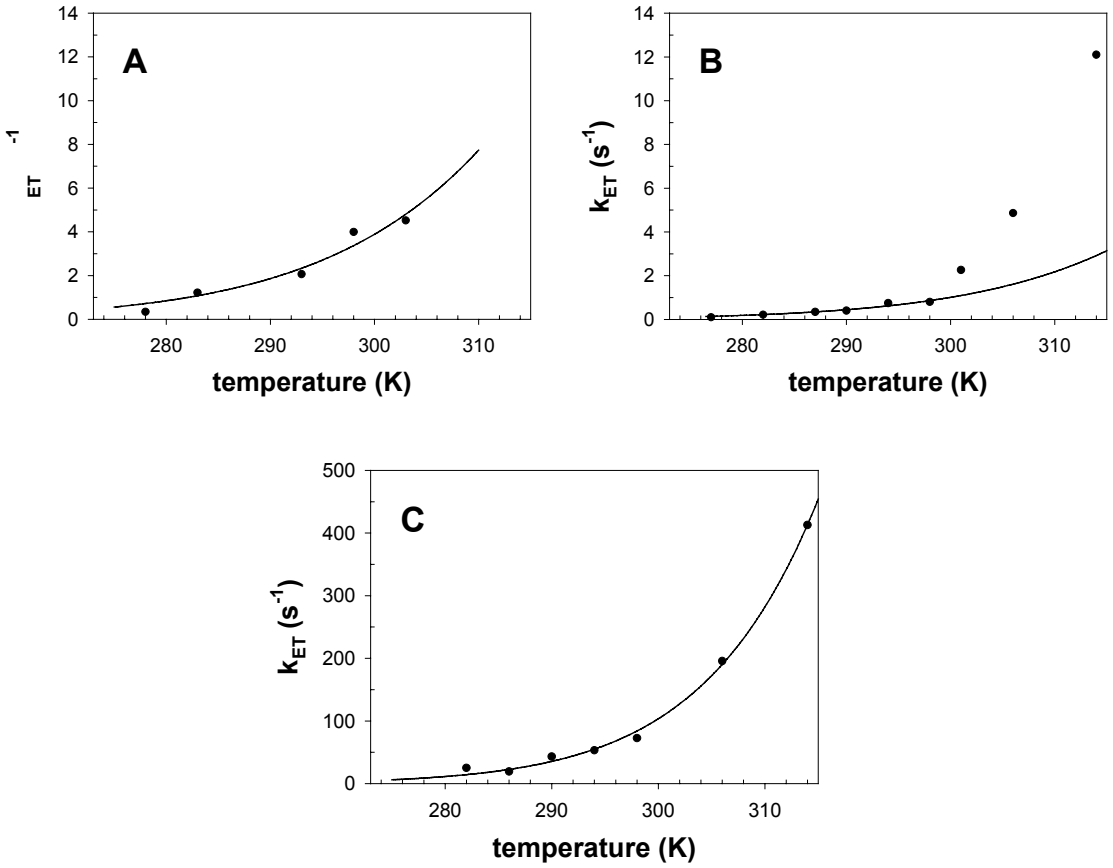

Figure 5. Temperature dependence of the electron transfer rates from reduced MADH to amicyanin. **A)** Dithionite-reduced MADH in 0.01 M phosphate, pH 7.5. **B)** Methylamine-reduced MADH in 0.01 M Ca-HEPES, pH 7.5. **C)** Methylamine-reduced MADH in 0.01 M phosphate, pH 7.5, + 0.2 M KCl. Solid line represents the fitting to equation (4). In panel B only points below 300 K fit to the equation. The et parameters resulting from the fitting are reported in table 2.

The value of the strength of the coupling factor H_{AB} calculated for electron-transfer from dithionite-reduced MADH to amicyanin (8.5 cm^{-1}) is indicative of a true electron transfer and the value of the reorganization energy λ = 2.4 eV is the same as reported for the *P. denitrificans* system *(5)*. Similarly, the reaction of methylamine-reduced MADH in the absence of monovalent cations appears to be a true electron transfer, in the temperature range 277-300 K, with et parameters close to those calculated for dithionite-reduced MADH (H_{AB} = 15.6 cm^{-1}, λ = 2.7 eV). However, at temperatures above 300 K, a drastic increase of the rate is observed and the process cannot be described as non-adiabatic electron transfer.

The analysis of the temperature dependence of the rate constant for the reaction of substrate-reduced MADH with amicyanin in the presence of monovalent cations produced parameters evidencing the adiabatic nature of this process. This is consistent with a possible role of the activation mechanism in the kinetic separation of the two electrons to be transferred, one at a time, to the one-electron carrier reversibly bound to the dehydrogenase.

From equation (5), assuming the distance of 9.3 Å between the TTQ edge ($C^{\eta 2}$) close to the surface of the protein and the copper ion of amicyanin, as determined in the crystal structure, a decay coefficient β of 0.94 and 1.1 $Å^{-1}$ is calculated from the et rates, in the methylamine-reduced (in the absence of ions) and the dithionite-reduced system, respectively, in agreement with the values observed in a large number of other proteins with β structure *(49)*.

The dissociation constant of the complex $MADH_{red}$/$amicyanin_{ox}$ calculated according to equation (3) is in the micromolar range and is only slightly affected by the presence of KCl (Table 2).

Table 2. Electron transfer parameters and dissociation constant for the reaction of reduced MADH and amicyanin.

	dithionite-reduced MADH	**methylamine reduced-MADH**	
Buffer	phosphate (10 mM)	Ca-HEPES (10 mM)	0.2 M KCl
H_{AB} (cm^{-1})	8.5	15.5	[6100]
H_{AB} (KJ/mol)	102	185	
λ (eV)	2.40	2.6	[3.4]
λ (KJ/mol)	231	251	
β * ($Å^{-1}$)	1.1	0.94	[-1]
K_d (µM)	7.3	2.7	12

* β is calculated on the basis of the distance observed in the crystal 9.4 A

In the crystal, MADH is reduced by the methylamine present in the surrounding medium. The rate is likely to be diffusion-limited but still too fast to be measured. In fact, within the time of spectrophotometric observation, the methylamine derived electrons distribute between TTQ and the amicyanin copper. As in the case of the *P. denitrificans* binary complex *(19)*, the reversible distribution of electrons is pH dependent, with a higher proportion of reduced copper as pH increases. This is shown by the single crystal polarized spectra reported in figure 6. With increasing pH, the absorption of the reduced TTQ at 330 nm decreases with the concomitant increase of the absorption of the semiquinone form at 425 nm, indicative of electron transfer to the copper.

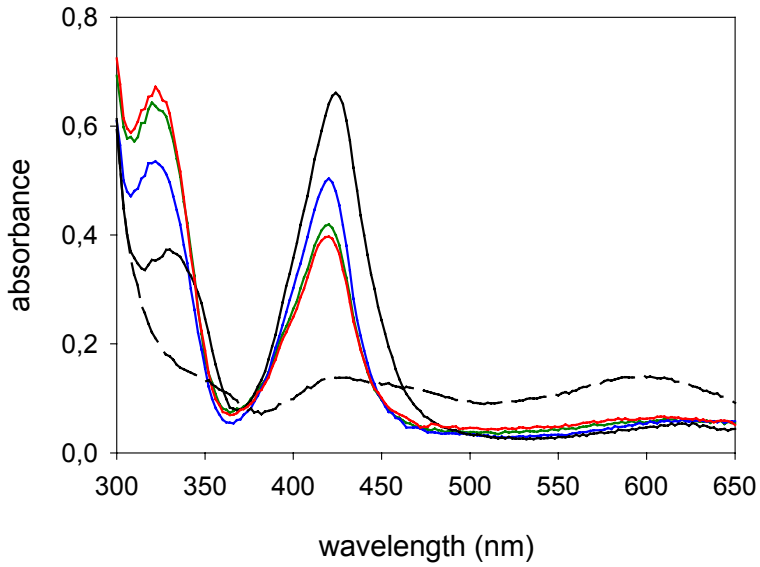

Figure 6. Single crystal polarized absorption spectra of the amicyanin-MADH complex before (dashed line) and after (continuous lines) reaction with methylamine at pH 6.5 (red), 7.0 (green), 7.5 (blue) and 9.5 (black).

Chemical shift perturbation analysis

MADH-amicyanin binary complex

To study the complex of MADH and amicyanin in both redox states, Zn(II) amicyanin used as a mimic for Cu(II) amicyanin. Cu(II) is paramagnetic, resulting in extensive broadening of resonances of many nuclei around the metal. It has been shown that metal substitution in blue copper proteins only affects the position of the ligand side-chains and otherwise has very few structural effects. The rmsd of cobalt and copper amicyanin structures (PDB entries 1TK5 *(50)* and 2OV0, respectively) is 0.55 Å rmsd for the backbone atoms. For Zn(II) forms of azurin *(51)* and pseudoazurin *(32)* similar results were found.

To investigate its binding site to MADH in solution, amicyanin was enriched in ^{15}N, as well as ^{2}H for all non-exchangeable protons. It is well established that in perdeuterated proteins dipolar relaxation of the amide protons is strongly reduced, leading to sharp signals in the [^{15}N-^{1}H] HSQC spectrum. In combination with TROSY-type experiments *(21)*, this approach allows the observation of amicyanin amide resonances in the complex with MADH (figure 7A,B). Upon titration with MADH numerous resonances of amicyanin decrease in intensity and new resonances appear at 1.0 mol. eq. of MADH protomers. For resonances with small perturbations, shifting signals were observed. It can be concluded that the exchange rate is slow-intermediate for most signals. The off-rate is estimated to be on the order of 250 s^{-1}.

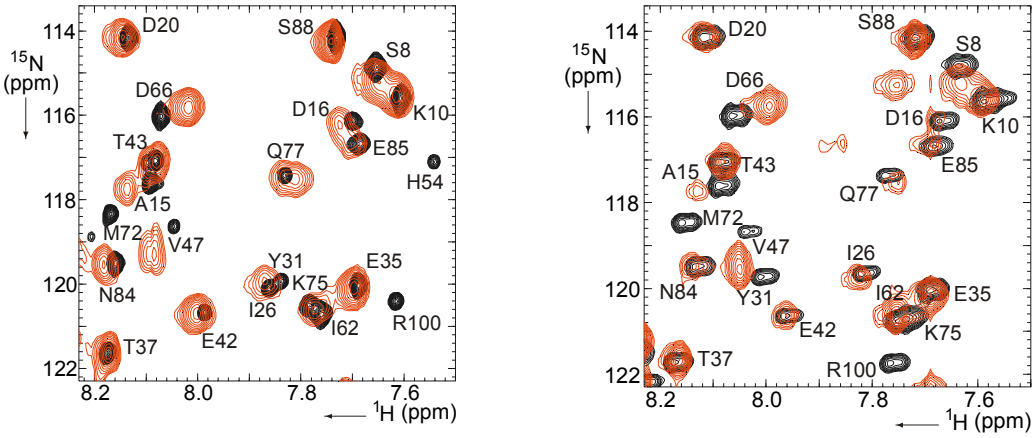

Figure 7. Regions of the TROSY spectra of Cu(I) amicyanin (**A**) and Zn(II) amicyanin (**B**), free (black contours) and bound to MADH (red contours). The amicyanin-MADH protomer ratio was 1:5 in (A) and 1:3 in (B).

A clear difference was observed between the titration performed with Cu(I) amicyanin and Zn(II) substituted amicyanin. In the case of Cu(I) amicyanin, nineteen resonances of amides close to the copper site disappeared upon addition of MADH without new resonances appearing. With Zn(II) amicyanin, the number of new peaks was equivalent to that of the signals that disappeared. This suggests that in the case of Cu(I) amicyanin an exchange process takes place within the complex, leading to broadening of the resonances of amides close the copper. The possible reason for this behaviour will be discussed later.

The formation of the complex has large effects on the chemical shifts of the amides. Figure 8 presents the $\Delta\delta_{avg}$ values for all observed residues in Cu(I) and Zn amicyanin bound to MADH and in the figure 9 these $\Delta\delta_{avg}$ values have been mapped onto the surface representation of amicyanin using the color code indicated by the vertical bar on the right in the figure 8. In the spectra of the complex of MADH with Zn(II) amicyanin, most peaks could be assigned by comparison of the free and bound forms. Five resonances of amides in the hydrophobic patch show such large chemical shift changes that they could not be assigned. However, they could be classified as ‘large perturbation’ and are shown in red in figure 9B. The predominant effects are at the hydrophobic patch, surrounding the exposed copper ligand His96 with lesser effects observed around the positive patch located around Lys60. These regions can be identified as the interface for binding. Considerable perturbations are also observed on the other side of the protein. Many of these amides are buried, suggesting that these are secondary effects, caused by small structural changes inside the protein upon binding. This is confirmed by the crystal structure of the complex (see below). Except for the perturbation observed for Arg69 in Zn(II) amicyanin, the effects of binding are similar for the Cu(I) and Zn(II) amicyanin.

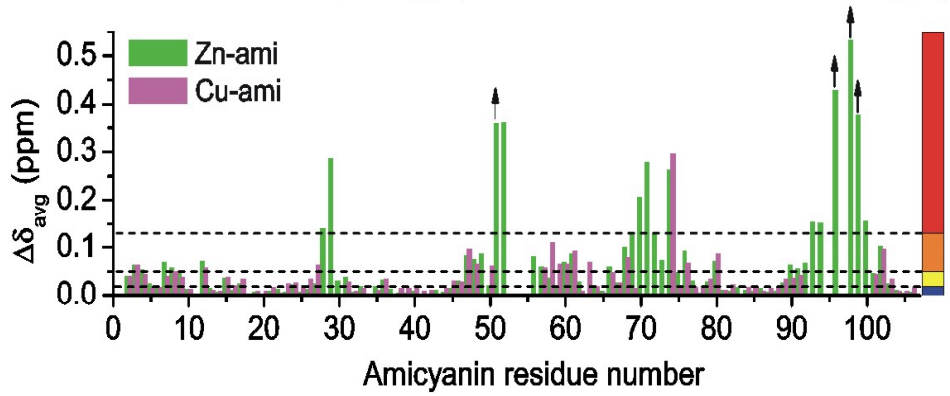

Figure 8. The $\Delta\delta_{avg}$ values are shown for all observed residues in Cu (magenta bars) and Zn (green bars) amicyanin. The arrows indicate residues for which only a minimum shift could be determined (see Material and Methods).

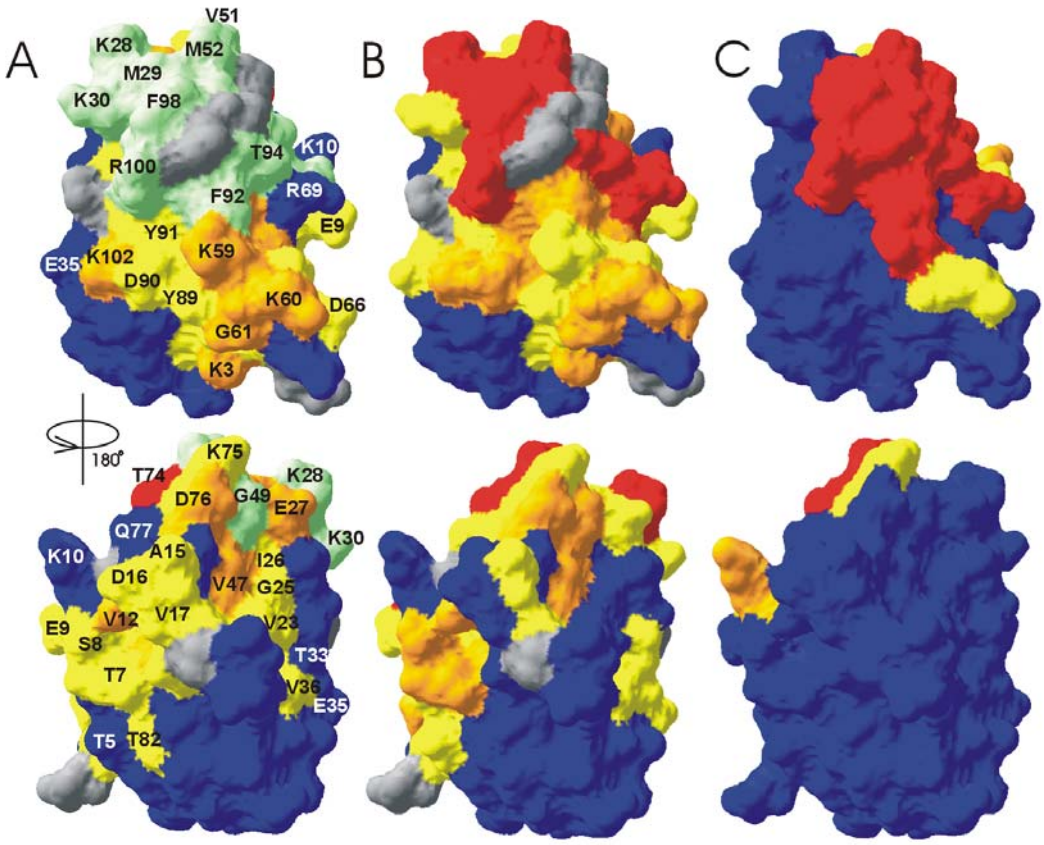

Figure 9. Maps of the chemical shift perturbations on the structure of amicyanin in the complex, with the results for Cu(I) and Zn(II) amicyanin shown in panels **A** and **B**, respectively. The unassigned residues and prolines are in grey and in panel A the missing residues are coloured in green. In panel **C** the residues of amicyanin have been colored according to the distance from MADH in the crystal structure of the complex, with residues with atoms within 4, 5 and 6 Å from MADH in red, orange and yellow, respectively and other residues in blue.

Interaction with cytochrome c-550

To study the interaction between amicyanin and its possible redox partner in the *P.versutus* respiratory chain, cytochrome *c*-550, two experiments were performed. The first one was the titration of the binary complex (MADH/Cu(I)-amicyanin) and the second one was the titration of the free uncomplexed Cu(I)-amicyanin with cytochrome *c*-550. For the experiment on free amicyanin the ^{15}N form of this protein was used, while in the case of the binary complex the double-labelled ^{15}N-^{2}H form of amicyanin was used because the perdeuteration strongly reduces the dipolar relaxation of amide, leading to sharper signals. So it becomes possible to observe the amicyanin signals in the TROSY spectra also when the protein is in complex with the large enzyme, MADH.

In both experiments, small aliquots of a concentrated (1.6 mM) stock of cytochrome *c*-550 were added to a 0.2-0.25 mM sample of either the free Cu(I)-amicyanin or the binary complex, until a final ratio of 2:1 molar equivalents of cytochrome were added and no perturbations in the amicyanin signals were observed. These results suggest that cytchrome *c*-550 is not the physiological partner of amicyanin in this bacteria.

DISCUSSION

The MADH/amicyanin complexes of *P. denitrificans* and *P. versutus* are similar, with an overall root-mean-square deviation (rmsd) of 1.0 Å for all corresponding atoms in the crystal structures of the complexes. This finding, together with the competence in electron transfer, clearly indicates that in both cases a functional complex – and not merely a co-crystal – has been described. The structural resemblance is consistent with the similarity of the et rates and the role of monovalent cations in the oxidation of methylamine-reduced MADH in solution. The lower efficiency in the ion activation agrees with the higher dissociation constants for ions reported for *P. versutus* MADH (34). These findings suggest that the subtle changes occurring within amicyanin upon its association with MADH, revealed by the new NMR data on the *P. versutus* complex, are likely to be a general feature of these systems.

The behaviour of several resonances of amicyanin upon complex formation with MADH indicate that the dissociation rate constant for oxidized amicyanin is about 250 s^{-1}, enabling a fast turn-over of the enzyme, with the lifetime of the complex being 4 ms. Notwithstanding the transient nature of the complex, it is likely that MADH spends most time in the bound state, given the K_d in the low μM range *(6)* and the high protein concentrations in the periplasm.

Disappearance of signals in the Cu(I) amicyanin

Complex formation of Cu amicyanin with MADH results in the loss of signals from residues close to the copper. This is not observed for Zn-substituted amicyanin, suggesting that broadening of the signals is due to a process that can occur only in the Cu amicyanin. Two possibilities are considered.

First, a small fraction of Cu(II) amicyanin could cause extensive linebroadening due to paramagnetic relaxation, provided electron exchange within as well as between the MADH-amicyanin complexes is sufficiently fast. Only in this case, all amicyanin molecules will experience the broadening effect. Although the samples contained 1 mM methylamine and 1 mM sodium ascorbate to create a reducing environment, it is possible that during the long experiments the sample did not remain anaerobic. However, given the low rate constant values measured at low concentrations of monovalent ions, intra-complex et is likely to be too slow in the NMR samples to result in linebroadening.

Second, slow flipping of the His96 ring in the complex could lead to intermediate exchange of the amides surrounding the copper site. His96 is known to protonate and flip around pH 7 in free amicyanin and has been reported not to protonate in the complex between amicyanin and MADH from *P. denitrificans* due to steric hindrance observed in the crystal *(52)*. It cannot be excluded, however, that protonation and flipping occurs in the complex in solution, leading to exchange broadening.
For Zn amicyanin the line broadening is not observed. This result does not allow to distinguish between the two explanations, because Zn-ami neither is redox active, nor is expected to exhibit protonation of His96.

Comparison between solution and crystal state complexes

The chemical shift perturbations observed for amicyanin can be analysed by comparison with the crystal structure of the complex. The most strongly affected residues are centered around Phe98 (figure 9 A-B), suggesting that this area of the amicyanin surface is part of the interface. This is in accordance with the crystal structure, as can be seen in figure 9C, which shows the residues that are part of the interface of the complex in red. It has been shown that mutagenesis of the equivalent Phe in the *P. denitrificans* complex has a large effect on the et rate, which was attributed to reduced electronic coupling between the redox sites *(48)*.
The area of residues exhibiting chemical shift perturbations is, however, noticeably larger, involving the positive patch around Lys60 and numerous residues at the back of amicyanin. Two explanations have been provided to account for large areas of perturbations observed for electron transfer complexes. First, the effects can be caused by small structural changes in the interface area that result in carry-on effects due to slight movements in secondary structure elements or changes in hydrogen bond networks (secondary perturbations). Second, the extended area can indicate that the complex in solution comprises a dynamic state as well as a well-defined state. In the dynamic state other areas of the protein make contact with the partner, causing additional chemical shift perturbations, as observed for other proteins *(53,54)*. Although it is not straightforward to differentiate between the two possibilities, it is expected that a dynamic state affects surface residues, while the secondary perturbations can affect also residues in the interior of the protein. Highly dynamic

protein complexes show small $\Delta\delta_{avg}$ values, compared to well-defined complexes *(55,56)*.

In the complex with MADH, amicyanin shows large $\Delta\delta_{avg}$ values, suggesting that the complex is mostly well-defined. This idea is supported by the fact that amicyanin is ordered in the crystal structure of the complex. Many perturbed amides are buried. Thus, it seems most likely that the extensive perturbations are of a secondary nature. The crystal structure offers the opportunity to check for structural changes involving residues with perturbed amides. The average rmsd for backbone atoms between free (PDB entry 1ID2 *(7)*) and MADH-bound amicyanin is 0.54 (±0.06) Å (figure 10). This value and those given below represent the average (± SD) over the three amicyanin molecules found in the asymmetric unit of the structure in entry 1ID2, which was solved at 2.15 Å resolution. In the interface the biggest differences are observed for the ligand loops, with 0.6 (±0.1) and 1.0 (±0.1 Å displacements for the carbonyl oxygens of Phe98 and Val51, respectively.

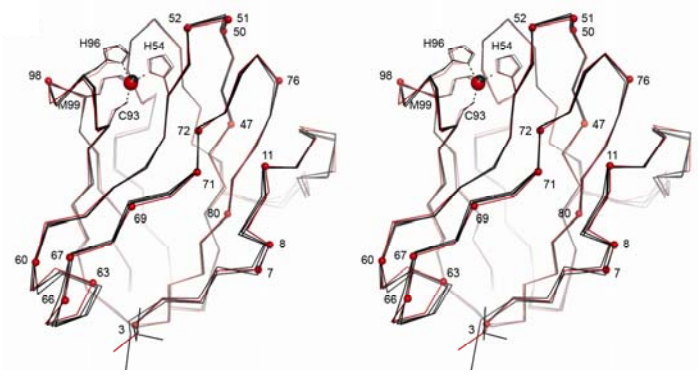

Figure 10. Stereo view of a superimposition of *P. versutus* amicyanin from the complex with MADH (red) with the three copies in the asymmetric unit of unbound amicyanin crystals (black, PDB 1ID2).

The perturbations of residues 47-50 and 76 (figure 11B) may be a consequence of changes around Val51, because of the hydrogen bond network that connects the buried Asn48 with Met52, Glu50 and Asp76.

Significant is the displacement of the β-strand that runs down from the interface −in N-terminal direction− from Met72 to Ala67 (figure 11A). Arg69 in this strand is involved in complex formation with MADH and may be the cause of the observed distortion. Also the loop from Asp66 to Lys60 has moved. The distance between the carbonyl oxygen of Val63 and the amide nitrogen of Lys3 has increased from 2.9 (±0.2) to 3.8 Å, thus disrupting the hydrogen bond that connects the loop to the N-

terminal residues (figure 11C). These effects may be attributed to interactions of Arg69 with MADH and they explain that perturbations are observed for the residues in this β-strand and residues 3 and 4, located far from the interface. Also the relatively mobile loop of residues 7-11 appears to have assumed a different average structure, perhaps because it is connected to Glu71 via ordered water molecules. This is in line with the perturbations observed for Thr7 and Ser8, as well as Ala80, which is connected via another water molecule to Ser8. This water (HOH numbers 104, 146 and 141 in the three chains in 1ID2 and HOH160 in chain A of the structure of the complex) moves by about 1 Å upon complex formation, increasing the distance to the carbonyl of Ser8 from 2.43 (±0.04) to 3.2 Å (figure 11D). This water is buried and more than 14 Å away from the nearest atom of MADH. It is observed in all chains of the free amicyanin, but only in the A chain of the bound protein. These results illustrate that complex formation leads to subtle structural changes deep inside amicyanin. The chemical shift differences observed for buried amides can clearly be correlated to such changes, in particular to changes in hydrogen bond networks.

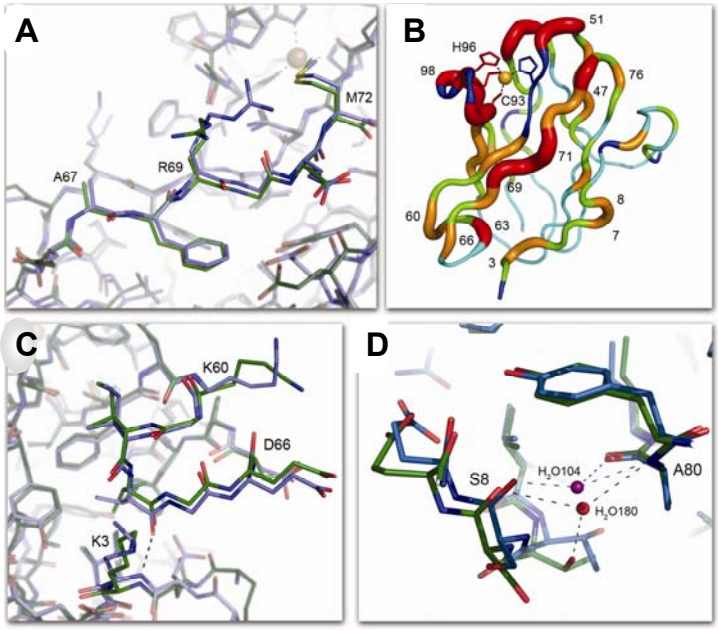

Figure 11. **A**) Detail view of the β-strand from residues 67 to 72 with free amicyanin in blue and the protein from the MADH complex in green. **B)** Backbone trace of amicyanin with tube width and color coding according to the $\Delta\delta_{avg}$ value of the amide groups; cyan, $\Delta\delta_{avg}$ < 0.02 ppm, green, $\Delta\delta_{avg}$ < 0.05 ppm, yellow $\Delta\delta_{avg}$ < 0.13 ppm, red $\Delta\delta_{avg}$ > 0.13 ppm, blue, no data. **C)** Detail view of the loop region from residues 60 to 66. In the complex with MADH, this loop (green) adopts a conformation that disrupts a backbone hydrogen bond from Val 63 to Lys 3. **D)** Detail view of area around Ser 8, showing the displacement of a buried water molecule in the bound form of amicyanin (green; water molecule labeled as H_2O180).

CHAPTER 4

NMR studies on protein- protein complexes from *Paracoccus denitrificans*

INTRODUCTION AND AIM OF THE WORK

Many structural and kinetic studies have been performed on the proteins of the *Paracoccus denitrificans* respiratory chain. The crystal structures of MADH *(3)* and amicyanin *(57)* have been solved, as well has those of their binary complex *(10)* and of the ternary complex that these two proteins form with cytochrome *c*-551 *(12)*. Cytochrome *c*-551 is supposed to be the physiological carrier of electrons from amicyanin to the membrane acceptor. In the crystal of the ternary complex, electrons are transferred from the methylamine-reduced MADH to the heme of the cytochrome via amicyanin *(17)*. The ternary complex is assumed to exist in solution on the basis of the results of many kinetic experiments *(15,58)*. Nevertheless, no NMR studies have been performed until now to investigate this system in solution. In the present work the complete assignments of amides resonances of amicyanin in both its redox states have been performed, using Zn(II) as a mimic for Cu(II) because the latter is paramagnetic and this property causes an extensive broadening of resonances of nuclei around the metal. It has been shown that metal substitution in blue copper proteins only affects the position of the ligand side-chains and, otherwise, has very few structural effects *(32,51)*. By perdeuteration and labelling with ^{15}N, which enable selective observation of amicyanin in the complex, it has been possible to characterize the recognition surfaces of amicyanin in the binary complexes with MADH and with cytochrome *c*-551i. Similar studies have been performed to investigate the interaction of the MADH-amicyanin binary complex with cytochrome *c*-551i, with the aim to test whether confirm the ternary complex exists in solution as well as in the crystal.

EXPERIMENTAL PROCEDURES

Proteins production and purification

Amicyanin

Escherichia coli BL21 cells were transformed with the plasmid pET28a-ami and cultured at 37 °C in LB medium containing 50 mg/L kanamycin (Sigma-Aldrich, St. Louis, MO). Expression was induced by adding 1 mM isopropyl-β-galactoside when OD_{600}=0.7. After 16 hours, the cells were harvested by centrifugation at 6000 rpm for 20 minutes. Cells were lysed by sonication after adding DNase (Sigma-Aldrich, St. Louis, MO) and 0.5 mM phenylmethanesulphonylfluoride (Sigma-Aldrich, St. Louis, MO). In the presence of about 20 μM $CuSO_4$ to convert apo to holo-protein, $K_3Fe(CN)_6$ was slowly added in amounts sufficient to fully oxidize the bound metal. Holo-amicyanin was purified following the published procedure *(31)* with slight modifications. After sonication and centrifugation at 10000 rpm for 30 minutes, the supernatant was dialysed overnight in a 3500 MWCO dialysis tube against 2 L of 20 mM sodium phosphate buffer, pH 7, which was replaced twice. The supernatant was then loaded on a DEAE column equilibrated with 10 mM sodium phosphate, pH 7. The protein bound weakly to the column material and could be eluted with 10 mM sodium phsphate plus 150 mM sodium chloride buffer, pH 7, using a flow rate of 1.5 ml/min. The protein solution was then dialysed overnight in a 3500 MWCO dialysis tube against 2 L of 10 mM sodium phosphate buffer, pH 7, which was replaced twice. Then the protein solution was loaded on a Hi-Trap-Q column (CV=10 ml) in a FPLC machine; the column was equilibrated with 10 mM potassium phosphate buffer, pH 7.5 and the protein was eluted with 10 mM potassium phosphate plus 0.5 M sodium chloride buffer, pH 7.5, using a linear gradient (0-100%) and a flow rate of 3 ml/min. Then, the buffer of the protein solution was exchanged again by centrifugation in Centricon (MWCO=5000 Kda) at 4000 rpm; the final buffer was 10 mM potassium phosphate, pH 7.5. The resulting solution was loaded on a CM column equilibrated with 20 mM sodium phosphate buffer, pH 7. The protein was eluted with 20 mM sodium phosphate plus 0.5 M sodium chloride buffer, pH 7, using a linear gradient (0-100%) and a flow rate of 3 ml/min. Purity was checked by the A_{280}/A_{595} ratio (about 3 for pure protein). The yield was 60 mg/L (estimated from ε=4610 $M^{-1}cm^{-1}$ at 595 nm). ^{15}N-labelled protein was produced as above, but growing the cells at 30°C in M9 minimal medium supplemented with 1 g/L $^{15}NH_4Cl$; then, after induction the

temperature was lowed to 22°C. The protein yield after purification was about 25 mg/L. ^{15}N-^{13}C-amicyanin was produced in the same conditions described for the ^{15}N-labelled protein, but using 2 g/L of $^{13}C_6$-glucose (as the sole carbon source) with a yield of 30 mg/L of pure protein. A minimal medium with D_2O substituting H_2O and 5 g/L CD_3COONa as the sole carbon source was used to produce ^{15}N-^{2}H-amicyanin (yield after purification: about 15 mg/L). Due to possibly incomplete exchange of the amide protons it was only possible to establish that the deuteration level of non-exchangeable protons was high that 83%, on the basis of mass spectrometry.

Zn-replacement

Substitution of copper with zinc was performed as described *(32)*. To remove the unfolded protein, Zn-amicyanin was passed through an anionic exchange column (Source 30Q) equilibrated with 20 mM sodium phosphate, pH 7. The protein was eluted with 100 mM NaCl in the same buffer.

MADH and cytochrome c-551i

MADH and cytochrome *c*-551i from *P. denitrificans* were prepared as described in *(59)* and *(60)*, respectively.

NMR spectroscopy

For the assignment of the backbone amide resonances of reduced Cu-amicyanin, HNCACB *(22)*, HNCO *(23)*, HN(CA)CO *(24)*, CC(CO)NH *(25)* and [^{15}N-^{1}H] HSQC spectra were acquired at 300 K on a Bruker Avance DMX 600 MHz NMR spectrometer equipped with a TCI-Z-GRAD ATM cryo-probe using a 2.0 mM ^{13}C,^{15}N labelled sample of amicyanin, in 10 mM potassium phosphate, pH 6.8, 5 mM sodium ascorbate and containing 10% D_2O for lock. Zn-substituted amicyanin was assigned on the basis of NOESY-[^{15}N-^{1}H] HSQC and TOCSY-[^{15}N-^{1}H] HSQC spectra on a 1.2 mM ^{15}N labelled sample in 20 mM potassium phosphate, pH 7.9 and 6% of D_2O. These data were acquired using a TXI-Z-GRAD probe on the same spectrometer. The assignment of Zn-amicyanin bound to MADH was done on the basis of TROSY and NOESY-TROSY of 1.9 mM of free ^{15}N-^{2}H-Zn-amicyanin and 1.15 mM of ^{15}N-^{2}H-Zn-amicyanin in the presence of 1 molar equivalent of MADH. In both cases the buffer was 20 mM potassium phosphate, pH=7.8, 6% of D_2O and the spectra were acquired at 300 K on a Bruker Avance DMX 600 MHz NMR spectrometer equipped with a TCI-Z-GRAD ATM cryo-probe for the free amicyanin and on a Bruker Avance 900 MHz NMR spectrometer equipped with a cryo-probe system for the complex. Chemical shift perturbation experiments and all other experiments on the binary complex were performed at 300 K on the same 900 MHz machine.

To study the interaction of the binary complex with cytochrome *c*-551i, we used a 0.2 mM sample of ^{2}H-^{15}N labelled Zn-substituted amicyanin in the presence of 1 molar equivalent of oxidized MADH (amicyanin-MADH protomer ratio: 1:2) in 20 mM potassium phosphate, pH 8, 6% of D_2O, to which small aliquots of a concentrated stock of oxidized cytochrome *c*-551i were added up to 3.3 molar equivalents. The same experiment was repeated using sodium ascorbate-reduced MADH and cytochrome *c*-551i; in this case, 2 mM sodium ascorbate was added to the same buffer. TROSY *(21)* spectra were acquired for 3 h, and in the indirect dimension 80 complex points were acquired.

Also the interaction of free amicyanin with citochrome *c*-551i was studied. In these case, we used 0.2 mM ^{15}N labelled Cu(I)-amicyanin in 10 mM potassium phosphate, pH 6.8, 2 mM sodium ascorbate and 6% of D_2O, to which small aliquots of sodium ascorbate-reduced cytochrome *c*-551i in the same buffer were added up to 2.4 molar equivalents. The same experiment was performed on ^{15}N labelled Zn-substituted

amicyanin in the same buffer, but in the absence of ascorbate and using the oxidized form of cytochrome *c*-551i (up to 2.3 molar equivalents). Than, at the end of this experiment the cytochrome was reduced by adding of 1mM sodium ascorbate to the NMR sample. HSQC spectra were acquired on Bruker Avance DMX 600 MHz NMR spectrometer for 10-40 minutes, depending on the concentration of the protein added.

NMR data analysis

NMR data were processed using AZARA (http://www.bio.cam.ac.uk/azara/). Backbone assignment of Cu(I)-amicyanin was performed using the semi-automated procedure in Ansig-for-Windows *(46)*. All non-proline residues were assigned except for Asn54 for which no signals were observed. Amides in Zn-substituted amicyanin were assigned by comparison with Cu(I)-amicyanin and confirmed by analysis of the NOESY-[^{15}N-^{1}H] HSQC and TOCSY-[^{15}N-^{1}H] HSQC spectra. In this case four residues were not assigned: His53, Asn54, Phe57 and His95. TROSY spectra were compared using Ansig-for-Windows.

Amides resonances in the HSQC of amicyanin bound to cytochrome *c*-551i were assigned by comparison with the free form, except for the residue His36 in the Zn-substituted form, which is not assigned also in the HSQC of the free protein.

The signals in the TROSY spectra of the Zn-amicyanin were assigned by comparison with the previously assigned HSQC spectrum and, with respect to it, all residues were assigned except for Asp1 and Lys27, for which no signals were observed in the TROSY spectrum. The resonances in the TROSY spectrum of the Zn-amicyanin bound to MADH were assigned by comparison with the TROSY of the free form and, for the residues that shifted much, using the corresponding NOESY-TROSY spectra. For this bound form all residues were assigned except for Met51, Leu62, Thr93, Met98 and Arg99; for these residues a minimum perturbation was determined on the basis of the closest unassigned peak in the bound form.

For the assigned residues, the perturbation was quantified as $\Delta\delta_{avg} = (½(\Delta\delta N^2/25 + \Delta\delta H^2))^{0.5}$, where $\Delta\delta N$ and $\Delta\delta H$ are the chemical shift changes of ^{15}N and ^{1}H nuclei upon binding. Annotated HSQC spectra for Cu(I) and Zn-amicyanin are shown in figure 1 and 2, respectively, while the assignments and perturbations tables are shown in Appendix B.

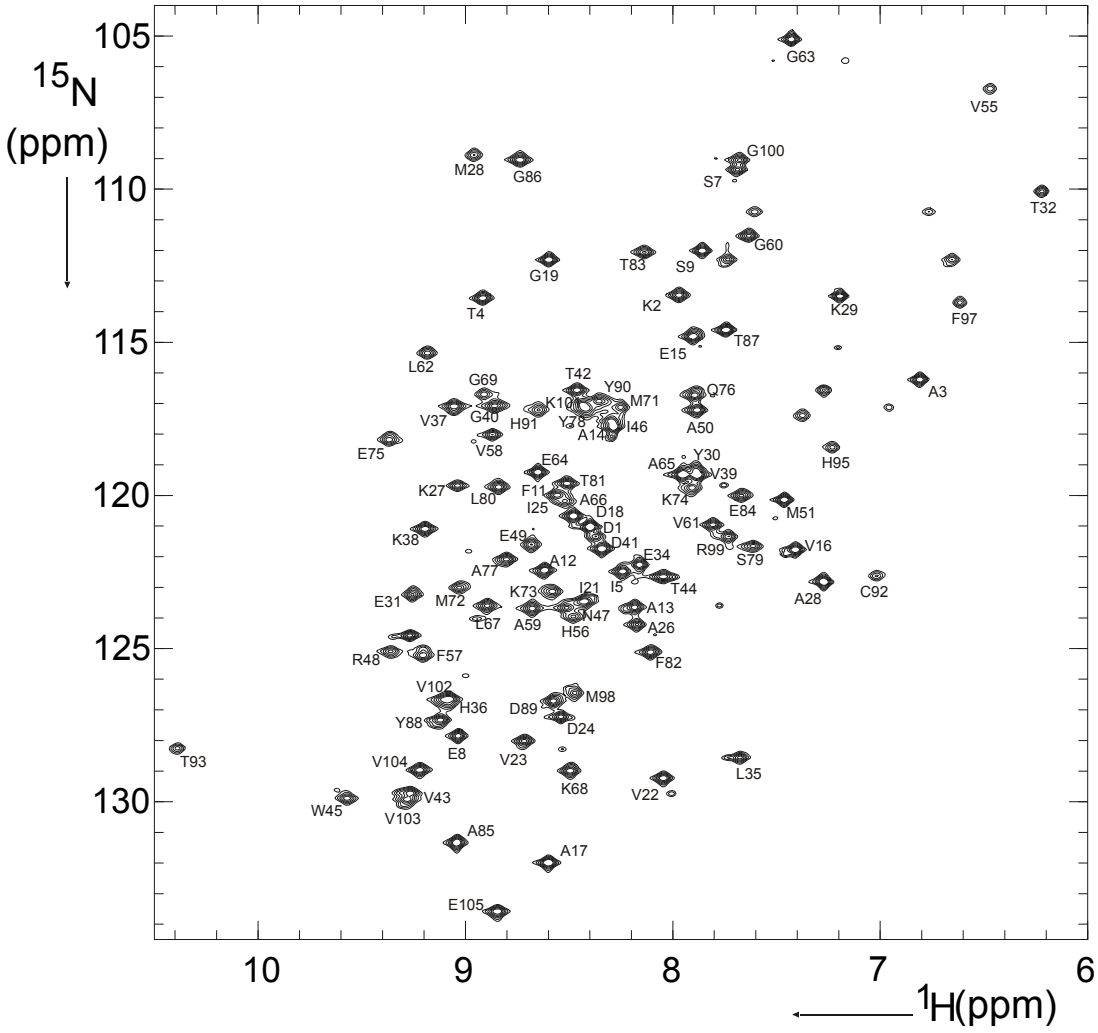

Figure 1. Annotated ^{15}N-HSQC spectrum of *P. denitrificans* Cu(I)-amicyanin

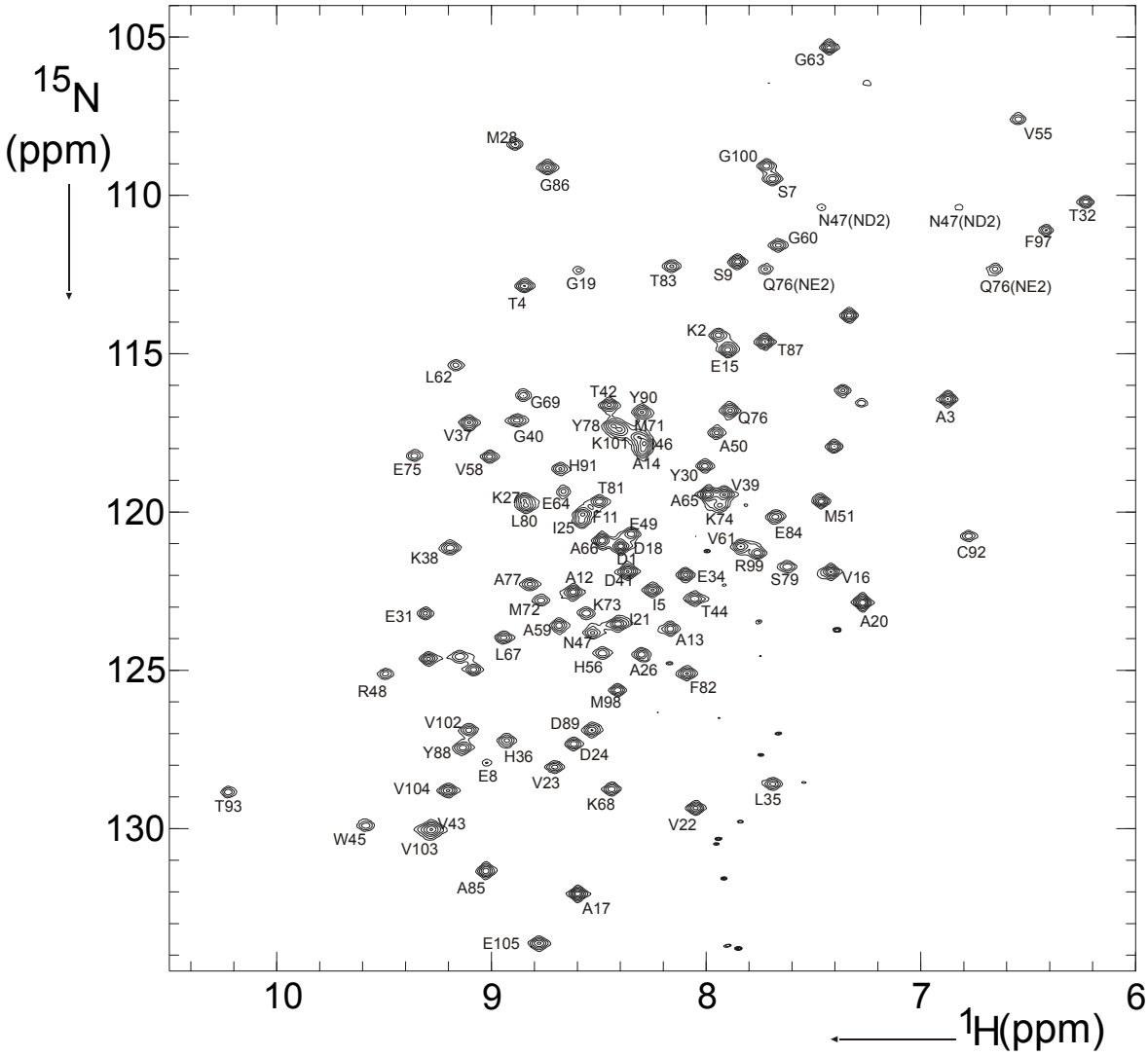

Figure 2. Annotated ^{15}N-HSQC spectrum of *P. denitrificans* Zn-substituted amicyanin

RESULTS

Chemical shift perturbation analysis

MADH-amicyanin complex

The complex between MADH and amicyanin was studied in the oxidized form, using a Zn(II) substitited amicyanin as a mimic for Cu(II) to avoid the broadening of the signals caused by the paramagnetic properties of the latter. To investigate its binding site to MADH in solution, amicyanin was enriched in ^{15}N, as well as ^{2}H for all non-exchangeable protons. It is well established that in perdeuterated proteins dipolar relaxation of the amide protons is strongly reduced, leading to sharp signals in the [^{15}N-^{1}H] HSQC spectrum. This approach, in combination with TROSY-type experiments *(21)*, allows the observation of amicyanin amide resonances also in the complex with MADH.

The formation of the complex has large effects on the chemical shifts of the amides. Figure 3 shows the $\Delta\delta_{avg}$ values for all observed residues in Zn-substituted amicyanin bound to MADH (amicyanin-MADH protomer ratio of 1:2) and in the figure 4 these $\Delta\delta_{avg}$ values were mapped onto the surface representation of amicyanin using the color code indicated by the vertical bar on the right in the figure 3. In the TROSY spectra of the complex most of the peaks could be assigned by comparison of the free and bound forms and, for the residues that shift more, by confirmation of the relative NOESY-TROSY spectra. Five resonances show such a large chemical shift changes that they could not be assigned, also because of the not sufficiently high quality of the NOESY-TROSY spectra. However, they could be classified as 'large perturbed' on the basis of the closest not assigned peak in the spectra of the complex. These residues are: Met51, Leu62, Thr93, Phe97 and Arg99. Figure 4B shows a map of the surface of the crystal structure of the amicyanin in the complex where the residues are coloured on the basis of their distance from the MADH. By comparison of the chemical shift perturbations map (figure 4A) and the map of the contacts in the crystal (figure 4B) it is clear that also in solution the predominant effects are at the hydrophobic patch that surrounds the exposed copper ligand His95 but, in solution, the formation of the complex involves a larger area than in the crystal. In particular the region of the residues 58-62 shows considerable perturbations and, together with the hydrophobic patch region, it is identified as the principal interface for binding.

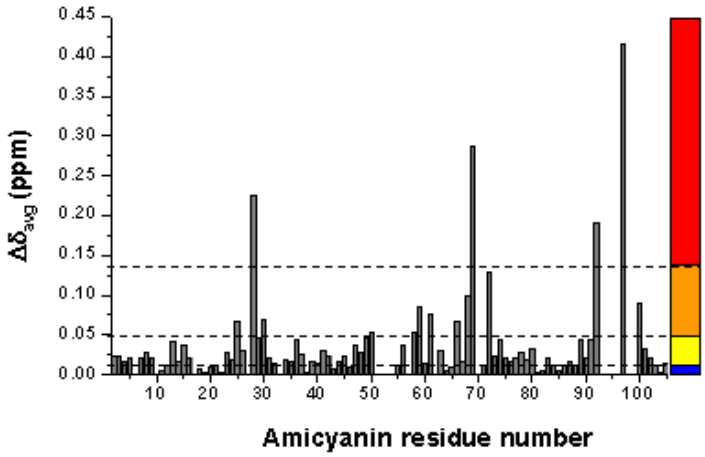

Figure 3. The $\Delta\delta_{avg}$ values for all observed residues Zn amicyanin bound to MADH. The vertical bar indicates the classification of these values as follows: $\Delta\delta_{avg}$<0.018 "no shift", <0.05 "small", <0.13 "medium" and >0.13 "large"

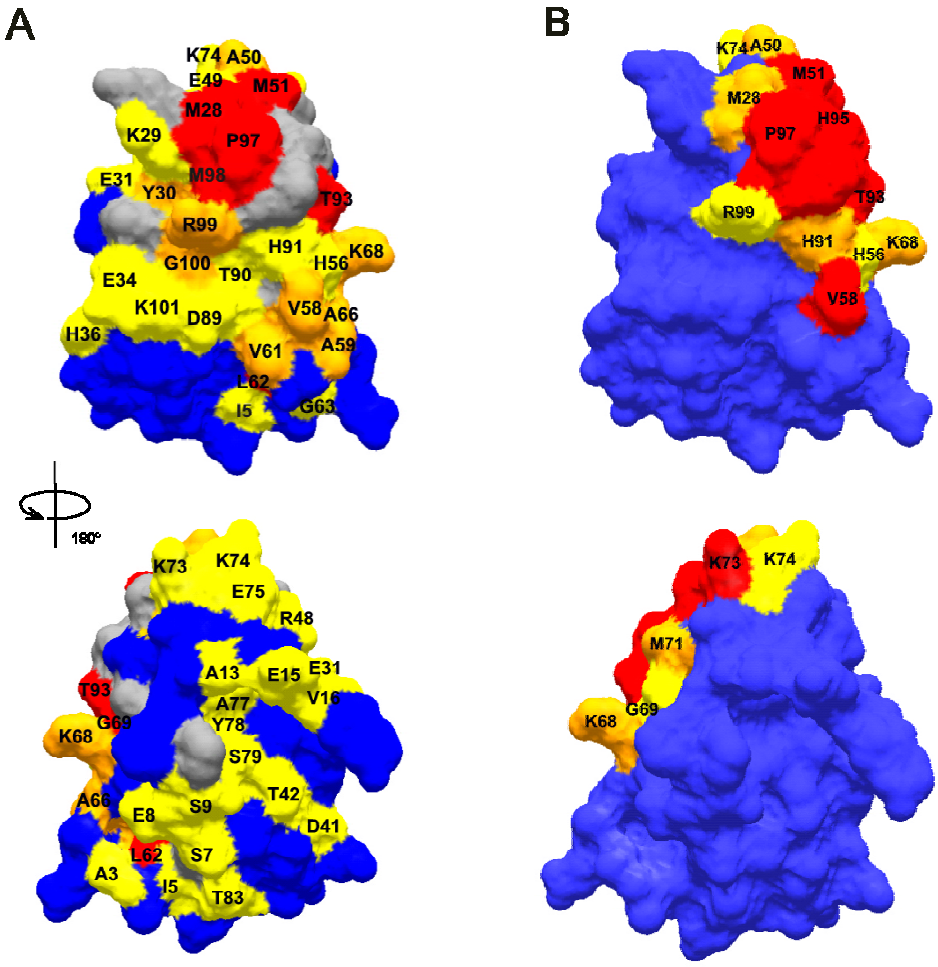

Figure 4. A) Map of the chemical shift perturbations on the structure of Zn-amicyanin in the complex with MADH. The unassigned residues and prolines are in grey In panel **B** the residues of amicyanin were colored according to the distance from MADH in the crystal structure of the complex (PDB entry: 1MDA), with residues with atoms within 4, 5 and 6 Å from MADH in red, orange and yellow, respectively and other residues in blue.

Effect of pH and of the redox state of MADH

In order to study the effect of pH and of the different redox states of MADH on the amides resonances of bound amicyanin, some spectra of the binary complex were acquired at different pH values and with different redox forms of MADH.

The reference spectrum is the TROSY of the complex between Zn-amicyanin and methylamine-reduced MADH at pH 8. Then, pH was changed and spectra were collected at pH 7.5 and 8.5. Furthermore, spectra of the complexes with oxidized MADH and with sodium ascorbate-reduced MADH, both at pH 8, were collected. Table 1 shows the $\Delta\delta_{avg}$ classification for the perturbed residues in these spectra, calculated on the basis of the chemical shifts of the reference sample; furthermore, in the table the residues are also reported which, due to a high perturbation (large shift or high decrease of the intensity), disappear and for which it is not possible to calculate the $\Delta\delta_{avg}$. The pH changes have large effect on the resonances of the amicyanin amides, causing the disappearance or small/medium perturbations of many residues on the amicyanin surface. On the contrary the change of the MADH redox state causes just small perturbations on a few amicaynin residues which are localized, except for Gly19, within the binding interface of the complex.

Table 1. Perturbed residues of Zn amicyanin bound to MADH due to changes in the pH or in the redox state of MADH

compared spectra*	$\Delta\delta_{avg}$ classification**			disappeared residues
	small	medium	large	
A-B	Phe11, Met28, Ala50 Gly69, Met72,His91 Phe97,Gly100	-	-	Gly19 (in A)
A-C	Ala13, Met28, Arg48	-	-	Gly19 (in A)
A-D	Lys2, Ala3, Glu15 Glu34, Val37, Gly40 Val61, Glu64, Ala65 Leu67, Gly69, Lys74 Tyr78, Thr83, Va104 Glu105	Thr4, His36, His91	-	Glu8 (in D) Glu49 (in D) Val58 (in D) Gly100 (in D)
A-E	Ala3, Glu15, Met28 Glu34, Val58, Val61 Gly63, Ala65, Leu67 Lys68, Glu84, Cys92 Phe97, Gly100, Glu105	Lys2, Thr4, His36	-	Gly19 (in A) Trp45 (in E) Arg48 (in E) His56 (in E) His91 (in E)

* The spectra are the TROSYs of the complex between Zn amicyanin and: **A**:methylamine-reduced MADH at pH 8; **B**:oxidized MADH at pH 8; **C**:ascorbate-reduced MADH at pH 8; **D**:methylamine-reduced MADH at pH 8.5; **E**:methylamine-reduced MADH at pH 7.5. ** The $\Delta\delta_{avg}$ are classified as: "no shift" if <0.018 (residues not indicated); "small" if <0.05; "medium" if <0.13 and "large if >0.13 ppm.

Interaction between the MADH-amicyanin binary complex and cytochrome c-551i

In order to study the interaction which could occur in solution between the MADH-amicyanin binary complex and its supposed physiologically electron acceptor cytochrome *c*-551i, two NMR experiments were performed: a titration of the complex of Zn-amicyanin and sodium ascorbate-reduced MADH with the reduced form of cytochrome *c*-551i and a similar experiment using a complex of Zn-amicyanin and oxidized MADH titrated with the oxidized form of cytochrome *c*-551i. Upon titration with cytochrome c-551i some amicyanin resonances are perturbed by the presence of the protein added. Table 2 reports the $\Delta\delta_{avg}$ classification for the affected residues in the TROSY spectra of the binary complexes in the titration with cytochrome *c*-551i; furthermore in the table the residues are also reported which, due to a high perturbation (large shift or high decrease of the intensity), disappear and for which it is not possible to calculate the $\Delta\delta_{avg}$.

Table 2. . Perturbed residues of amides resonances of amicyanin in the complex with MADH due to the titration with cytochrome *c*-551i

Experiment*	$\Delta\delta_{avg}$ classification**			disappeared residues
	small	medium	large	
1	Lys2, Ala3, Glu15,Glu34, Trp45, Val61, Ala65, Leu67, Gly69, Thr83, Cys92, Phe97, Val102, Glu105	Thr4, His36	-	Gly63, His91
2	Ala13, Glu15, Gly69	-	-	Arg48, Glu49 Gly63, His91

*The experiments are the titration at pH 6.8 of **1)** Zn-amicyanin/ascorbate-reduced MADH complex with ascorbate-reduced cyt c-551i and **2)** Zn-amicyanin/oxidized MADH with oxidized cyt c-551i. The data are relative to a final points of the titrations, when 3.3 molar equivalents of cytochrome were added. **The $\Delta\delta_{avg}$ are classified as: “no shift” if <0.018 (residues not indicated); “small” if <0.05; “medium” if <0.13 and “large if >0.13 ppm.

The perturbed residues, indicated in table 2, are scattered on the amicyanin surface and far away from the binding interface with cytochrome *c*-551i found in the crystal structure of the ternary complex *(12)*, a fact that suggests that these perturbations could not reflect the formation of a complex. Furthermore, by comparison of the results presented in table 1 and 2 it is evident that the perturbations occurring during the titrations of the binary complex with cytochrome *c*-551i are the same observed for small changes in the pH . Considering that in the course of a long experiment, as

these titrations, which require continuous additions of an external solution, it is very difficult to keep the pH exactly the same initial value, it is likely that small changes in the pH of the NMR sample occur and could be the cause of the observed perturbations on the amicyanin resonances.

Amicyanin-cytochrome c-551i complex

The interaction between free, uncomplexed, amicyanin and cytochrome *c*-551i was studied in both reduced and oxidized states, using the Cu(I) and Zn(II) form of amicyanin, respectively. To investigate its binding site to cytochrome *c*-551i in solution, amicyanin was enriched in ^{15}N in order to collect the 2D-[^{15}N-^{1}H] HSQC spectra. Upon titration with cytochrome *c*-551i, some resonances experience small perturbations and shifts of the signals were observed, while other few resonances showed a decrease of intensity. So, it can be concluded that the exchange rate is fast or fast-intermediate for most signals, both for Cu(I) and Zn-amicyanin.
The off-rate for the Cu(I)-amicyanin/cytochrome *c*-551i complex is estimated to be of the order of 600-1000 s^{-1}. All residues assigned in the free form of amicyanin were assigned also in the spectra of the complexes by comparison of the free and bound forms, except for Phe97 which disappears in the spectrum of bound Cu(I)-amicyanin. However, this residue was classified as “large perturbed” on the basis of the shift shown after addition of 1.0 equivalent of cytochrome *c*-551i. The effects of the formation of the complex on the chemical shifts of the amides were quantified by the $\Delta\delta_{avg}$ values, that are shown in the figure 5 for all assigned residues of Cu(I) and Zn-amicyanin bound to cytochrome *c*-551i (the data are relative to the final point of the titrations, when 2.4 molar equivalents of cytochrome were added in the case of Cu(I)-amicyanin and 2.3 in the case of the Zn-substituted form). In figure 6 these $\Delta\delta_{avg}$ values were mapped onto the surface representation of amicyanin using the color code indicated by the vertical bar on the right in figure 5. Some differences were observed in the perturbations of the signals between Cu(I) and Zn-amicyanin due to the formation of the complex. In the case of Cu(I), the effects of the binding are more localized on the hydrophobic patch that surrounds the exposed ligand His95, while in the case of Zn-amicyanin the binding seems to involve a larger area, resulting in more numerous, but in general smaller, shifts. This could have two explanation: 1) a more dynamic nature of the complex in the case of the Zn-amicyanin compared to

the Cu(I) protein or 2) it could be just a consequence of the higher affinity of cytochrome *c*-551i for the Zn- substituted with respect to the Cu(I)-amicyanin (see the calculated values of K_d at page 73) which could be responsible for a more extended perturbation of the amicyanin surface.

As it is clear from the binding maps shown in figure 6, the major differences involve the residue Phe97, which show a very large shift in the case of Cu(I) and no shift in the case of Zn-amicyanin.

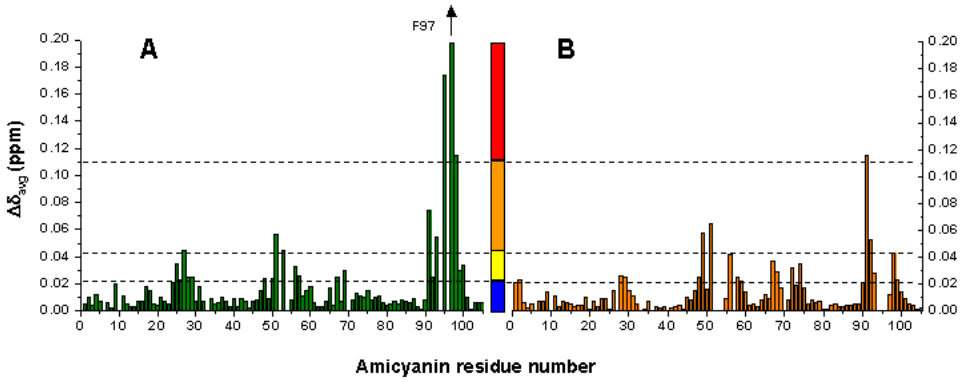

Figure 5. The $\Delta\delta_{avg}$ values for all observed residues in **A)** Cu(I) and **B)** Zn amicyanin bound to *c*ytochrome *c*-551i; the vertical bar indicates the classification of these values as follows: $\Delta\delta_{avg}$<0.02 “no shift”, <0.04 “small”, <0.1 “medium” and >0.1 “large”

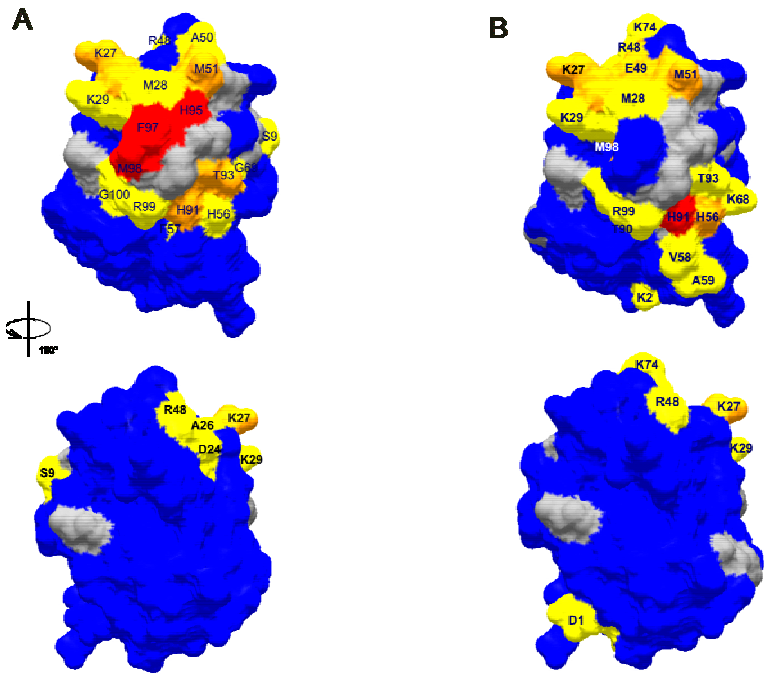

Figure 6. Maps of the chemical shift perturbations on the structure of amicyanin (PDB entry: 1AAN) due to the formation of the complex with cytochrome *c*-551i, with the results for Cu(I) and Zn(II) amicyanin shown in panels **A** and **B**, respectively. The unassigned residues and prolines are in grey.

Cytochrome *c*-551i contains a single iron atom that in its oxidized state (+3) is paramagnetic, with one unpaired electron in the 3d orbitals, while in its reduced state (+2) is diamagnetic. This change in the magnetic properties has an effect on the nuclear relaxation rates and on the chemical shifts of the signals of the residues close to the metal (i.e. pseudocontact shifts). These pseudocontact shifts *(61-64)* provide longer-range distance constraints with respect to the NOEs and are particularly useful in the vicinity of the paramagnetic metal ion; they further allow to relate the position of the metal ion to those of the protein protons.

So, comparing the spectra of the amicyanin bound to oxidized and reduced form of cytochrome *c*-551i it should be possible to evidence the amicyanin residues that in the complex are close to the iron ion. For this reason at the end of the titration of Zn-amicyanin with oxidized cytochrome *c*-551i the latter was reduced by sodium ascorbate and a spectrum of the resulting sample was acquired. This experiment was done only on Zn-amicyanin because in the case of Cu(I)-amicyanin it is not possible titrate with oxidized cytochrome because the electron transfer from amicyanin to cytochrome would cause the formation of Cu(II) with a consequent wide broadening of the signals around the copper site. However, the comparison of the spectra of Zn amicyanin bound to the two different redox forms of cytochrome *c*-551i does not show differences, suggesting that the complex must be quite mobile (mainly electrostatic). For this reason, only the data of the titration of Zn-amicyanin with oxidized cytochrome *c*-551i are shown.

Binding constants

The fast or fast-intermediate character of the exchange rate for most signals, for both Cu(I) and Zn-amicyanin in complex with cytochrome *c*-551i makes it possible to calculate the binding constants for the formation of these complexes. Chemical shift changes of amides, in ^{1}H or ^{15}N dimension, were plotted against the molar ratio of citochrome *c*-551i and amicyanin. Than the data were fitted using a one-site binding model which corrects for dilution effects (it is convenient to perform the calculation on residues showing larger shifts):

$$y = \frac{1}{2} P2 \left(Q - \sqrt{Q^2 - 4 * x * P3} \right) \qquad \text{equation 1}$$

$$Q = 1 + P + P3 * x$$

$$P = \frac{B + A * P3 * x}{A * B * K_a}$$

where:

A = the molar concentration of amicyanin in the NMR tube;
B = the molar concentration of the cytochrome *c*-551i stock;
P2 = the maximum effect on observable ($\Delta\delta_{max}$)
P3 = a parameter that can be used to adjust for uncertainty in concentration determination of the proteins;
x = the ratio of the protein added (cytochrome) over the one in the tube (amicyanin);
K_a = the binding constant (in M^{-1}).

This fitting, performed in the program Origin version 7.5, has given values for K_d ($1/K_a$) of 62±12 μM and 17± 6 μM for the complexes of cytochrome *c*-551i with Cu(I) and Zn amicyanin, respectively (figure 7).

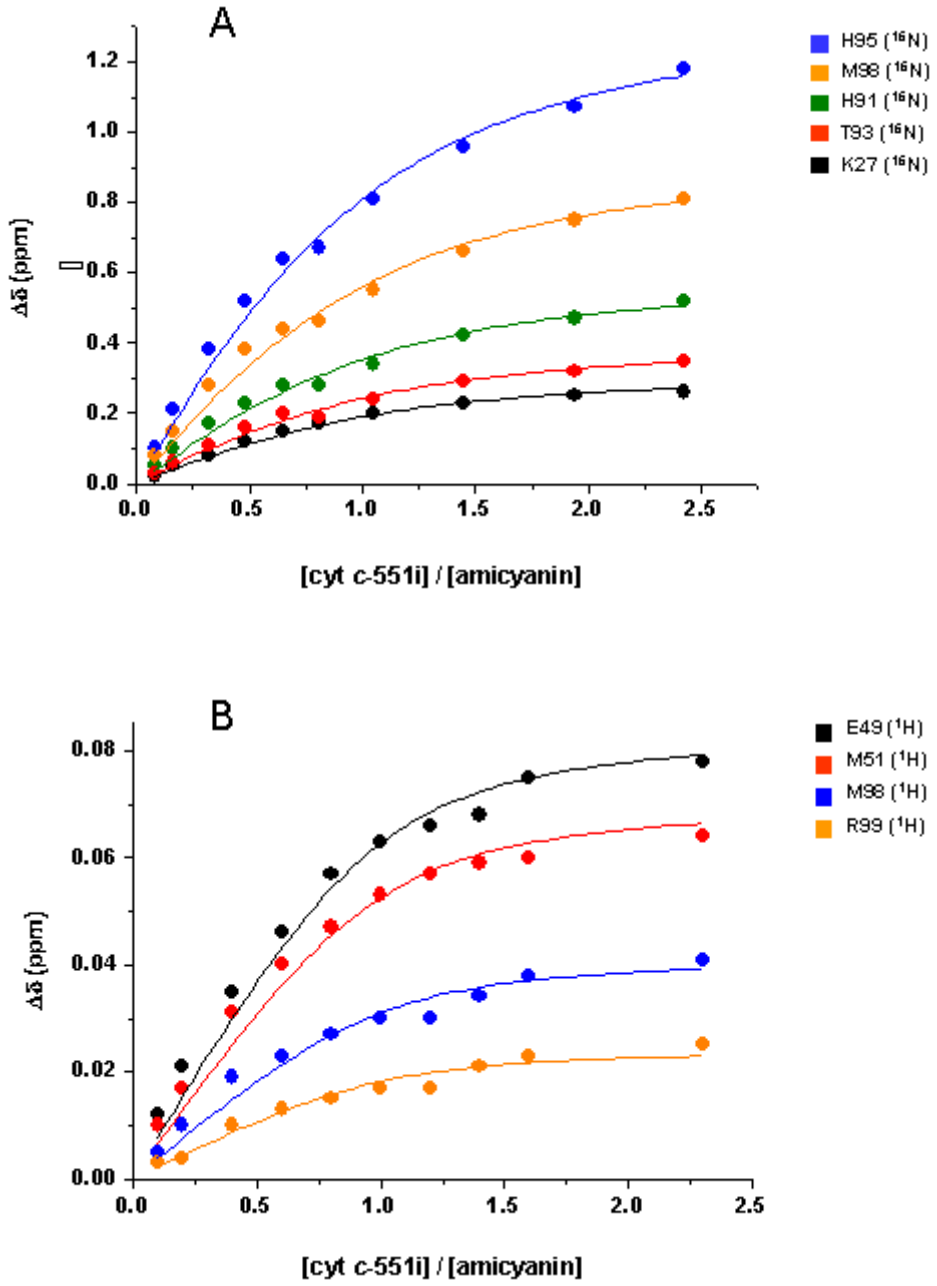

Figure 7. Titration curves for **A)** Cu(I) and **B)** Zn-amicyanin with cytochrome *c*-551i with the chemical shift changes ($\Delta\delta$) in the ^{1}H or ^{15}N dimension plotted against the ratio between [cyt c-551i] and [amicyanin] and fitted globally with the equation 1 (using P3=1) for a 1:1 complex.

.

DISCUSSION

The interactions of amicyanin with MADH and with its possible electron acceptor, cytochrome *c*-551i, were investigated by high-resolution NMR techniques, in particular with the aim of characterizing the binding interface on the amicyanin surface. The extensive chemical shifts perturbations of the amides resonances of Zn-amicyanin caused by the formation of the binary complex with MADH were analyzed by comparison with the crystal structure of the complex. The most strongly affected residues are those in the region of the hydrophobic patch that surrounds the exposed ligand His95 and in particular those centered around Phe97 (figure 4A), suggesting that this area of the amicyanin surface is part of the interface. This is in accordance with the crystal structure, as can be seen in figure 4B in which the residues that constitute the interface are colored in red. Furthermore, it has been shown that replacement of Phe97 by mutagenesis has a large effect on the electron transfer rate in the complex, which was attributed to reduced electronic coupling between the redox sites *(48)*. However, the area of residues exhibiting chemical shift perturbations is noticeably larger, involving in particular the region of the residues 58-62 and also numerous residues at the back side of amicyanin. A similar result was found for the same complex from *Paracoccus versutus* (see chapter 3) and, as in that case, two explanations were provided to account for this larger area of perturbations observed in solution with respect to the crystal structure. First, these effects might be caused by slight movements in secondary structure elements or changes in hydrogen bond networks (secondary perturbations) as a result of small structural changes in the interface area. Second, this wide area could indicate a dynamic nature for this complex in solution. In fact, for other protein complexes it has been shown that, beside a major area of contact, other region of the protein make contacts with the partner, causing additional chemical shift perturbations *(53,54)*. These two possibilities are not easily distinguishable and one does not exclude the other one, while it is expected that the existence of a dynamic state results in small $\Delta\delta_{avg}$ values, compared to well-defined complexes *(55,56)*. So, the fact that in the complex with MADH the amicyanin residues show large $\Delta\delta_{avg}$ values, suggest that the nature of the complex is mostly well-defined and that the larger area of chemical shift perturbations observed in solution with respect to the crystal structure is due mostly to secondary effects.

One of the open questions about the *P. denitrificans* system is which is the physiological electron acceptor of amicyanin. Cytochrome *c*-551i is shown to be, *in vitro*, the most efficient acceptor of electrons from amicyanin *(11)* and it forms with amicyanin and MADH a crystalline ternary complex for which the structure has been solved at 2.4 Å resolution *(12)*. The existence of this ternary complex in solution is supposed on the base of many kinetic experiments, even if the question of the physiologically role of the cytochrome *c*-551i remains unanswered *(15,58)*.

In the present work the interaction of amicyanin, both free and in the complex of MADH, with cytochrome *c*-551i was investigated by NMR titration experiments and different results were found for the two cases. The interaction between free, uncomplexed, amicyanin and cytochrome *c*-551i was investigated for both the reduced and the oxidized state of amicyanin, using Cu(I) and Zn(II)-substituted amicyanin, respectively. In both cases the results clearly show the formation of a complex, even if some differences were observed in the perturbations of the signals of the two forms of amicyanin. In the case of Cu(I) the effects of the binding are fairly localized on the hydrophobic patch that surrounds the exposed ligand His95 and the shifts are reasonably small, but not very much. This result is in accord with the hypothesis, based on kinetic experiments, that in the absence of MADH the surface of amicyanin binding cytochrome *c*-551i is the same that binds MADH in the binary complex MADH-amicyanin *(58)*. In the case of Zn-amicyanin cytochrome *c*-551i seems to bind over a larger area (figure 6), resulting in smaller shifts. This result, together with the absence of the differences between the spectra of the Zn amicyanin bound to oxidized and reduced cytochrome *c*-551i (i.e. absence of pseudocontact shifts caused by the heme), indicates that the complex must be quite mobile (mainly electrostatic). However, an effect due to a higher affinity of the cytochrome *c*-551i for the Zn-amicyanin with respect to the Cu(I) form should be take in account as a possible explanation for the larger perturbed area observed in the case of the Zn-amicyanin. The K_d for these complexes, calculated on the base of these NMR titrations, result to be of 62$\pm$12 μM and 17$\pm$ 6 μM for Cu(I) and Zn-amicyanin, respectively.

Completely different are the results of the chemical shifts analysis obtained in the case of the titration of the binary complex with cytochrome *c*-551i. The experiments were performed on the complexes of Zn-amicyanin with ascorbate-reduced and

oxidized forms of MADH which were titrated, respectively, with ascorbate-reduced and oxidized forms of cytochrome *c*-551i.

During the titrations, some residues are affected, showing small or medium shifts or disappearance because of larger shifts or a high decrease of intensity (table 2). However, these residues are scattered on the surface of amicyanin and far away from the binding interface with cytochrome *c*-551i in the crystal structure of the ternary complex *(12)*. Therefore, these perturbations might not be due to the formation of a complex, but they could be an effect of small changes in the pH conditions which can have occurred during these long lasting experiments. These explanation is suggested by the results of the experiments on the effects of pH changes on the amicyanin resonances (table 1).

APPENDIX A

Table 1. Assignment of *Paracoccus versutus* ^{15}N-Zn- amicyanin, 20mM NaPi pH=7, T=300K (n.a.: not assigned)

Residue		^{15}N	$^{1}H^{N}$	Others
0	**Gly**	n.a.	n.a.	
1	**Gln**	n.a.	n.a.	NE2 111.69, HE21 7.48, HE22 6.73
2	**Asp**	121.05	8.33	
3	**Lys**	120.13	8.61	
4	**Ile**	106.78	7.03	
5	**Thr**	116.48	8.57	
6	**Val**	128.05	8.87	
7	**Thr**	122.54	7.76	
8	**Ser**	114.31	7.72	
9	**Glu**	125.65	8.77	
10	**Lys**	115.17	7.68	
11	**Pro**	-	-	
12	**Val**	115.97	8.76	
13	**Ala**	123.29	8.59	
14	**Ala**	123.99	8.23	
15	**Ala**	117.07	8.15	
16	**Asp**	115.69	7.77	
17	**Val**	124.25	7.14	
18	**Pro**	-	-	
19	**Ala**	123.39	8.43	
20	**Asp**	113.65	8.21	
21	**Ala**	120.89	6.99	
22	**Val**	123.67	8.74	
23	**Val**	126.47	7.75	
24	**Val**	130.27	9.28	
25	**Gly**	113.39	8.76	
26	**Ile**	119.13	7.93	
27	**Glu**	122.60	8.16	
28	**Lys**	119.80	8.90	
29	**Met**	107.96	8.98	
30	**Lys**	113.98	7.29	
31	**Tyr**	119.38	8.09	
32	**Leu**	123.18	9.37	
33	**Thr**	110.18	6.36	
34	**Pro**	-	-	
35	**Glu**	119.53	7.77	
36	**Val**	122.31	7.70	
37	**Thr**	121.34	8.25	
38	**Ile**	121.19	9.10	
39	**Lys**	118.93	8.63	
40	**Ala**	121.93	8.34	
41	**Gly**	111.20	9.40	
42	**Glu**	120.10	8.05	
43	**Thr**	116.65	8.16	
44	**Val**	126.77	8.59	
45	**Tyr**	122.70	8.37	
46	**Trp**	123.93	9.66	NE1 123.25, HE1 8.65
47	**Val**	118.27	8.14	
48	**Asn**	124.92	8.81	ND2 108.74, HD21 7.43, HD22 6.32

49	**Gly**	116.32	9.37	
50	**Glu**	120.17	8.41	
51	**Val**	112.40	7.73	
52	**Met**	121.27	7.38	
53	**Pro**	-	-	
54	**His**	n.a.	n.a.	
55	**Asn**	n.a.	n.a.	
56	**Val**	115.11	6.70	
57	**Ala**	127.46	8.24	
58	**Phe**	111.42	8.81	
59	**Lys**	122.38	9.56	
60	**Lys**	120.92	8.80	
61	**Gly**	111.21	7.24	
62	**Ile**	120.14	7.84	
63	**Val**	109.00	8.71	
64	**Gly**	108.43	7.42	
65	**Glu**	118.31	8.61	
66	**Asp**	115.59	8.14	
67	**Ala**	123.27	8.84	
68	**Phe**	120.61	8.53	
69	**Arg**	130.01	8.09	
70	**Gly**	115.09	8.38	
71	**Glu**	119.17	6.61	
72	**Met**	118.14	8.26	
73	**Met**	119.85	8.83	
74	**Thr**	115.55	8.63	
75	**Lys**	120.36	7.84	
76	**Asp**	119.02	9.15	
77	**Gln**	116.89	7.88	NE2 110.49, HE21 7.45, HE22 6.50
78	**Ala**	121.24	9.26	
79	**Tyr**	121.33	9.17	
80	**Ala**	128.66	7.60	
81	**Ile**	118.71	8.49	
82	**Thr**	124.48	8.51	
83	**Phe**	125.75	8.04	
84	**Asn**	119.10	8.25	ND2 111.81, HD2 6.66
85	**Glu**	116.17	7.75	
86	**Ala**	128.04	8.87	
87	**Gly**	108.45	9.02	
88	**Ser**	113.63	7.80	
89	**Tyr**	125.40	9.31	
90	**Asp**	126.71	8.30	
91	**Tyr**	119.80	8.65	
92	**Phe**	119.25	8.93	
93	**Cys**	119.59	6.84	
94	**Thr**	127.41	9.98	
95	**Pro**	-	-	
96	**His**	116.12	7.02	
97	**Pro**	-	-	
98	**Phe**	111.48	6.54	
99	**Met**	124.87	8.60	
100	**Arg**	121.35	7.86	
101	**Gly**	108.33	7.38	
102	**Lys**	119.23	8.60	
103	**Val**	126.93	8.89	
104	**Ile**	130.40	9.42	
105	**Val**	127.21	9.14	
106	**Glu**	133.46	9.14	

Table 2. Assignment of *Paracoccus versutus* ^{15}N-^{13}C-Cu(I)- amicyanin, 300K, 10mM KPi pH 6.8 (n.a.: not assigned)

Residue		^{15}N	$^{1}H^{N}$	C^{α}	C^{β}	CO	Others
0	**Gly**	n.a.	n.a.	n.a.	n.a.	n.a.	
1	**Gln**	n.a.	n.a.	56.07	29.81	172.42	CG 34.10, NE2 112.19 HE21 7.47, HE22 6.72
2	**Asp**	121.48	8.33	55.09	41.68	174.44	
3	**Lys**	120.52	8.60	59.40	33.81	172.90	
4	**Ile**	107.06	7.00	58.48	42.25	171.76	
5	**Thr**	116.89	8.54	62.11	72.61	169.88	
6	**Val**	128.41	8.85	62.78	32.48	173.14	
7	**Thr**	123.11	7.74	65.65	68.87	171.52	
8	**Ser**	114.68	7.71	55.91	64.69	170.91	
9	**Glu**	126.04	8.76	59.24	30.22	174.27	
10	**Lys**	115.41	7.66	53.06	33.09	171.07	
11	**Pro**	-	-	63.85	n.a.	n.a.	
12	**Val**	116.30	8.73	59.24	34.43	172.19	
13	**Ala**	123.63	8.56	52.85	19.08	176.21	
14	**Ala**	124.38	8.24	55.28	18.73	176.62	
15	**Ala**	117.51	8.15	54.06	19.00	174.66	
16	**Asp**	115.96	7.74	54.71	41.05	173.36	
17	**Val**	124.70	7.12	61.45	32.53	171.16	
18	**Pro**	-	-	63.29	32.79	174.04	
19	**Ala**	123.80	8.43	54.50	18.95	175.17	
20	**Asp**	113.99	8.19	53.40	39.91	172.42	
21	**Ala**	121.26	6.96	52.21	21.58	174.41	
22	**Val**	124.03	8.71	64.24	31.35	171.06	
23	**Val**	126.82	7.73	60.44	35.80	173.35	
24	**Val**	130.76	9.27	62.02	32.21	172.31	
25	**Gly**	113.65	8.70	45.17	-	n.a.	
26	**Ile**	119.51	7.86	61.09	41.35	172.64	
27	**Glu**	122.89	8.00	56.85	34.57	171.63	
28	**Lys**	120.65	9.02	-	29.85	173.04	
29	**Met**	109.11	9.02	-	29.03	171.28	
30	**Lys**	114.09	7.10	55.78	36.19	172.05	
31	**Tyr**	120.24	7.95	57.98	37.84	174.82	
32	**Leu**	123.70	9.36	58.22	42.18	174.74	
33	**Thr**	110.40	6.32	58.72	70.26	169.73	
34	**Pro**	-	-	65.35	-	172.61	
35	**Glu**	120.04	7.75	56.59	32.75	171.24	
36	**Val**	122.76	7.68	60.16	35.87	169.70	
37	**Thr**	121.69	8.24	61.75	70.32	171.16	
38	**Ile**	121.57	9.08	59.59	42.48	171.57	
39	**Lys**	119.21	8.61	54.36	34.28	173.76	
40	**Ala**	122.30	8.31	54.55	17.68	175.44	
41	**Gly**	111.59	9.39	44.83	-	n.a.	
42	**Glu**	120.39	8.02	57.09	31.31	171.08	
43	**Thr**	116.97	8.14	62.36	71.56	169.97	
44	**Val**	127.13	8.56	61.87	34.57	170.40	
45	**Tyr**	123.01	8.33	56.74	41.13	171.74	
46	**Trp**	124.53	9.62	58.42	33.12	173.21	NE1 123.78, HE1 8.61
47	**Val**	118.53	8.10	61.26	35.45	172.56	
48	**Asn**	125.23	8.73	53.58	38.41	172.92	ND2 109.54, HD21 7.51, HD22 6.28
49	**Gly**	116.59	9.170	45.61	-	n.a.	
50	**Glu**	121.27	8.60	54.20	34.06	169.46	
51	**Val**	112.30	7.63	64.04	32.25	174.48	

52	**Met**	122.03	7.35	53.40	32.62	168.95	
53	**Pro**	-	-	n.a.	n.a.	n.a.	
54	**His**	117.17	7.64	n.a.	n.a.	n.a.	
55	**Asn**	n.a.	n.a.	n.a.	42.20	168.89	
56	**Val**	114.00	6.56	62.61	34.71	169.84	
57	**Ala**	127.62	8.32	50.63	22.47	170.86	
58	**Phe**	111.40	8.76	56.16	44.37	174.40	
59	**Lys**	122.76	9.55	56.56	34.08	173.51	
60	**Lys**	121.33	8.79	58.81	33.36	172.67	
61	**Gly**	111.66	7.20	46.87	-	172.07	
62	**Ile**	120.45	7.82	63.06	38.37	174.02	
63	**Val**	109.3	8.69	60.55	31.56	171.15	
64	**Gly**	108.89	7.40	44.68	-	168.93	
65	**Glu**	118.63	8.59	59.40	30.43	174.72	
66	**Asp**	115.91	8.13	53.06	43.20	174.25	
67	**Ala**	123.64	8.82	53.16	20.06	172.47	
68	**Phe**	121.08	8.52	57.66	43.95	170.67	
69	**Arg**	107.89	8.05	55.07	32.64	170.56	
70	**Gly**	115.60	8.46	44.98	-	171.41	
71	**Glu**	119.30	6.43	56.84	31.32	172.57	
72	**Met**	118.23	8.24	55.15	31.20	173.31	
73	**Met**	120.53	8.99	54.95	39.31	174.46	
74	**Thr**	115.54	8.62	60.45	69.57	170.01	
75	**Lys**	120.32	7.87	59.24	33.44	174.31	
76	**Asp**	119.44	9.14	57.03	38.98	172.12	
77	**Gln**	117.18	7.87	55.36	32.52	170.47	NE2 110.74, HE21 7.41, HE22 6.44
78	**Ala**	121.44	9.25	50.14	25.98	172.77	
79	**Tyr**	121.88	9.15	58.53	44.36	170.00	
80	**Ala**	104.98	7.56	50.71	22.52	173.48	
81	**Ile**	119.02	8.46	61.58	42.77	170.87	
82	**Thr**	124.77	8.48	62.26	69.93	170.19	
83	**Phe**	126.11	8.01	57.56	41.17	172.13	
84	**Asn**	119.46	8.21	55.29	40.36	171.61	ND2 112.30, HD2 6.64
85	**Glu**	116.51	7.74	55.00	34.08	172.38	
86	**Ala**	128.42	8.87	53.12	19.51	173.63	
87	**Gly**	108.85	8.99	45.16	-	183.16	
88	**Ser**	114.00	7.79	57.68	64.57	170.95	
89	**Tyr**	125.80	9.29	57.65	39.96	171.25	
90	**Asp**	127.04	8.27	55.22	42.71	171.51	
91	**Tyr**	120.27	8.61	55.89	42.45	171.65	
92	**Phe**	120.52	8.92	55.91	42.43	182.41	
93	**Cys**	121.32	6.79	57.61	31.54	n.a.	
94	**Thr**	125.36	9.79	70.01	65.76	n.a.	
95	**Pro**	-	-	n.a.	n.a.	172.50	
96	**His**	118.50	7.26	n.a.	n.a.	170.47	
97	**Pro**	-	-	n.a.	n.a.	172.70	
98	**Phe**	114.50	6.66	57.13	37.96	173.86	
99	**Met**	126.99	8.62	57.16	32.28	n/a	
100	**Arg**	120.56	7.69	54.87	35.64	172.45	
101	**Gly**	109.05	7.38	44.59	-	168.38	
102	**Lys**	119.64	8.58	56.39	37.81	172.71	
103	**Val**	127.37	8.88	62.06	34.84	171.12	
104	**Ile**	130.71	9.39	61.90	38.31	170.51	
105	**Val**	127.53	9.12	60.52	33.21	173.14	
106	**Glu**	133.75	9.13	57.74	32.81	177.65	

Table 3. Shift perturbations (ppm) for *P.versutus* Cu(I) and Zn-substituted amicyanin bound to MADH (d:disappeared, n.a.: not assigned)

Residue		Cu(I)-amicyanin +5eq of MADH				Zn-amicyanin +3eq of MADH		
		^{15}N	$^{1}H^{N}$	$\Delta\delta_{avg}$		^{15}N	$^{1}H^{N}$	$\Delta\delta_{avg}$
0	**Gly**							
1	**Gln**	n.a.	n.a.	n.a.		n.a.	n.a.	n.a.
2	**Asp**	0.29	0.001	0.041		0.29	0.001	0.041
3	**Lys**	0.33	0.062	0.064		0.33	0.062	0.064
4	**Ile**	0.27	0.053	0.054		0.27	0.053	0.054
5	**Thr**	0.13	0.023	0.025		0.13	0.023	0.025
6	**Val**	0.12	0.017	0.021		0.12	0.017	0.021
7	**Thr**	0.48	0.015	0.069		0.48	0.015	0.069
8	**Ser**	0.40	0.003	0.057		0.40	0.003	0.057
9	**Glu**	0.33	0.009	0.047		0.33	0.009	0.047
10	**Lys**	0.06	0.014	0.013		0.06	0.014	0.013
11	**Pro**	-	-	-		-	-	-
12	**Val**	0.36	0.070	0.071		0.36	0.070	0.071
13	**Ala**	0.06	0.017	0.015		0.06	0.017	0.015
14	**Ala**	0.05	0.003	0.007		0.05	0.003	0.007
15	**Ala**	0.14	0.042	0.036		0.14	0.042	0.036
16	**Asp**	0.02	0.015	0.011		0.02	0.015	0.011
17	**Val**	0.15	0.020	0.025		0.15	0.020	0.025
18	**Pro**	-	-	-		-	-	
19	**Ala**	0.03	0.006	0.006		0.03	0.006	0.006
20	**Asp**	0.01	0.001	0.002		0.01	0.001	0.002
21	**Ala**	0.02	0.010	0.008		0.02	0.010	0.008
22	**Val**	0.02	0.016	0.012		0.02	0.016	0.012
23	**Val**	0.05	0.002	0.007		0.05	0.002	0.007
24	**Val**	0.08	0.028	0.023		0.08	0.028	0.023
25	**Gly**	0.04	0.000	0.006		0.04	0.000	0.006
26	**Ile**	0.09	0.003	0.013		0.09	0.003	0.013
27	**Glu**	0.04	0.034	0.025		0.04	0.034	0.025
28	**Lys**	0.56	0.164	0.140		0.56	0.164	0.140
29	**Met**	1.84	0.167	0.286		1.84	0.167	0.286
30	**Lys**	0.14	0.032	0.030		0.14	0.032	0.030
31	**Tyr**	0.15	0.046	0.039		0.15	0.046	0.039
32	**Leu**	0.05	0.001	0.007		0.05	0.001	0.007
33	**Thr**	0.13	0.008	0.019		0.13	0.008	0.019
34	**Pro**	-	-	-		-	-	-
35	**Glu**	0.13	0.002	0.018		0.13	0.002	0.018
36	**Val**	0.23	0.001	0.033		0.23	0.001	0.033
37	**Thr**	0.06	0.011	0.012		0.06	0.011	0.012
38	**Ile**	0.00	0.005	0.004		0.00	0.005	0.004
39	**Lys**	0.02	0.005	0.005		0.02	0.005	0.005
40	**Ala**	0.01	0.011	0.008		0.01	0.011	0.008
41	**Gly**	0.01	0.000	0.001		0.01	0.000	0.001
42	**Glu**	0.00	0.004	0.003		0.00	0.004	0.003
43	**Thr**	0.01	0.014	0.010		0.01	0.014	0.010
44	**Val**	0.02	0.007	0.006		0.02	0.007	0.006
45	**Tyr**	0.06	0.016	0.014		0.06	0.016	0.014
46	**Trp**	0.20	0.012	0.030		0.20	0.012	0.030
47	**Val**	0.58	0.012	0.082		0.58	0.012	0.082
48	**Asn**	0.53	0.018	0.076		0.53	0.018	0.076
49	**Gly**	0.02	0.122	0.086		0.02	0.122	0.086
50	**Glu**	0.14	0.006	0.020		0.14	0.006	0.020

51	**Val**	d	d	d		2.47*	0.130*	0.361*
52	**Met**	d	d	d		2.56	0.002	0.362
53	**Pro**	-	-	-		-	-	-
54	**His**	n.a.	n.a.	n.a.		n.a.	n.a.	n.a.
55	**Asn**	n.a.	n.a.	n.a.		n.a.	n.a.	n.a.
56	**Val**	0.27	0.101	0.081		0.27	0.101	0.081
57	**Ala**	0.00	0.084	0.059		0.00	0.084	0.059
58	**Phe**	0.17	0.039	0.037		0.17	0.039	0.037
59	**Lys**	0.06	0.024	0.019		0.06	0.024	0.019
60	**Lys**	0.15	0.093	0.069		0.15	0.093	0.069
61	**Gly**	0.61	0.026	0.088		0.61	0.026	0.088
62	**Ile**	0.17	0.022	0.029		0.17	0.022	0.029
63	**Val**	d	d	d		d	d	d
64	**Gly**	0.10	0.005	0.015		0.10	0.005	0.015
65	**Glu**	0.06	0.002	0.009		0.06	0.002	0.009
66	**Asp**	0.22	0.071	0.059		0.22	0.071	0.059
67	**Ala**	0.10	0.031	0.026		0.10	0.031	0.026
68	**Phe**	0.46	0.108	0.100		0.46	0.108	0.100
69	**Arg**	0.66	0.128	0.130		0.66	0.128	0.130
70	**Gly**	1.43	0.059	0.206		1.43	0.059	0.206
71	**Glu**	0.30	0.389	0.278		0.30	0.389	0.278
72	**Met**	0.41	0.162	0.128		0.41	0.162	0.128
73	**Met**	0.13	0.100	0.073		0.13	0.100	0.073
74	**Thr**	1.85	0.010	0.262		1.85	0.010	0.262
75	**Lys**	0.27	0.041	0.048		0.27	0.041	0.048
76	**Asp**	0.52	0.077	0.092		0.52	0.077	0.092
77	**Gln**	0.18	0.025	0.031		0.18	0.025	0.031
78	**Ala**	0.01	0.006	0.004		0.01	0.006	0.004
79	**Tyr**	0.19	0.010	0.028		0.19	0.010	0.028
80	**Ala**	0.23	0.090	0.071		0.23	0.090	0.071
81	**Ile**	0.01	0.014	0.010		0.01	0.014	0.010
82	**Thr**	0.03	0.012	0.009		0.03	0.012	0.009
83	**Phe**	0.05	0.021	0.016		0.05	0.021	0.016
84	**Asn**	0.01	0.015	0.011		0.01	0.015	0.011
85	**Glu**	0.04	0.008	0.008		0.04	0.008	0.008
86	**Ala**	0.09	0.007	0.014		0.09	0.007	0.014
87	**Gly**	0.04	0.004	0.006		0.04	0.004	0.006
88	**Ser**	0.06	0.002	0.009		0.06	0.002	0.009
89	**Tyr**	0.18	0.009	0.026		0.18	0.009	0.026
90	**Asp**	0.12	0.087	0.064		0.12	0.087	0.064
91	**Tyr**	0.39	0.006	0.055		0.39	0.006	0.055
92	**Phe**	0.48	0.003	0.068		0.48	0.003	0.068
93	**Cys**	0.57	0.186	0.154		0.57	0.186	0.154
94	**Thr**	0.83	0.137	0.152		0.83	0.137	0.152
95	**Pro**	-	-	-		-	-	-
96	**His**	d	d	d		2.99*	0.100*	0.429*
97	**Pro**	-	-	-		-	-	-
98	**Phe**	d	d	d		3.09*	0.430*	0.532*
99	**Met**	d	d	d		0.35*	0.532*	0.379*
100	**Arg**	1.10	0	0.156		1.10	0.000	0.156
101	**Gly**	0.27	0.036	0.046		0.27	0.036	0.046
102	**Lys**	0.71	0.033	0.103		0.71	0.033	0.103
103	**Val**	0.18	0.002	0.025		0.18	0.002	0.025
104	**Ile**	0.07	0.008	0.011		0.07	0.008	0.011
105	**Val**	0.01	0.007	0.005		0.01	0.007	0.005
106	**Glu**	0.04	0.002	0.006		0.04	0.002	0.006

* These are the minimum shifts because assignment was not possible

APPENDIX B

Table 1. Assignment of *Paracoccus denitrificans* ^{15}N-Zn- amicyanin, 20mM KPi pH=7,9 T=300K (n.a.: not assigned)

Residue		^{15}N	$^{1}H^{N}$	Others
0	**Gly**	n.a.	n.a.	
1	**Asp**	121.39	8.38	
2	**Lys**	114.37	7.94	
3	**Ala**	116.44	6.87	
4	**Thr**	112.86	8.85	
5	**Ile**	122.46	8.25	
6	**Pro**	-	-	
7	**Ser**	109.47	7.69	
8	**Glu**	127.93	9.02	
9	**Ser**	112.10	7.85	
10	**Pro**	-	-	
11	**Phe**	120.07	8.57	
12	**Ala**	122.53	8.62	
13	**Ala**	123.68	8.17	
14	**Ala**	117.84	8.28	
15	**Glu**	114.87	7.89	
16	**Val**	121.89	7.41	
17	**Ala**	132.06	8.59	
18	**Asp**	121.08	8.40	
19	**Gly**	112.36	8.59	
20	**Ala**	122.86	7.27	
21	**Ile**	123.53	8.40	
22	**Val**	129.35	8.05	
23	**Val**	128.06	8.70	
24	**Asp**	127.33	8.62	
25	**Ile**	120.29	8.58	
26	**Ala**	124.50	8.30	
27	**Lys**	119.65	8.90	
28	**Met**	108.40	8.88	
29	**Lys**	113.78	7.33	
30	**Tyr**	118.55	8.17	
31	**Glu**	123.20	9.30	
32	**Thr**	110.19	6.23	
33	**Pro**	-	-	
34	**Glu**	121.99	8.09	
35	**Leu**	128.59	7.69	
36	**His**	127.22	8.93	
37	**Val**	117.18	9.10	
38	**Lys**	121.13	9.19	
39	**Val**	119.45	7.92	
40	**Gly**	117.11	8.87	
41	**Asp**	121.88	8.36	
42	**Thr**	116.62	8.45	
43	**Val**	129.77	9.27	
44	**Thr**	122.75	8.05	
45	**Trp**	129.91	9.58	
46	**Ile**	117.67	8.31	
47	**Asn**	123.81	8.53	ND2 110.38, HD21 7.46, HD22 6.82

48	**Arg**	125.12	9.49	
49	**Glu**	120.68	8.35	
50	**Ala**	117.50	7.94	
51	**Met**	119.66	7.46	
52	**Pro**	-	-	
53	**His**	n.a.	n.a.	
54	**Asn**	n.a.	n.a.	
55	**Val**	107.59	6.55	
56	**His**	124.47	8.48	
57	**Phe**	n.a.	n.a.	
58	**Val**	118.25	9.00	
59	**Ala**	123.59	8.68	
60	**Gly**	111.58	7.66	
61	**Val**	121.09	7.84	
62	**Leu**	115.37	9.16	
63	**Gly**	114.78	7.42	
64	**Glu**	119.34	8.66	
65	**Ala**	119.44	7.98	
66	**Ala**	120.86	8.48	
67	**Leu**	123.97	8.94	
68	**Lys**	128.75	8.44	
69	**Gly**	116.32	8.85	
70	**Pro**	-	-	
71	**Met**	117.22	8.31	
72	**Met**	122.80	8.77	
73	**Lys**	123.20	8.56	
74	**Lys**	119.79	7.94	
75	**Glu**	118.22	9.35	
76	**Gln**	116.81	7.89	NE2 112.33, HE21 7.72, HE22 6.65
77	**Ala**	122.28	8.82	
78	**Tyr**	117.27	8.43	
79	**Ser**	121.73	7.62	
80	**Leu**	119.80	8.84	
81	**Thr**	119.67	8.49	
82	**Phe**	125.10	8.09	
83	**Thr**	112.24	8.15	
84	**Glu**	120.15	7.67	
85	**Ala**	131.34	9.03	
86	**Gly**	109.08	8.74	
87	**Thr**	114.63	7.72	
88	**Tyr**	127.44	9.13	
89	**Asp**	126.89	8.53	
90	**Tyr**	116.85	8.30	
91	**His**	118.64	8.68	
92	**Cys**	120.76	6.78	
93	**Thr**	128.84	10.23	
94	**Pro**	-	-	
95	**His**	n.a.	n.a.	
96	**Pro**	-	-	
97	**Phe**	111.11	6.41	
98	**Met**	125.63	8.41	
99	**Arg**	121.30	7.76	
100	**Gly**	109.08	7.71	
101	**Lys**	117.44	8.38	
102	**Val**	126.89	9.10	
103	**Val**	130.03	9.28	
104	**Val**	128.81	9.18	
105	**Glu**	133.61	8.77	

Table 2. Assignment of *Paracoccus denitrificans* ^{15}N-^{13}C-Cu(I)- amicyanin, 300K, 10mM KPi pH 6.8 (n.a.: not assigned)

Residue		^{15}N	$^{1}H^{N}$	C^{α}	C^{β}	CO
0	**Gly**	n.a.	n.a.	n.a.	n.a.	n.a.
1	**Asp**	121.32	8.38	57.21	41.03	173.17
2	**Lys**	113.36	7.97	55.75	33.20	175.52
3	**Ala**	116.19	6.80	51.12	22.84	174.64
4	**Thr**	113.60	8.92	60.25	70.71	177.94
5	**Ile**	122.47	8.25	59.15	39.85	174.95
6	**Pro**	-	-	60.89	32.37	173.43
7	**Ser**	109.32	7.69	56.17	64.27	175.92
8	**Glu**	127.81	9.04	59.27	29.84	172.82
9	**Ser**	111.98	7.86	55.69	63.50	178.85
10	**Pro**	-	-	63.07	32.75	174.99
11	**Phe**	119.93	8.55	54.25	41.43	176.56
12	**Ala**	122.42	8.62	53.26	18.75	171.83
13	**Ala**	123.64	8.19	54.74	n.a.	170.95
14	**Ala**	117.75	8.29	53.99	18.79	171.92
15	**Glu**	114.74	7.90	56.35	29.73	173.73
16	**Val**	121.73	7.41	63.64	31.67	174.82
17	**Ala**	131.95	8.60	52.15	19.49	172.24
18	**Asp**	120.99	8.40	56.09	40.66	172.62
19	**Gly**	112.25	8.59	45.14	-	174.98
20	**Ala**	122.79	7.27	52.50	19.55	173.27
21	**Ile**	123.43	8.43	62.55	37.37	174.90
22	**Val**	129.18	8.05	60.40	35.96	174.01
23	**Val**	127.95	8.71	61.39	32.91	175.65
24	**Asp**	127.15	8.55	55.12	43.28	174.51
25	**Ile**	120.13	8.52	60.61	39.06	175.91
26	**Ala**	124.17	8.17	52.04	22.15	173.86
27	**Lys**	119.62	9.03	56.51	29.31	174.17
28	**Met**	108.89	8.96	55.14	28.17	175.99
29	**Lys**	113.48	7.20	55.42	35.83	175.72
30	**Tyr**	119.13	7.89	57.61	37.82	172.69
31	**Glu**	123.17	9.25	60.56	29.99	173.81
32	**Thr**	110.09	6.22	58.83	69.70	n.a.
33	**Pro**	-	-	n.a.	n.a.	n.a.
34	**Glu**	122.25	8.17	56.01	30.35	177.33
35	**Leu**	128.51	7.67	53.83	45.84	175.52
36	**His**	126.62	9.08	54.71	28.83	176.11
37	**Val**	117.05	9.05	58.67	34.09	176.01
38	**Lys**	121.05	9.19	53.59	34.20	173.07
39	**Val**	119.30	7.88	66.21	31.37	173.11
40	**Gly**	117.04	8.86	44.64	-	175.99
41	**Asp**	121.70	8.34	55.25	41.32	174.84
42	**Thr**	116.53	8.46	62.09	70.33	176.67
43	**Val**	129.77	9.27	64.22	34.33	176.65
44	**Thr**	122.64	8.05	61.70	71.19	177.75
45	**Trp**	129.85	9.58	58.53	31.80	174.74
46	**Ile**	117.52	8.30	60.72	41.25	174.88
47	**Asn**	123.65	8.51	52.94	37.82	174.09
48	**Arg**	125.05	9.36	53.53	30.13	173.36
49	**Glu**	121.57	8.68	54.01	33.79	177.98
50	**Ala**	117.20	7.89	53.10	18.54	171.02

51	**Met**	120.07	7.47	52.90	32.60	178.32
52	**Pro**	-	-	n.a.	n.a.	n.a.
53	**His**	117.47	7.36	n.a.	n.a.	n.a.
54	**Asn**	n.a.	n.a.	n.a.	n.a.	n.a.
55	**Val**	106.72	6.47	60.98	33.83	176.21
56	**His**	123.86	8.48	52.98	33.57	174.04
57	**Phe**	125.19	9.21	55.24	40.68	174.27
58	**Val**	117.97	8.85	62.35	32.38	174.90
59	**Ala**	123.71	8.68	54.64	18.10	172.71
60	**Gly**	111.50	7.63	45.88	-	174.94
61	**Val**	120.91	7.80	66.58	32.93	173.75
62	**Leu**	115.35	9.18	53.56	42.61	174.94
63	**Gly**	105.07	7.43	44.08	-	178.51
64	**Glu**	119.22	8.65	59.79	29.96	172.49
65	**Ala**	119.28	7.95	50.52	20.40	172.83
66	**Ala**	120.64	8.48	52.45	19.93	173.44
67	**Leu**	123.48	8.87	54.60	43.47	176.77
68	**Lys**	128.97	8.50	55.09	31.42	175.22
69	**Gly**	116.65	8.90	44.54	-	n.a.
70	**Pro**	-	-	61.94	31.75	173.74
71	**Met**	117.10	8.25	54.54	29.19	174.08
72	**Met**	122.96	9.02	55.20	37.42	173.47
73	**Lys**	123.11	8.58	54.97	33.19	95.27
74	**Lys**	119.73	7.91	59.09	33.28	172.98
75	**Glu**	118.11	9.36	58.30	26.33	174.73
76	**Gln**	116.67	7.89	55.13	31.89	177.40
77	**Ala**	122.05	8.80	49.85	25.02	175.05
78	**Tyr**	117.13	8.41	59.51	43.51	176.72
79	**Ser**	121.65	7.62	57.47	67.23	177.65
80	**Leu**	119.69	8.84	54.61	48.18	175.97
81	**Thr**	119.61	8.51	61.54	69.33	176.23
82	**Phe**	125.08	8.11	59.58	41.55	173.55
83	**Thr**	112.02	8.14	62.10	69.06	176.23
84	**Glu**	119.92	7.67	55.31	33.82	174.58
85	**Ala**	131.29	9.04	52.93	18.54	173.67
86	**Gly**	109.01	8.74	44.88	-	179.82
87	**Thr**	114.57	7.74	62.26	70.39	177.06
88	**Tyr**	127.28	9.12	56.57	39.92	176.15
89	**Asp**	126.65	8.58	54.53	42.94	175.19
90	**Tyr**	116.89	8.36	56.31	39.45	175.98
91	**His**	117.11	8.64	54.62	33.18	179.71
92	**Cys**	122.62	7.02	58.03	30.48	n.a.
93	**Thr**	128.25	10.39	69.55	65.15	n.a.
94	**Pro**	-	-	64.08	n.a.	174.30
95	**His**	118.29	7.23	52.73	29.47	n.a.
96	**Pro**	-	-	n.a.	n.a.	n.a.
97	**Phe**	113.69	6.62	56.81	37.48	173.56
98	**Met**	126.35	8.47	56.62	31.52	n.a.
99	**Arg**	121.34	7.73	54.66	34.81	174.74
100	**Gly**	108.97	7.67	43.78	-	179.03
101	**Lys**	116.97	8.44	55.91	36.78	174.48
102	**Val**	126.61	9.10	61.83	34.35	176.67
103	**Val**	129.75	9.27	61.87	32.04	176.84
104	**Val**	128.95	9.22	60.85	32.15	174.58
105	**Glu**	133.54	8.85	57.39	32.63	170.05

Table 3. Shift perturbations (ppm) for *P.denitrificans* Cu(I) and Zn-substituted amicyanin bound to cytochrome *c*-551i (d:disappeared, n.a.: not assigned)

Residue		Cu(I)-amicyanin +2.4eq of cyt *c*-551i				Zn-amicyanin +2.3eq of cyt *c*-551i		
		^{15}N	$^{1}H^{N}$	$\Delta\delta_{avg}$		^{15}N	$^{1}H^{N}$	$\Delta\delta_{avg}$
0	**Gly**	n.a.	n.a.	n.a.		n.a.	n.a.	n.a.
1	**Asp**	0.02	0.006	0.005		0.15	0.003	0.021
2	**Lys**	0.02	0.014	0.010		0.13	0.020	0.023
3	**Ala**	0.01	0.006	0.005		0.00	0.009	0.006
4	**Thr**	0.06	0.013	0.013		0.01	0.002	0.002
5	**Ile**	0.02	0.010	0.008		0.04	0.000	0.006
6	**Pro**	-	-	-		-	-	-
7	**Ser**	0.02	0.007	0.006		0.05	0.001	0.007
8	**Glu**	0.01	0.003	0.003		0.02	0.009	0.007
9	**Ser**	0.08	0.024	0.020		0.04	0.018	0.014
10	**Pro**	-	-	-		-	-	-
11	**Phe**	0.07	0.008	0.011		0.08	0.003	0.012
12	**Ala**	0.03	0.004	0.005		0.02	0.003	0.004
13	**Ala**	0.02	0.001	0.003		0.03	0.008	0.007
14	**Ala**	0.02	0.003	0.004		0.02	0.008	0.006
15	**Glu**	0.05	0.002	0.007		0.02	0.006	0.005
16	**Val**	0.04	0.006	0.007		0.01	0.005	0.004
17	**Ala**	0.06	0.022	0.018		0.02	0.005	0.005
18	**Asp**	0.07	0.017	0.016		0.01	0.006	0.005
19	**Gly**	0.00	0.007	0.005		0.07	0.004	0.010
20	**Ala**	0.03	0.003	0.005		0.01	0.001	0.002
21	**Ile**	0.03	0.013	0.010		0.05	0.004	0.008
22	**Val**	0.02	0.009	0.007		0.01	0.004	0.003
23	**Val**	0.02	0.006	0.005		0.06	0.006	0.010
24	**Asp**	0.02	0.029	0.021		0.02	0.013	0.010
25	**Ile**	0.09	0.046	0.035		0.00	0.002	0.001
26	**Ala**	0.04	0.031	0.023		0.00	0.022	0.016
27	**Lys**	0.26	0.035	0.044		0.24	0.095	0.075
28	**Met**	0.03	0.035	0.025		0.12	0.028	0.026
29	**Lys**	0.06	0.033	0.025		0.13	0.024	0.025
30	**Tyr**	0.05	0.002	0.007		0.02	0.022	0.016
31	**Glu**	0.02	0.025	0.018		0.07	0.007	0.011
32	**Thr**	0.01	0.010	0.007		0.03	0.004	0.005
33	**Pro**	-	-	-		-	-	-
34	**Glu**	0.04	0.010	0.009		0.01	0.001	0.002
35	**Leu**	0.02	0.006	0.005		0.04	0.006	0.007
36	**His**	0.01	0.009	0.007		n.a.	n.a.	n.a.
37	**Val**	0.03	0.013	0.010		0.02	0.003	0.004
38	**Lys**	0.04	0.007	0.008		0.01	0.002	0.002
39	**Val**	0.01	0.004	0.003		0.02	0.002	0.003
40	**Gly**	0.04	0.011	0.010		0.00	0.001	0.001
41	**Asp**	0.01	0.004	0.003		0.02	0.000	0.003
42	**Thr**	0.03	0.012	0.010		0.01	0.005	0.004
43	**Val**	0.05	0.004	0.008		0.01	0.006	0.005
44	**Thr**	0.01	0.003	0.003		0.01	0.000	0.001
45	**Trp**	0.02	0.010	0.008		0.06	0.008	0.010
46	**Ile**	0.02	0.011	0.008		0.05	0.007	0.009
47	**Asn**	0.01	0.021	0.015		0.01	0.022	0.016
48	**Arg**	0.04	0.033	0.024		0.09	0.031	0.025
49	**Glu**	0.02	0.012	0.009		0.13	0.078	0.058
50	**Ala**	0.03	0.033	0.024		0.11	0.005	0.016

51	**Met**	0.24	0.064	0.057		0.33	0.064	0.065
52	**Pro**	-	-	-		-	-	-
53	**His**	0.28	0.029	0.045		n.a.	n.a.	n.a.
54	**Asn**	n.a.	n.a.	n.a.		n.a.	n.a.	n.a.
55	**Val**	0.03	0.010	0.008		0.05	0.009	0.010
56	**His**	0.17	0.032	0.033		0.23	0.038	0.042
57	**Phe**	0.16	0.018	0.026		n.a.	n.a.	n.a.
58	**Val**	0.02	0.015	0.011		0.03	0.036	0.026
59	**Ala**	0.04	0.019	0.015		0.11	0.023	0.023
60	**Gly**	0.09	0.019	0.019		0.05	0.017	0.014
61	**Val**	0.01	0.008	0.006		0.00	0.006	0.004
62	**Leu**	0.02	0.003	0.004		0.02	0.007	0.006
63	**Gly**	0.00	0.004	0.003		0.01	0.004	0.003
64	**Glu**	0.03	0.009	0.008		0.05	0.006	0.008
65	**Ala**	0.04	0.022	0.017		0.00	0.018	0.013
66	**Ala**	0.02	0.005	0.005		0.02	0.013	0.010
67	**Leu**	0.15	0.019	0.025		0.23	0.025	0.037
68	**Lys**	0.05	0.002	0.007		0.18	0.021	0.030
69	**Gly**	0.18	0.021	0.030		0.08	0.019	0.018
70	**Pro**	-	-	-		-	-	-
71	**Met**	0.00	0.012	0.009		0.05	0.007	0.009
72	**Met**	0.09	0.006	0.013		0.03	0.045	0.032
73	**Lys**	0.03	0.015	0.011		0.03	0.027	0.020
74	**Lys**	0.01	0.014	0.010		0.05	0.048	0.035
75	**Glu**	0.05	0.018	0.015		0.01	0.024	0.017
76	**Gln**	0.03	0.010	0.008		0.02	0.007	0.006
77	**Ala**	0.04	0.012	0.010		0.05	0.007	0.009
78	**Tyr**	0.05	0.013	0.012		0.04	0.004	0.006
79	**Ser**	0.04	0.003	0.006		0.05	0.002	0.007
80	**Leu**	0.01	0.006	0.005		0.01	0.000	0.001
81	**Thr**	0.01	0.007	0.005		0.01	0.001	0.002
82	**Phe**	0.02	0.009	0.007		0.00	0.006	0.004
83	**Thr**	0.00	0.007	0.005		0.00	0.007	0.005
84	**Glu**	0.03	0.010	0.008		0.01	0.004	0.003
85	**Ala**	0.02	0.010	0.008		0.02	0.003	0.004
86	**Gly**	0.01	0.009	0.007		0.01	0.006	0.005
87	**Thr**	0.01	0.013	0.009		0.03	0.003	0.005
88	**Tyr**	0.01	0.004	0.003		0.02	0.006	0.005
89	**Asp**	0.01	0.000	0.001		0.01	0.008	0.006
90	**Tyr**	0.05	0.006	0.008		0.12	0.019	0.022
91	**His**	0.52	0.013	0.074		0.79	0.044	0.116
92	**Cys**	0.13	0.024	0.025		0.30	0.046	0.054
93	**Thr**	0.35	0.034	0.055		0.20	0.001	0.028
94	**Pro**	-	-	-		-	-	-
95	**His**	1.18	0.070	0.174		n.a.	n.a.	n.a.
96	**Pro**	-	-	-		-	-	-
97	**Phe**	d	d	d ($\Delta\delta_{avg}$>0.196*)		0.07	0.010	0.012
98	**Met**	0.81	0.017	0.115		0.23	0.041	0.044
99	**Arg**	0.20	0.015	0.030		0.11	0.025	0.024
100	**Gly**	0.19	0.028	0.033		0.03	0.020	0.015
101	**Lys**	0.07	0.002	0.010		0.05	0.008	0.009
102	**Val**	0.00	0.002	0.001		0.02	0.007	0.006
103	**Val**	0.03	0.007	0.007		0.03	0.001	0.004
104	**Val**	0.01	0.008	0.006		0.00	0.002	0.001
105	**Glu**	0.03	0.006	0.006		0.01	0.003	0.003

* Value calculate for the shift at 1.0 eq. of cyt *c*-551i added (peak 114.14-6.839)

Table 4. Shift perturbations (ppm) for *P.denitrificans* d Zn-substituted amicyanin bound to MADH (d:disappeared, n.a.: not assigned)

Residue		Zn-amicyanin +2eq of MADH		
		^{15}N	$^{1}H^{N}$	$\Delta\delta_{avg}$
0	**Gly**	n.a.	n.a.	n.a.
1	**Asp**	n.a.	n.a.	n.a.
2	**Lys**	0.16	0.011	0.024
3	**Ala**	0.08	0.028	0.023
4	**Thr**	0.11	0.006	0.016
5	**Ile**	0.12	0.017	0.021
6	**Pro**	-	-	-
7	**Ser**	0.10	0.020	0.020
8	**Glu**	0.12	0.034	0.029
9	**Ser**	0.07	0.026	0.021
10	**Pro**	-	-	-
11	**Phe**	0.03	0.006	0.006
12	**Ala**	0.03	0.015	0.011
13	**Ala**	0.22	0.039	0.042
14	**Ala**	0.11	0.008	0.017
15	**Glu**	0.17	0.037	0.036
16	**Val**	0.07	0.026	0.021
17	**Ala**	0.01	0.000	0.001
18	**Asp**	0.05	0.001	0.007
19	**Gly**	0.01	0.001	0.002
20	**Ala**	0.05	0.010	0.010
21	**Ile**	0.07	0.009	0.012
22	**Val**	0.01	0.001	0.002
23	**Val**	0.17	0.019	0.028
24	**Asp**	0.04	0.025	0.019
25	**Ile**	0.39	0.050	0.066
26	**Ala**	0.20	0.019	0.031
27	**Lys**	n.a.	n.a.	n.a.
28	**Met**	1.56	0.059	0.225
29	**Lys**	0.27	0.035	0.046
30	**Tyr**	0.33	0.071	0.069
31	**Glu**	0.11	0.019	0.021
32	**Thr**	0.10	0.008	0.015
33	**Pro**	-	-	-
34	**Glu**	0.01	0.027	0.019
35	**Leu**	0.11	0.010	0.017
36	**His**	0.15	0.055	0.044
37	**Val**	0.16	0.019	0.026
38	**Lys**	0.01	0.004	0.003
39	**Val**	0.00	0.023	0.016
40	**Gly**	0.04	0.018	0.014
41	**Asp**	0.16	0.027	0.030
42	**Thr**	0.16	0.006	0.023
43	**Val**	0.05	0.001	0.007
44	**Thr**	0.02	0.024	0.017
45	**Trp**	0.10	0.026	0.023
46	**Ile**	0.07	0.003	0.010
47	**Asn**	0.24	0.017	0.036
48	**Arg**	0.04	0.037	0.027
49	**Glu**	0.31	0.019	0.046
50	**Ala**	0.38	0.009	0.054
51	**Met**	2.93	0.313	0.470*

52	**Pro**	-	-	-
53	**His**	n.a.	n.a.	n.a.
54	**Asn**	n.a.	n.a.	n.a.
55	**Val**	0.02	0.016	0.012
56	**His**	0.15	0.043	0.037
57	**Phe**	n.a.	n.a.	n.a.
58	**Val**	0.00	0.075	0.053
59	**Ala**	0.21	0.113	0.085
60	**Gly**	0.09	0.010	0.015
61	**Val**	0.53	0.010	0.075
62	**Leu**	4.74	0.262	0.695*
63	**Gly**	0.19	0.021	0.031
64	**Glu**	0.03	0.003	0.005
65	**Ala**	0.05	0.010	0.010
66	**Ala**	0.21	0.083	0.066
67	**Leu**	0.11	0.004	0.016
68	**Lys**	0.62	0.068	0.100
69	**Gly**	1.90	0.148	0.288
70	**Pro**	-	-	-
71	**Met**	0.03	0.015	0.011
72	**Met**	0.84	0.068	0.128
73	**Lys**	0.00	0.033	0.023
74	**Lys**	0.13	0.058	0.045
75	**Glu**	0.04	0.030	0.022
76	**Gln**	0.03	0.022	0.016
77	**Ala**	0.10	0.020	0.020
78	**Tyr**	0.20	0.004	0.028
79	**Ser**	0.06	0.024	0.019
80	**Leu**	0.20	0.024	0.033
81	**Thr**	0.00	0.003	0.002
82	**Phe**	0.04	0.000	0.006
83	**Thr**	0.08	0.023	0.020
84	**Glu**	0.07	0.007	0.011
85	**Ala**	0.02	0.005	0.005
86	**Gly**	0.08	0.008	0.013
87	**Thr**	0.10	0.012	0.016
88	**Tyr**	0.04	0.017	0.013
89	**Asp**	0.28	0.026	0.044
90	**Tyr**	0.05	0.026	0.020
91	**His**	0.14	0.057	0.045
92	**Cys**	0.89	0.201	0.190
93	**Thr**	0.60	1.303	0.925*
94	**Pro**	-	-	
95	**His**	n.a.	n.a.	n.a.
96	**Pro**	-	-	-
97	**Phe**	2.37	0.348	0.416
98	**Met**	1.32	0.049	0.190*
99	**Arg**	0.58	0.134	0.125*
100	**Gly**	0.52	0.071	0.089
101	**Lys**	0.22	0.010	0.032
102	**Val**	0.15	0.006	0.022
103	**Val**	0.07	0.006	0.011
104	**Val**	0.01	0.004	0.003
105	**Glu**	0.06	0.016	0.014

* These are the minimum shifts because assignment was not possible

REFERENCES

1. Dennison, C., Canters, G. W., De Vries, S., Vijgenboom, E., and Van Spanning, R. J. (1998) The methylamine dehydrogenase electron transfer chain, *Adv. Inorg. Chem. 45*, 351-407.
2. Davidson, V. L., Jones, L. H., Graichen, M. E., Mathews, F. S., and Hosler, J. P. (1997) Factors which stabilize the methylamine dehydrogenase-amicyanin electron transfer protein complex revealed by site-directed mutagenesis, *Biochemistry 36*, 12733-12738.
3. Chen, L., Doi, M., Durley, R. C., Chistoserdov, A. Y., Lidstrom, M. E., Davidson, V. L., and Mathews, F. S. (1998) Refined crystal structure of methylamine dehydrogenase from Paracoccus denitrificans at 1.75 A resolution, *J Mol Biol 276*, 131-149.
4. Bishop, G. R., and Davidson, V. L. (1995) Intermolecular electron transfer from substrate-reduced methylamine dehydrogenase to amicyanin is linked to proton transfer, *Biochemistry 34*, 12082-12086.
5. Brooks, H. B., and Davidson, V. L. (1994) Kinetic and thermodynamic analysis of a physiologic intermolecular electron-transfer reaction between methylamine dehydrogenase and amicyanin, *Biochemistry 33*, 5696-5701.
6. Davidson, V. L., Graichen, M. E., and Jones, L. H. (1993) Binding constants for a physiologic electron-transfer protein complex between methylamine dehydrogenase and amicyanin. Effects of ionic strength and bound copper on binding, *Biochim Biophys Acta 1144*, 39-45.
7. Romero, A., Nar, H., Huber, R., Messerschmidt, A., Kalverda, A. P., Canters, G. W., Durley, R., and Mathews, F. S. (1994) Crystal structure analysis and refinement at 2.15 A resolution of amicyanin, a type I blue copper protein, from Thiobacillus versutus, *J Mol Biol 236*, 1196-1211.
8. Kalverda, A. P., Wymenga, S. S., Lommen, A., van de Ven, F. J., Hilbers, C. W., and Canters, G. W. (1994) Solution structure of the type 1 blue copper protein amicyanin from Thiobacillus versutus, *J Mol Biol 240*, 358-371.
9. Van Beeumen, J., Van Bun, S., Canters, G. W., Lommen, A., and Chothia, C. (1991) The structural homology of amicyanin from Thiobacillus versutus to plant plastocyanins, *J Biol Chem 266*, 4869-4877.
10. Chen, L., Durley, R., Poliks, B. J., Hamada, K., Chen, Z., Mathews, F. S., Davidson, V. L., Satow, Y., Huizinga, E., Vellieux, F. M., and Hol, W. G. J. (1992) Crystal structure of an electron-transfer complex between methylamine dehydrogenase and amicyanin, *Biochemistry 31*, 4959-4964.
11. Husain, M., and Davidson, V. L. (1986) Characterization of two inducible periplasmic c-type cytochromes from Paracoccus denitrificans, *J Biol Chem 261*, 8577-8580.
12. Chen, L., Durley, R. C., Mathews, F. S., and Davidson, V. L. (1994) Structure of an electron transfer complex: methylamine dehydrogenase, amicyanin, and cytochrome c551i, *Science 264*, 86-90.
13. Van Spanning, R. J., Wansell, C. W., Reijnders, W. N., Harms, N., Ras, J., Oltmann, L. F., and Stouthamer, A. H. (1991) A method for introduction of unmarked mutations in the genome of Paracoccus denitrificans: construction of strains with multiple mutations in the genes encoding periplasmic cytochromes c550, c551i, and c553i, *J Bacteriol 173*, 6962-6970.
14. Mathews, F. S., Chen, Z.-W., Durley, R. C. E., Davidson, V. L., Jones, L. H., Graichen, M. E., Hosler, J. H., Merli, A., Brodersen, D. E., and Rossi, G. L. (1998) Structural Research on the Methylamine Dehydrogenase Redox Chain of Paracoccus Denitrificans, in *Biological Electron-Transfer Chains: Genetics, Composition and Mode of Operation* (Canters, G. W., and Vijgenboom, E., Eds.), pp 129-146, Kluwer Academic Publishers, Dordrecht, The Netherlands.

15. Davidson, V. L., and Jones, L. H. (1996) Electron transfer from copper to heme within the methylamine dehydrogenase--amicyanin--cytochrome c-551i complex, *Biochemistry 35*, 8120-8125.
16. Davidson, V. L. (2000) What controls the rates of interprotein electron-transfer reactions, *Acc Chem Res 33*, 87-93.
17. Merli, A., Brodersen, D. E., Morini, B., Chen, Z., Durley, R. C., Mathews, F. S., Davidson, V. L., and Rossi, G. L. (1996) Enzymatic and electron transfer activities in crystalline protein complexes, *J Biol Chem 271*, 9177-9180.
18. Ferrari, D., Di Valentin, M., Carbonera, D., Merli, A., Chen, Z. W., Mathews, F. S., Davidson, V. L., and Rossi, G. L. (2004) Electron transfer in crystals of the binary and ternary complexes of methylamine dehydrogenase with amicyanin and cytochrome c551i as detected by EPR spectroscopy, *J Biol Inorg Chem 9*, 231-237.
19. Ferrari, D., Merli, A., Peracchi, A., Di Valentin, M., Carbonera, D., and Rossi, G. L. (2003) Catalysis and electron transfer in protein crystals: the binary and ternary complexes of methylamine dehydrogenase with electron acceptors, *Biochim Biophys Acta 1647*, 337-342.
20. Marcus, R. A., and Sutin, N. (1985) Electron transfers in chemistry and biology, *Biochim Biophys Acta 811*, 265-322.
21. Pervushin, K., Riek, R., Wider, G., and Wuthrich, K. (1997) Attenuated T2 relaxation by mutual cancellation of dipole-dipole coupling and chemical shift anisotropy indicates an avenue to NMR structures of very large biological macromolecules in solution, *Proc Natl Acad Sci U S A 94*, 12366-12371.
22. Wittekind, M., and Mueller, L. (1993) HNCACB, a High-Sensitivity 3D NMR Experiment to Correlate Amide-Proton and Nitrogen Resonances with the Alpha- and Beta-Carbon Resonances in Proteins, *J Magn Reson B 101*, 201-205.
23. Grzesiek, S., and Bax, A. (1992) Improved 3D triple-resonance NMR techniques applied to a 31 kDa protein, *J Magn Reson B 96*, 432-440.
24. Clubb, R. T., Thanabal, V., and Wagner, G. (1992) A constant-time three-dimensional triple-resonance pulse scheme to correlate intraresidue 1HN, 15N, and 13C? chemical shifts in 15N---13C-labelled proteins, *J Magn Reson B 97*, 213-217.
25. Montelione, G. T., Lyons, B. A., Emerson, S. D., and Tashiro, M. (1992) An efficient triple resonance experiment using carbon-13 isotropic mixing for determining sequence-specific resonance assignments of isotopically-enriched proteins, *J. Am. Chem. Soc. 114*, 10974-10975.
26. Vellieux, F. M., Huitema, F., Groendijk, H., Kalk, K. H., Jzn, J. F., Jongejan, J. A., Duine, J. A., Petratos, K., Drenth, J., and Hol, W. G. (1989) Structure of quinoprotein methylamine dehydrogenase at 2.25 A resolution, *Embo J 8*, 2171-2178.
27. Kalverda, A. P., Lommen, A., Wymenga, S., Hilbers, C. W., and Canters, G. W. (1991) Three dimensional structure determination of amicyanin by NMR and MD simulations., *J Inorg Biochem 43*, 171.
28. van Wielink, J. E., Frank, J. J., and Duine, J. A. (1989) in *PQQ and Quinoproteins* (Jongejan, J. A., and Duine, J. A., Eds.), pp 269-278, Kluwer Academic Publisher, Dordrecht.
29. Winkler, J. R., and Gray, H. B. (1992) Electron transfer in ruthenium-modified proteins, *Chem. Rev. 92*, 369-379.
30. Elkær Jørgensen, L., Ubbink, M., and Danielsen, E. (2004) Amicyanin metal-site structure and interaction with MADH: PAC and NMR spectroscopy of Ag- , Cd-, and Cu-amicyanin, *J. Biol. Inorg. Chem. 9*, 27-38.
31. van Houwelingen, T., Canters, G. W., Stobbelaar, G., Duine, J. A., Frank, J., Jr., and Tsugita, A. (1985) Isolation and characterization of a blue copper protein from Thiobacillus versutus, *Eur J Biochem 153*, 75-80.
32. Prudencio, M., Rohovec, J., Peters, J. A., Tocheva, E., Boulanger, M. J., Murphy, M. E., Hupkes, H. J., Kosters, W., Impagliazzo, A., and Ubbink, M. (2004) A caged lanthanide complex as a paramagnetic shift agent for protein NMR, *Chemistry 10*, 3252-3260.

33. van Wielink, J. E., Frank, J., and Duine, J. A. (1990) Methylamine dehydrogenase from Thiobacillus versutus, in *Methods in Enzymology*, pp 235-241, Academic Press, New York.
34. Gorren, A. C., and Duine, J. A. (1994) The effects of pH and cations on the spectral and kinetic properties of methylamine dehydrogenase from Thiobacillus versutus, *Biochemistry 33*, 12202-12209.
35. Ubbink, M., Van Beeumen, J., and Canters, G. W. (1992) Cytochrome c550 from Thiobacillus versutus: cloning, expression in Escherichia coli, and purification of the heterologous holoprotein, *J Bacteriol 174*, 3707-3714.
36. Otwinowski, Z., and Minor, W. (1996) Processing of X-ray diffraction data collected in oscillation mode, in *Methods in Enzymology*, pp 307-326, Academic Press, New York.
37. Collaborative Computational Project, N. (1994) The CCP4 suite: programs for protein crystallography, *Acta Crystallogr D Biol Crystallogr 50*, 760-763.
38. Jones, T. A., Zou, J. Y., Cowan, S. W., and Kjeldgaard, M. (1991) Improved methods for building protein models in electron density maps and the location of errors in these models, *Acta Crystallogr A 47 (Pt 2)*, 110-119.
39. Emsley, P., and Cowtan, K. (2004) Coot: model-building tools for molecular graphics, *Acta Crystallogr D Biol Crystallogr 60*, 2126-2132.
40. Brunger, A. T., Adams, P. D., Clore, G. M., DeLano, W. L., Gros, P., Grosse-Kunstleve, R. W., Jiang, J. S., Kuszewski, J., Nilges, M., Pannu, N. S., Read, R. J., Rice, L. M., Simonson, T., and Warren, G. L. (1998) Crystallography & NMR system: A new software suite for macromolecular structure determination, *Acta Crystallogr D Biol Crystallogr 54*, 905-921.
41. Weiss, M. S., and Hilgenfeld, R. (1997) On the use of the merging R factor as a quality indicator for X-ray data, *J. Appl. Crystallogr. D55*, 203-205.
42. Husain, M., Davidson, V. L., Gray, K. A., and Knaff, D. B. (1987) Redox properties of the quinoprotein methylamine dehydrogenase from paracoccus denitrificans, *Biochemistry 26*, 4139-4143.
43. Strickland, S., Palmer, G., and Massey, V. (1975) Determination of dissociation constants and specific rate constants of enzyme-substrate (or protein-ligand) interactions from rapid reaction kinetic data, *J Biol Chem 250*, 4048-4052.
44. Bishop, G. R., and Davidson, V. L. (1998) Electron transfer from the aminosemiquinone reaction intermediate of methylamine dehydrogenase to amicyanin, *Biochemistry 37*, 11026-11032.
45. Rivetti, C., Mozzarelli, A., Rossi, G. L., Henry, E. R., and Eaton, W. A. (1993) Oxygen binding by single crystals of hemoglobin, *Biochemistry 32*, 2888-2906.
46. Helgstrand, M., Kraulis, P., Allard, P., and Hard, T. (2000) Ansig for Windows: an interactive computer program for semiautomatic assignment of protein NMR spectra, *J Biomol NMR 18*, 329-336.
47. Huizinga, E. G., van Zanten, B. A., Duine, J. A., Jongejan, J. A., Huitema, F., Wilson, K. S., and Hol, W. G. (1992) Active site structure of methylamine dehydrogenase: hydrazines identify C6 as the reactive site of the tryptophan-derived quinone cofactor, *Biochemistry 31*, 9789-9795.
48. Davidson, V. L., Jones, L. H., and Zhu, Z. (1998) Site-directed mutagenesis of Phe 97 to Glu in amicyanin alters the electronic coupling for interprotein electron transfer from quinol methylamine dehydrogenase, *Biochemistry 37*, 7371-7377.
49. Gray, H. B., and Winkler, J. R. (1996) Electron transfer in proteins, *Annu Rev Biochem 65*, 537-561.
50. Carrell, C. J., Wang, X., Jones, L., Jarrett, W. L., Davidson, V. L., and Mathews, F. S. (2004) Crystallographic and NMR investigation of cobalt-substituted amicyanin, *Biochemistry 43*, 9381-9389.

51. Nar, H., Huber, R., Messerschmidt, A., Filippou, A. C., Barth, M., Jaquinod, M., van de Kamp, M., and Canters, G. W. (1992) Characterization and crystal structure of zinc azurin, a by-product of heterologous expression in Escherichia coli of Pseudomonas aeruginosa copper azurin, *Eur J Biochem 205*, 1123-1129.
52. Zhu, Z., Cunane, L. M., Chen, Z., Durley, R. C., Mathews, F. S., and Davidson, V. L. (1998) Molecular basis for interprotein complex-dependent effects on the redox properties of amicyanin, *Biochemistry 37*, 17128-17136.
53. Ubbink, M., and Bendall, D. S. (1997) Complex of plastocyanin and cytochrome c characterized by NMR chemical shift analysis, *Biochemistry 36*, 6326-6335.
54. Volkov, A. N., Worrall, J. A., Holtzmann, E., and Ubbink, M. (2006) Solution structure and dynamics of the complex between cytochrome c and cytochrome c peroxidase determined by paramagnetic NMR, *Proc Natl Acad Sci U S A 103*, 18945-18950.
55. Worrall, J. A., Liu, Y., Crowley, P. B., Nocek, J. M., Hoffman, B. M., and Ubbink, M. (2002) Myoglobin and cytochrome b5: a nuclear magnetic resonance study of a highly dynamic protein complex, *Biochemistry 41*, 11721-11730.
56. Worrall, J. A., Reinle, W., Bernhardt, R., and Ubbink, M. (2003) Transient protein interactions studied by NMR spectroscopy: the case of cytochrome C and adrenodoxin, *Biochemistry 42*, 7068-7076.
57. Durley, R., Chen, L., Lim, L. W., Mathews, F. S., and Davidson, V. L. (1993) Crystal structure analysis of amicyanin and apoamicyanin from Paracoccus denitrificans at 2.0 A and 1.8 A resolution, *Protein Sci 2*, 739-752.
58. Davidson, V. L., and Jones, L. H. (1995) Complex formation with methylamine dehydrogenase affects the pathway of electron transfer from amicyanin to cytochrome c-551i, *J Biol Chem 270*, 23941-23943.
59. Davidson, V. L. (1990) Methylamine dehydrogenases from methylotrophic bacteria, *Methods Enzymol 188*, 241-246.
60. Husain, M., and Davidson, V. L. (1985) An inducible periplasmic blue copper protein from Paracoccus denitrificans. Purification, properties, and physiological role, *J Biol Chem 260*, 14626-14629.
61. Horrocks, W. D., Jr., and Greenberg, E. S. (1973) Evaluation of dipolar nuclear magnetic resonance shifts in low-spin hemin systems: ferricytochrome c and metmyoglobin cyanide, *Biochim Biophys Acta 322*, 38-44.
62. Kurland, R. J. M., B.R. (1977) Isotropic NMR shifts in transition metal complexes: the calculation of the Fermi contact and pseudocontact terms, *J. Magn. Reson. 2*, 286-301.
63. LaMar, G. N. d. R., J.S. (1993) NMR methodology for paramagnetic proteins, *Biol. Magn. Reson. 12*, 1-78.
64. Ubbink, M., Ejdeback, M., Karlsson, B. G., and Bendall, D. S. (1998) The structure of the complex of plastocyanin and cytochrome f, determined by paramagnetic NMR and restrained rigid-body molecular dynamics, *Structure 6*, 323-335.

LIST OF PUBLICATIONS

Chiara Cavalieri et al., Structural comparison of crystal and solution states of the 138 kDa complex of methylamine dehydrogenase and amicyanin from *Paracoccus versutus*. Manuscript submitted to *Biochemistry*

Chiara Cavalieri et al., NMR studies on protein-protein complexes from *Paracoccus denitrificans*. Manuscript in preparation.

RINGRAZIAMENTI

Ringrazio Gian Luigi Rossi per l'aiuto, la costante fiducia e per la possibilità che mi ha dato di vivere un'importante esperienza di lavoro e di vita all'estero.

Grazie a Marcellus Ubbink per l'accoglienza che mi ha riservato e per i preziosi ed indispensabili insegnamenti che mi ha dato durante i mesi trascorsi al Leiden Insitute of Chemistry.

Grazie ad Angelo Merli per la disponibilità nel risolvere tanti dubbi, soprattutto durante la stesura di questa tesi.

Infine ringrazio tutti gli amici ed i compagni di laboratorio, qui a Parma e a Leiden, per l'aiuto che mi hanno dato tutte le volte che ne ho avuto bisogno, ma soprattutto per l'amicizia, che ha reso ancora più belli questi anni trascorsi insieme.